UNIVERSITY OF CALIFORNIA,
IRVINE

Spatial and Temporal Control of Immune Cell Activation

DISSERTATION

submitted in partial satisfaction of the requirements
for the degree of

DOCTOR OF PHILOSOPHY

in Chemistry

by

Keun Ah Ryu

Dissertation Committee:
Associate Professor Aaron Esser-Kahn, Chair
Professor Kenneth Shea
Associate Professor Jennifer Prescher

2017

TABLE OF CONTENTS

LIST OF FIGURES

LIST OF SCHEMES

ACKNOWLEDGMENTS

I would like to thank my committee chair and mentor, Prof. Aaron Esser-Kahn. His faith in my abilities from the beginning of my graduate career has allowed me to learn and accomplish more than I could have ever imagined. I will always be thankful for his support. I also thank Prof. Kenneth Shea and Prof. Jennifer Prescher for always making the time to discuss my research progress with great encouragement during the entirety of my time at UCI.

I would like to thank administrative members of the UCI chemistry department. I would like to also thank scientists that have offered me technical aid. I would like to thank the members of the UCI Mass Spectrometry Facility, the UCI NMR Spectroscopy Facility, and the Laser Spectroscopy Facility. Particularly, I would like to thank Torin Dupper from the UCI Materials Characterization Lab for help with TEM imaging, Alex Fast and Dr. Dima Fishman with help with laser experiments.

I would like to thank past and present members of the Esser-Kahn lab. To Bethany McGonnigal, Samantha Goetz, Kyle Brubaker, Dr. Lien Lybaert, Dr. Lalisa Stutts, Dr. Maya Kleiman, Dr. Troy Moore, Dr. David Shaffer, and Prof. Kasha Slowinska, for your generous amount of time listening to my complaints and your never-ending support involving lots of buffet lunches, bbqs, happy hours, "5k" walks and coffee breaks. I would also like to thank my colleagues in the chemistry department. I have made some of my best friends at UCI. You have made my time at UCI truly unforgettable and my life in Irvine never boring. I will miss our special off campus lunches, weekend hangouts, late night homework assignments, and weekend trips. I wish everyone the best of luck on your future endeavors. I would like to thank Helen, Katie, and the rest of the Sterk-Van Halsemas for their support despite the distance.

Finally, I would like to thank my parents, Dae Young and Chulmi, and brother, Vincent, for their unconditional love and support. I truly would not be here today without them. This is as much your work as it is mine.

Partial text of Chapter 1 is a reprint of the material as it appears in *ACS Chemical Biology*. The co-author listed in this publication directed and supervised research which forms the basis for the thesis/dissertation.

The text of Chapter 2 is a reprint of the material as it appears in *ACS Chemical Biology*. The co-author listed in this publication directed and supervised research which forms the basis for the thesis/dissertation.

The text of Chapter 3 is a reprint of the material as it appears in *Journal of American Chemical Society*. The co-author listed in this publication directed and supervised research which forms the basis for the thesis/dissertation.

CURRICULUM VITAE

KEUN AH RYU

Education

University of California, Irvine, Irvine, CA 2012-2017
Ph.D. in Organic Chemistry
Advisor: Prof. Aaron Esser-Kahn

Calvin College, Grand Rapids, MI 2008-2011
B.S. Chemistry (ACS Certified)
Minor: Japanese

Laboratory Research Experience

Graduate Research Assistant, Chemistry Department, UCI 2012-2017

- Designed, synthesized, and characterized of photo-caged Toll-like receptor agonists
- Developed *in vitro* and *in vivo* experimental protocols to study photo-activation of innate immune cells.
- Developed polymeric immune agonists for Toll-like receptor synergy mechanism determination.

Research Intern, Chemical Engineering Department, POSTECH, South Korea 2011-2012
Advisor: Prof. Jinwoo Lee

- Synthesized and characterized of mesoporous silica and carbon nanoparticles (NPs) and functionalized NPs for water purification.

Research Assistant, Chemistry Department, Calvin College 2009-2011
Advisor: Prof. Carolyn Anderson

- Expanded scope and optimized LiI catalyzed synthesis of *N*-Alkyl pyridones *via O*- to *N*- alkyl migration.

Technical Skills

Advanced chemistry methods

NMR, UV-VIS, Fluorescence Spectroscopy, FTIR, HPLC, GPC, LC/GC-MS, MALDI, DLS, FPLC, glove box techniques, bioconjugation techniques

Advanced biology methods

Mammalian cell culture, primary cell harvest, gel purification, ELISA, Western blot, plate reader analysis, antibody staining, flow cytometry, single- and multi-photon confocal microscopy, murine *in-vivo* assays (dermal drug delivery, blood collection, adoptive transfer, bioluminescent imaging), thermocycler, tissue RNA extraction, qPCR

Honors and Achievements

UC Regents' Dissertation Fellowship	2016
Allergan Graduate Research Fellowship in Synthetic Organic Chemistry	2015
Justine Lambert Graduate Prize in the Foundations of Science	2015
AAUW International Scholarship	2014
John A. Bolt Memorial Scholarship	2010
Ann, Myrtle, Eunice, Faith and Marie Huizenga Scholarship for Women	2009
Calvin College Presidential Scholarship	2008-2011
Howard Hughes Medical Institute Scholarship	2008-2011

Publications

Ryu, K.; McGonnigal, B.; Moore, T.; Esser-Kahn, A.P. **2017**, "Photoactivation of Immune Response *In Vivo*." *under review.*

Lybaert, L.; **Ryu, K**.; Nuhn, L.; De Rycke, R.; De Wever, O.; Chon, A.; Esser-Kahn, A.; De Geest, B. "Cancer Cell Lysate Entrapment in $CaCO_3$ Engineered with Polymeric TLR-agonists-Immunomodulating Microparticles in View of Personalized Anti-tumor Vaccination." *Chem. Mater.,* **2017**, DOI: 10.1021/acs.chemmater.6b05062.

Lybeart, L.; **Ryu, K.;** De Rycke, R.; Wever, O.; Esser-Kahn, A.; De Geest, B. "Polyelectrolyte-enrobed Cancer Cells in View of Personalized Cancer Vaccination." *Adv. Sci*. **2017**, DOI:10.1002/advs.201700050R1.

Ryu, K.; Slowinska, K.; Moore. T.; Esser-Kahn, A. "Effect of Immunostimulant Spatial Presentation on Immune Response," *ACS Chem. Biol.* **2016**, *11,* 3347-3352.

Oldenhuis, N.; Eldredge, A.; Burts, A.; **Ryu, K**.; Chung, J.; Johnson, M.; Guan, Z. "Biodegradable Dendronized Polymers for Efficient mRNA Delivery," *ChemistrySelect*, **2016,** DOI: 10.1002/slct.201600939.

Chun, J.; Jo, C.; Sahgong, S.; Kim, M.; Lim, E.; Kim, D.; Hwang, J; Kang, E.; **Ryu, K**.; Jung, Y.; Kim, Y.; Lee, J. "Ammonium Fluoride-Mediated Synthesis of Anhydrous Metal Fluoride/Mesoporous Carbon Nanocomposites for High Performance Lithium-Ion Battery Cathodes," *ACS Appl. Mater. Interfaces,* **2016**, *8*, 35180–35190.

Kleiman, M.; **Ryu, K**.; Esser-Kahn, A. "Determination of factors influencing the wet etching of Polydimethylsiloxane using Tetra-n-butylammonium fluoride" *Macromolec. Chem. Phys***.,** **2016**, *217*, 284-291.

Lynn, G.; Laga, R.; Darrah, P.; Ishizuka, A.; Balaci, A.; Dulcey, A.; Pechar, M.; Pola, R.; Gerner, M.; Yamamoto, A.; Buechler, C.; Quinn, K.; Smelkinson, M.; Vanek, O.; Cawood, R.; Hills, T.; Vasalatiy, O.; Kastenmuller, K.; Francica, J.; Stutts, L.; Tom, J.; **Ryu, K**.; Esser-Kahn, A.; Etrych, T.; Fisher, K; Seymour, L.; Sedar, R., "Particle Formation is the Principal

Physicochemical Determinant for Enhancing Vaccine Immunogenicity by Polymer-bound TLR Agonists," *Nat. Biotech.*, **2015**, *33,* 1201–1210.

Ryu, K.; Stutts, L.; Tom, J.; Mancini, R.; Esser Kahn, A. "Stimulation of Innate Immune Cells by Light-Activated TLR7/8 Agonists," *J. Am. Chem. Soc*., **2014**,*136,* 10823–10825*.*

Mancini, R.J.; Stutts, L.; **Ryu, K.**; Tom, J.K.; and Esser-Kahn, A.P. "Directing the Immune System with Chemical Compounds," *ACS Chem. Biol.,* **2014**, *9*, 1075—1085.

Nguyen, D.T.; Kleiman, M.; **Ryu, K.**; Hiew, S.; Brubaker, K.; Mughnetsyan, R.; Truong, R.; Dolan, B.; Tackett, E.; and Esser-Kahn, A.P. "Three-Dimensional Conformal Coatings through the Entrapment of Polymer Membrane Precursors," *ACS Appl. Mat. Interfaces,* **2014**, *6*, 2830–2835.

Tasker, S.; Bosscher, M.; Shandro, C.; Lanni, E.; **Ryu, K**.; Snapper, G.; Utter, J.; Ellsworth, B.; Anderson, C. E. "Preparation of *N*-Alkyl 2-Pyridones *via* a Lithium Iodide Promoted *O*- to *N*-Alkyl Migration: Scope and Mechanism," *J. Org. Chem.*, **2012**, *77*, 8220–8230.

Tasker, S.; Brandsen. B. M.; **Ryu, K**.; Snapper, G. S.; Staples, R. J.; DeKock, R. L.; Anderson, C. E. "Synthesis of a New Class of β-Iodo *N*-Alkenyl 2-Pyridones," *Org. Lett.,* **2011**, 13, 6224–6227.

Teaching and Leadership Experience

Undergraduate Research Mentor, University of California, Irvine 2012-2016

Managed training and experimentation of four undergraduate researchers in *in vitro*, *in vivo* experiments, biochemical assays, organic synthesis and characterization.

Teaching Assistant, University of California, Irvine 2012-2015

Undergraduate Labs: General Chemistry I, General Chemistry II, Organic Chemistry I, Organic Chemistry II

Teaching Assistant, Calvin College 2010-2011

General Chemistry, Organic Chemistry I, Organic Chemistry II

Select Presentations

Ryu, K.; McGonnigal, B.; Esser-Kahn, A. "Light induced cell migration *in vivo* with photocaged TLR agonist," *253rd ACS National Meeting,* San Francisco, CA 2017 (poster presentation).

Ryu, K.; Esser-Kahn, A. "Photoactivation of Immune Cells" Gordon Research Conference-Bioorganic Chemistry, Andover, NH, 2016 (poster presentation).

Ryu, K.; Moore, T.; Esser-Kahn, A. **"**Photo-activation of immune system with caged agonists," *251st ACS National Meeting,* San Diego, CA 2016 (poster presentation).

Ryu, K.; Slowinska, K.; Mancini, R.; Esser-Kahn, A. "Effect of Spatially Predetermined Agonist Presentation on Immune Response *via* Polymeric Systems" *249th ACS National Meeting,* Denver, CO, 2015 (poster presentation).

Ryu, K.; Stutts, L.; Esser-Kahn, A. "Selective Immune Cell Activation *via* Photocaged TLR Agonist" 248th *ACS National Meeting,* San Francisco, CA, 2014 (poster presentation).

ABSTRACT OF THE DISSERTATION

Spatial and Temporal Control of Immune Cell Activation

By

Keun Ah Ryu

Doctor of Philosophy in Chemistry

University of California, Irvine, 2017

Professor Aaron P. Esser-Kahn, Chair

The innate control of adaptive immunity has been the target of various therapeutics. By the chemical modification of the chemical patterns recognized by the Toll-like receptors (TLRs) on innate immune cells, we can further control the systemic immune response. Chemical modifications can be used to control the spatial presentation of multiple TLR agonists by covalent conjugation of two TLR agonists which serve as a synthetic mimic of macromolecular pathogens. Additionally, photocaging of TLR agonists is used to control the spatial and temporal presentation of agonists. These strategies would further provide mechanistic insight in TLR synergy as well as therapeutic insight in modulating the immune response.

CHAPTER 1. INTRODUCTION

1. 1. Innate Immune Control of Adaptive Immune System

Current research in immunotherapies focuses on the function of the innate and adaptive immune system including activation and physiological consequences.[1] Activation of the whole immune system is initiated by the recognition of various components of invading pathogens by antigen presenting cells (APCs) of the innate immune system.[2] Once APCs have processed the antigen, they migrate to the lymph nodes or spleen, to relay information to recirculating T cells. Of the APCs, dendritic cells (DCs) play an essential role by communicating between innate and adaptive immunity.[3]

The manner of antigen recognition and processing by dendritic cells (DCs) is particularly efficient and powerful. First, DCs only need a small amount of antigen to be activated and pass on the antigenic information to T cells.[4] Second, activated DCs retain their activity over a period of a couple days while other immune cells like macrophages which has a turnover in a matter of hours.[5] As a result, the number of activated DCs required to activate a subset of T cells is 30-100 times less than an average cell population.[6] For example, as few as 250 FcR per Langerhans cell are needed to drive a T cell into cell cycle, and each Langerhans cell on average handles 10-20 T cells.[7] In terms of clonal expansion of T cell populations, 1-1000 DCs are required.[8]

Consequently, targeting the innate immune systems, particularly DCs, is advantageous due to their crucial role in directing the activation of adaptive immune cells. Moreover, because DCs are activated by molecular patterns, these patterns can be chemically manipulated to control degree of immune activation. To chemically modify immune stimulatory molecular patterns, we must establish and understand how immune-stimulatory molecular patterns are recognized and processed by DCs.

1. 2. TLRs and TLR agonists

In recognizing these pathogens and distinguishing from "self" and "not self", APCs rely on binding of molecular agonists by a class of receptors named pattern recognition receptors (PRRs).[9] The Esser-Kahn lab is interested in a subset of PRRs called Toll-like Receptors (TLRS). TLRs recognize a host of chemical species[10] and induce the production of cytokines and expression of costimulatory molecules, thereby ultimately activating the adaptive immunity.

Generally, TLRs signal from two different regions of the cell, the cell surface and endosomal compartments. The first location, the cell surface, contains TLRs 1, 2, 4, 5 and 6. Each of these TLRs bind molecules present on the surfaces of pathogens ranging from zymosan to the flagellin of bacteria.[17,18] Many agonists of surface TLRs also increase macro-pinocytosis.[19] The remaining TLRs, TLR3, 7, 8 and 9 all signal from the endosome. Endosomal TLRs recognize pathogenic nucleic acids including ssDNA, ssRNA, and dsDNA. Signaling of TLR9 is activated by a series of endosomal proteases,[20] and a similar mode of action is hypothesized or proven for other endosomal TLRs.

Binding of a pathogen by the TLR initiates a signaling cascade by dimerization of intracellular domain containing adaptor proteins, MyD88 or TRIF, resulting in the induction of pro-inflammatory cytokine producing transcription factors, type 1 interferons, and adhesion molecules (**Figure 1. 1**).[11-12] DC TLR activation therefore induces antigen specific T-cell expansion.[13] Additionally, T-cell differentiation of Th1 and Th2 responses can be controlled by DCs, depending on DC subset, DC maturation stage, DC to T cell ratio, or antigen doses.[14] The role of DCs in joining the immune system following TLR activation makes TLRs a promising target for immunotherapies. [15]

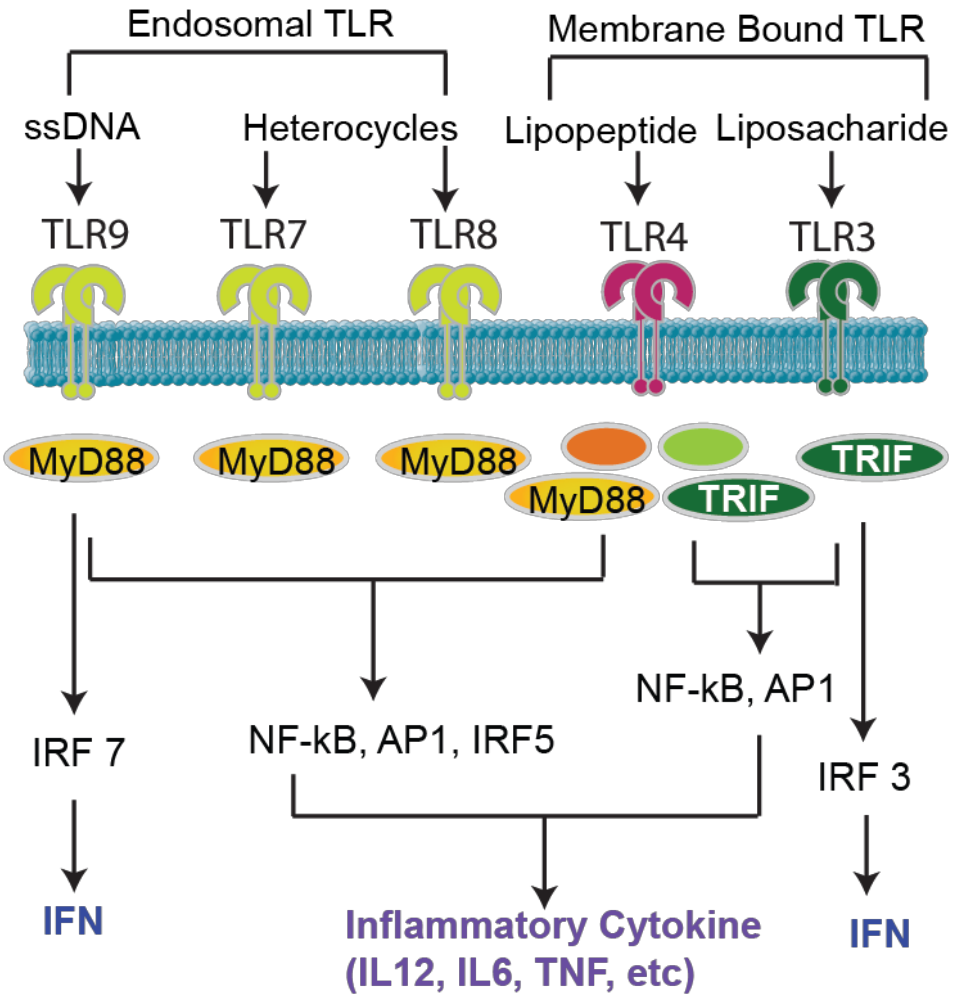

Figure 1. 1. Commonly studied TLRs in dendritic cells (DCs). TLRs except TLR 3 produce transcription factors NF-κB, AP1, and IRF to produce inflammatory cytokines and interferons *via* MyD88. TLR3 and 4 uses an independent pathway using TRIF. TLR4 requires the additional adaptor molecules TIRAP (orange) and TRAM (lime) for activation.

1. 3. TLR Synergies

On top of their crucial role in pathogen recognition, TLRs show synergistic immune activity. Furthermore, TLR synergies are a critical part of vaccines, cancer response, and tolerance. The yellow fever vaccine simultaneously and potently activates TLR2, 7, 8, and 9 on different DC subsets.[16] Additionally, several studies have shown improved efficacy of treatment with multiple TLR ligands compared with single TLR ligands in stimulating cellular immune responses.[17]

These synergies are currently attributed to multiple elements including the activation of multiple signaling pathways within a dendritic cell,[18] and the clustering of multiple receptors to form a hypothesized signalosome.[19] Particularly, many studies have focused on the cooperation between the MyD88 and TRIF pathways as well as the TRAM and TRIF pathway among different TLRs.[20] With the success of finding synergistic activity of TLRs and successful vaccine development, examination of the efficacy of multiple TLR- and PRR- ligand combinations in vaccines against infectious diseases is necessary. For example, agonists that stimulate endosomal TLRs (TLR 3, 7, 8, 9) synergize with agonists of cell surface membrane bound TLRs (TLR 2, 4).[21] Intriguingly, several TLR combinations also act in an inhibitory manner including combinations of multiple cell surface TLR targeting agonists like MPLA, Pam_3CSK_4 (TLR 2, 4) and LPS or combinations of endosomal TLR targeting agonists such as gardiquimod (TLR7) and CpGs (TLR9).[22] The activation of multiple pathways *via* the activation of multiple agonists also change the production of costimulatory molecules and cytokines that aid the production of response elements used to probe TLR synergism, leading to a panel of immune activity profile.

TLR synergies are an exciting opportunity to develop better immune therapies. Controlling the TLR signaling pathways utilizing chemically modified agonists might lead to a better

understanding of immune synergy, immune cell signaling, and ultimately better immunotherapies.

1. 4. Spatial Control of TLRs Through Covalent Conjugation of TLR Agonists

In the Esser-Kahn lab, we are developing TLR agonists that can efficiently activate the immune system. Particularly, we chemically modified TLR agonists with a degree of good spatial and temporal control of agonist presentation on immune cells like DCs. These chemically modified agonists can answer a variety of fundamental questions and can be used to optimize our approach in eliciting an immune response. Efforts to control spatial and temporal presentation of TLR agonists is reported herein.

First, we wanted to understand the spatial relationship of multiple TLR agonists. Naturally occurring pathogens are often large biomacromolecules. These pathogens consist of a variety of pathogen associated molecular patterns (PAMP). Many pathogens can activate multiple TLRs. Parasites such as *Leishmania* also interact with multiple TLR receptors including TLR 2, TLR 3, TLR 7, and predominantly TLR 4 and TLR 9[23] and treatments[24] also target the same TLRs. Bacteria like *Mycobacterium tuberculosis* induces the activation of TLR2 and TLR 9.[25]

More specifically, these biomacromolecules such as viruses consist of a viral capsid and viral nucleic acids and each component can activate a different TLR on a given cell in a spatially defined manner (**Figure 1. 2**a).[26] For example, Herpes Simplex Virus (HSV) activate TLR2 on the cell surface with the virions and TLR9 in the endosome of DCs with viral DNA. [27] The interaction of soluble TLR 2 agonist (lipoteichoic acid) and TLR 9 agonist (CpG DNA) in innate immune cell activation has been previously established.[28] However, this does not define the spatial orientation of the two agonists when interacting with the cell.

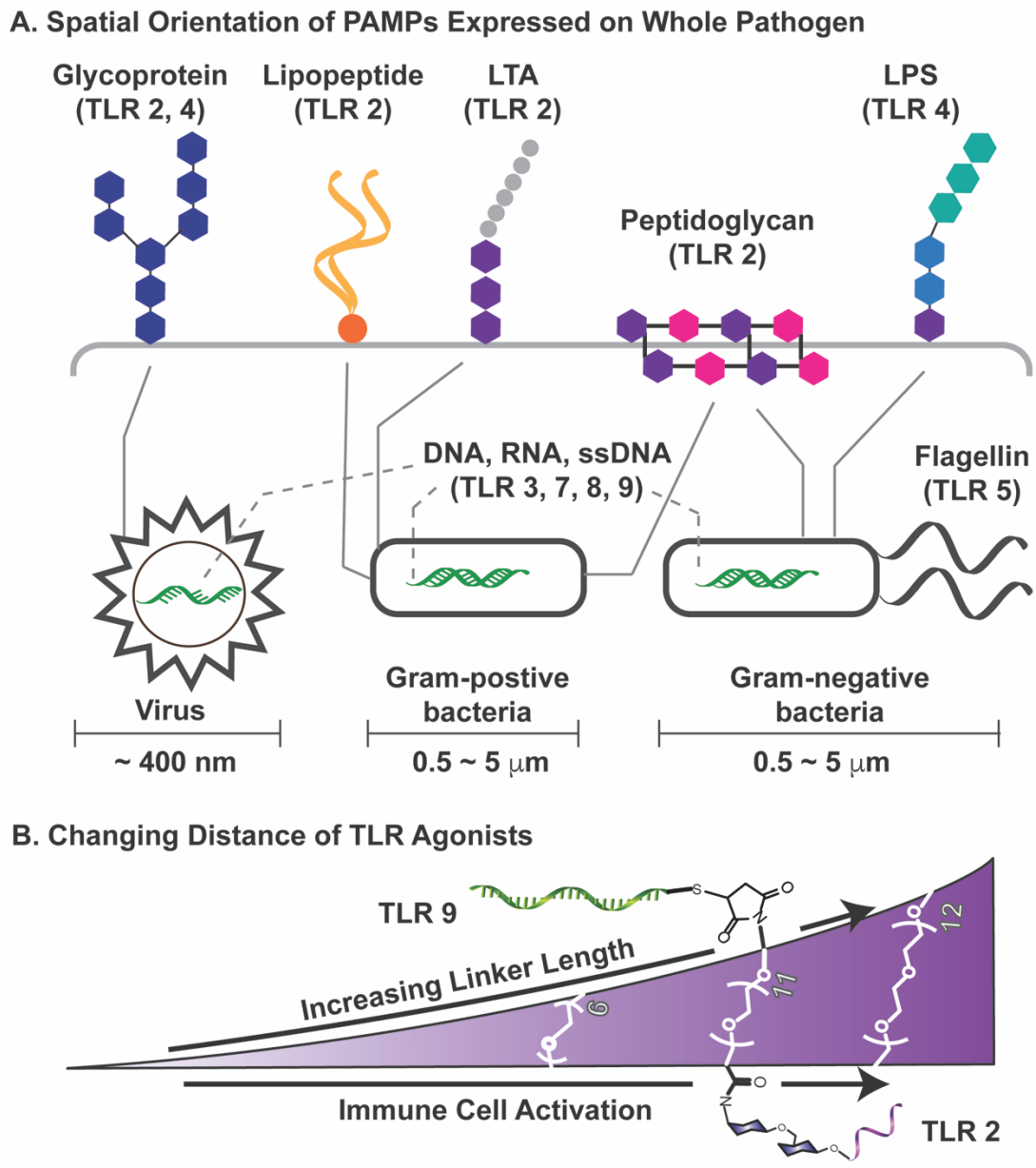

Figure 1. 2. (A) Pathogens express multiple PAMPs that can interact with a variety of TLRs. These PAMPs are organized in a specific spatial order. (B) Synthetic mimic of the spatially defined TLR agonist pairs can be synthesized by covalently linking agonists using linkers of varying lengths.

We sought to use this spatial information to prompt an increased immune signal to find the optimal immune response that can be elicited by a pair of TLR agonists. In tackling this question, we developed spatially restricted synergistic TLR agonists by covalently linking them together. This served as a synthetic mimic to pathogens that are large biomacromolecules. Examples of dual TLR agonists such as commercially available CL401™, CL531™, CL572™, and Adilipoline™ have shown to stimulate TLR synergy by the production of a variety of cytokines and retardation of tumor growth.[29] Though this serves as a convenient way of activating multiple TLRs with one compound, it lacks the spatial information of TLR activation of spatially constricted array of TLR agonists. Because the TLR agonists in the synthetic agonist heterodimers developed in the Esser-Kahn lab are covalently linked with a defined linker length, we can modulate the distance between the agonists by changing the length of the linker. The reported approach allowed us to probe for the distance dependent change in immune activity of these spatially confined synergistic agonists in macrophages and primary BMDCs (**Figure 1. 2**b).

1. 5. Spatial and Temporal Control of TLRs *in vitro*

TLR cross talk has both synergistic and antagonistic effects. In understanding the mechanism of TLR synergy, TLR activation sequence plays an important role in altering the immune response.[30] Natural examples include the activation mechanism of HSV where the activation of cell surface TLR2 is followed by the activation of intracellular TLR 9 by the viral DNA.[31] In many cases this has been observed in combinatorial methods with soluble agonists *via* pre-treating immune cells with a TLR agonist. Treating murine DCs with CpG before LPS induced an increase in IL-12 production, but the effect was not observed when DCs were treated in the

reverse order.[32] In some cases, the synergy is not effected. Macrophages pretreated with poly(I:C) followed by Pam_3CSK_4, flagellin, or CpG DNA produced increased amounts of TNF, and the reverse order of agonists did not change the production of TNF.[33] Changing the sequence of activation can also induce tolerance. Though LPS and mycoplasmal lipopeptide (macrophage activating lipopeptides, 2 kDa, (MALP-2)) can synergistically produce increased amounts of TNF when administered simultaneously, MALP-2 stimulation causes tolerance to subsequent LPS stimulation.[34] The specificity of TLR synergistic effects can further be altered by changing the cell type and TLR combinations.

Another challenge in understanding the mechanism of TLR synergy lies in elucidating the cell signaling mechanism of TLR synergy such as the distinction between paracrine and endocrine signaling. TLR agonists may interact with TLRs within the same cell or interact with TLRs over multiple cell types (**Figure 1. 3**a-c).[35] The result of the triggering of multiple receptors on one or between multiple cells can be either the enhancement of a single effector function[36] or the more effective control of pathogen growth mediated by distinct responses in tandem (**Figure 1. 3**d, e).[37]

One way of honing in on the mechanism is to control the spatio-temporal presentation of antigens through photocaging (**Figure 1. 3**f). Though simultaneous incubation of multiple agonists lacks such controls and does not give mechanistic insight into TLR synergies, photocaged agonists remain inactive until the agonists are irradiated at a certain location, at a given time, with a specific excitation wavelength of light. Therefore, orthogonally caged agonists can be incubated simultaneously without activation. Selective deprotection can then be used to determine the mechanism of TLR cooperation. Particularly, the use of non-linear 2 photon excitation (2PE) microscopy will allow focal bursts of release with a volume less than 1fl[38], with

spatio- control of agonist presentation on different regions of the cell surface and intracellular regions of a single cell. Additionally, 2PE uncaging can be close to the diffraction limit[39] and the ease of controlling multiple wavelengths of light at controllable time intervals *via* confocal microscope provides control of temporal- variables when measuring TLR activation.

The development of photocaged TLR agonists is reported herein. Additionally, we have shown the light dependent immune cell activation. We used the photocaged agonist to selectively activate a sub population of immune cells within a larger population, thus demonstrating the spatial control of immune cell activation by light (**Figure 1. 3**g). This approach can be applied to the use of 2PE photocages and 2PE uncaging techniques as discussed above to understand the mechanism of TLR synergy.

1. 6. Spatial and Temporal Control of TLRs *in vivo*

The unique spatial and temporal control of agonist activation provides a powerful way of elucidating fundamental immune cell activation mechanisms. It can further be applied as a new method of drug delivery *in vivo* to overcome some challenges in drug delivery.

Great strides have been made in the drug development process from the identification of targets and optimizing design of ligands to enhancing the stability of the drugs *in vivo*. Small molecule drugs are advantageous in the cost of manufacturing[40], pharmacokinetics[41], and can easily be chemically modified[42]. The availability of the drug must have high local concentration in the desired location which results in the drug being affective only where it is needed and the undesired side toxicities are diminished.[43] One great challenge that remains is the difficulty in reducing off target effects due to the lack of control in drug targeting and release kinetics. Various methods of enhancing drug release selectivity include development prodrug moieties,

addition of targeting ligands, and the incorporation of materials chemistry such as polymers and nanoparticles, or a combination of these strategies. For example, the use of nanoparticles, liposomes, or polymeric scaffolds to encapsulate the small molecule drug can enhance the pharmacokinetic and biodistribution of the active drug.[44] The addition of targeting ligands with the drug delivery scaffolds have greatly increased the efficiency of drug delivery greatly.[45] Further, the development of miniature drug delivery devices have made possible the creation of implantable devices with customizable drug release kinetics.[46] However, these approaches require the development and optimization of a variety of components outside of the design of the active drug.

Our photocaged TLR agonists can circumvent these challenges. First, the photocaged agonists acts as a prodrug. Due to the small size of the caged agonist, we can preserve the advantages of having a small molecule drug. Typically, prodrugs are released in its active form require only one to two chemical or enzymatic transformation steps *in vivo*.[47] This enzymatic activity causes some loss in the spatial control of drug release. However, because the active TLR agonist is released *via* exposure to light, this can dictate where the drug is released in a non-invasive manner. We also gain control of when and how much the drug is released by changing the number or length of irradiation. In this work, we have demonstrated the use of photocaged agonists *in vivo*, by eliciting light dependent immune cell activation and migration. with the advantage of non-invasive control of drug release *in vivo*.

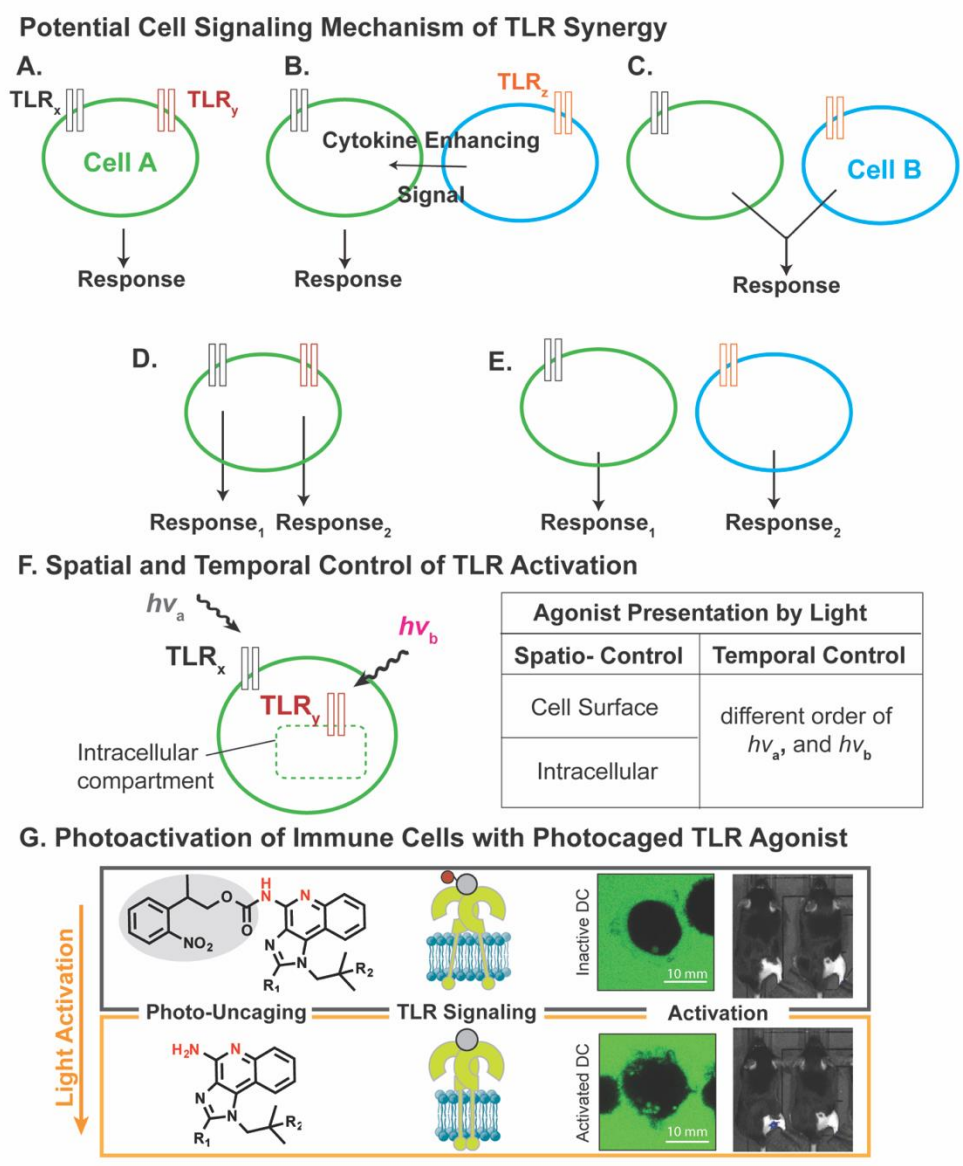

Figure 1. 3. Possible mechanisms of TLR synergy include (a) between multiple TLRs in a single cell with single effector response, (b) enhancement of one signal by stimulation of different TLR on different cell, (c) additive responses by distinct TLR activation of different cells, (d) independent stimulation of different TLRs on single cell (e) cooperation of different effector responses on different cells. (f) Spatial and temporal control of TLR activation *via* caged agonists and orthogonal photo-deprotection. (g) Photocaged TLR agonists can be used to activate immune cells with light.

1. 7. References

[1] Katsikis, P.; Schoenberger, S.; Pulendran B. *Nat. Immunol*. **2007**, *8,* 899-901.

[2] Steinman, R. *Annu. Rev. Immunol*. **2012**, *30*, 1-22.

[3] (a) R.M. Steinman, *Annu. Rev. Immunol*., **1991**, *9*, 271–296 (b) J. Banchereau, R.M. Steinman *Nature*, **1998**, *392*, 245–252

[4] (a) Pure', E., Inaba, K., Crowley, M. T., Tardelli, L., Witmer-Pack, M. D., Ruberti, G., Fathman, G., Steinman, R. M. *J. Exp. Med.* **1990**, *172*, 1459. (b) Inaba, K., MetJay, J. P., Crowley, M. T., Steinman, R. M. *J. Exp. Med.* **1990**. *172,* 63 1-40.

[5] Harding, C. V., Roof, R. W., Unanue, E. R.. *Proc. Natl. Acad. Sci. USA* **1990**, *86*, 4230-4234.

[6] Romani, N., Koide, S., Crowley, M., Witmer-Pack, M., Livingstone, A. M., Fathman, C. G., Inaba, K., Steinman, R. M. *J. Exp. Med*. **1989**, *169*, 1169- 1178.

[7] Romani, N., Inaba, K., Witmer-Pack, M., Crowley, M., Pure', E., Steinman, R. M. *J. Exp. Med.* **1989**, *169*, 1153-1168.

[8] Langhoff, E., Steinman, R. M. *J. Exp. Med*. **1990**, 169: 3 1 5-20

[9] Iwasaki, A.; Medzhitov, R. *Nat. Immunol*. **2004**, *5*, 987-995.

[10] Akira, S.; Takeda, K.; Kaisho, T. *Nat. Immunol*. **2001**, *2*, 675-680.

[11] Akira, S.; Kawai, T. *Sem. Immunol*. **2007**, *19*, 24-32.

[12] Karen, M. *Nature* **2006**, *441*, 431-436.

[13] Podojil, J.; Miller, S. *Immunol. Rev*. **2009**, *229*, 337-355.

[14] Moser, M.; Murphy, K. *Nat. Immunol*. **2000**, *1*, 199–205.

[15] Yarovinsky, F.; Kanzler, H.; Hieny, S.; Coffman, R. Sher, A. *Immunity*, **2006**, *25*, 655-664.

[16] Querec, T,; Bennouna, S,; Alkan, S,; Laouar, Y,; Gorden, K,; Flavell, R,; Akira, S,; Ahmed, R,; Pulendran, B. *J. Exp. Med.* **2006**, *203*, 413-424.

[17] (a) Tobias, W.; Osterloh, P.; Rechtsteiner, G.; Fassbender, M.; Heib, V.; Schmid, B.; Schmitt, E.; Schild, H.; Radsak, M. *Blood*, **2006**, *108*, 544-550. (b) Orr, M. T.; Beebe, E. A.; Hudson, T. E..; Moon, J. J.; Fox, C. B.; Reed, C. B.; Coler, R. N. *PLoS One* **2014**, *9*, e83884.

[18] (a) Zhu, Q., Egelston, C., Vivekanandhan, A., Uematsu, S., Akira, S., Klinman, D. M., Belyakov, I. M., and Berzofsky, J. A. *Proc. Natl. Acad. Sci. U.S.A.* **2008**, 105, 16260−16265. (b) Krummen, M., Balkow, S., Shen, L., Heinz, S., Loquai, C., Probst, H.-C., and Grabbe, S. J. *Leukocyte Biol*. **2008**, *88*, 189−199. (c) Makela, S. M., Strengell, M., Pietila, T. E., Osterlund, P., Julkunen, I. *J. Leukocyte Biol*. **2009**, *85*, 664−672.

[19] Wu, H. *Cell*, **2013**, *153*, 287−292.

[20] Beutler, E.; Gelbart, T.; West, C. *Blood Cells Mol. Dis*. **2001**, *27*, 728-730.

[21] (a) Napolitani, G.; Rinaldi, A.; Bertoni, F.; Sailusto, F.; Lanzavecchia, A. *Nature Immunol.* **2005**, *6*, 769–776. (b) Whitmore, M. M.; DeVeer, M.; Edling, A.; Oates, R. K.; Simons, B.; Lindner, D.; Williams, B. R. G. *Cancer Res.* **2004***, 64*, 5850–5860. (c) Roelofs, M. F.; Joosten, L. A. B.; Abdollahi-Roodsaz, S.; Van Lieshout, A. W. T.; Sprong, T.; van den Hoogen, F. H.; Van Den Berg, W. B.; Radstake, T. R. D. J. *Arthritis Rheum.* **2005**, *52*, 2313–2322.

[22] (a) Garcia-Cordero, J. L., Nembrini, C., Stano, A., Hubbell, J. A., and Maerkl, S. J. *Integr. Biol*. **2013**, *5*, 650− 658. (b) Gautier, G. M.; Humbert, M.; Deauvieau, F.; Scuiller, M.; Hiscott, J. Bates, E. E.; Trinchieri, G.; Caux, C.; Garrone, P. *J. Exp. Med.* **2005**, *201*, 1435–1446. (c)

Bekeredjian-Ding, I.; Roth, S. I.; Gilles, S.; Giese, T.; Ablasser, A.; Hornung, V.; Endres, S.; Hartmann, G. *J. Immunol.* **2006**, *176*, 7438–7446. (d) Bafica, A.; Scanga, C. A.; Feng, C. G.; Leifer, C.; Cheever, A.; Sher, A. *J. Exp. Med.* **2005**, *202*, 1715–1724.

[23] Singh, R. K.; Srivastava, A.; Singh, N., *Microbiol.l Res.* **2012,** *167* (8), 445-451.

[24] Mukherjee, A. K.; Gupta, G.; Adhikari, A.; Majumder, S.; Kar Mahapatra, S.; Bhattacharyya Majumdar, S.; Majumdar, S., *Int. Immunopharmacol.* **2012,** *12* (4), 565-572.

[25] Bafica, A.; Scanga, C. A.; Feng, C. G.; Leifer, C.; Cheever, A.; Sher, A., *J. Exp. Med.* **2005,** *202*, 1715-1724.

[26] Xagorari, A.; Chlichlia, K. *Open Microbiol. J.* **2008**, *2*, 49-59.

[27] Sato, A.; Linehan, M. M.; Iwasaki, A., *Proc. Natl. Acad. Sci. U.S.A.* **2006,** *103* (46), 17343-17348.

[28] Dalpke, A. H.; Frey, M.; Morath, S.; Hartung, T.; Heeg, K., *Immunobiology* **2002,** *206* (4), 392-407.

[29] Vernejou, F.; Debin, A.; Drocourt, D.; Perouzel, E.; Tiraby, G.; Lioux, T. U.S. Patent 20140141033 A1, 2014.

[30] Tan, R. S. T.; Ho, B.; Leung, B. P.; Ding, J. L., *Int. Rev. Immunol.* **2014,** *33* (6), 443-453.

[31] Sato, A.; Linehan, M. M.; Iwasaki, A., *Proc. Natl. Acad. Sci. U.S.A.* **2006,** *103* (46), 17343-17348.

[32] Theiner, G.; Rößner, S.; Dalpke, A.; Bode, K.; Berger, T.; Gessner, A.; Lutz, M. B., *Mol. Immunol.* **2008,** *45* (1), 244-252.

[33] Bagchi, A.; Herrup, E. A.; Warren, H. S.; Trigilio, J.; Shin, H.-S.; Valentine, C.; Hellman, J., *J. Immunol.* **2007,** *178* (2), 1164-1171.

[34] Sato, S.; Nomura, F.; Kawai, T.; Takeuchi, O.; Mühlradt, P. F.; Takeda, K.; Akira, S., *J. Immunol.* **2000,** *165* (12), 7096-7101.

[35] Tranchieri, G.; Sher, A. *Nat. Rev.* 2007, 7, 179-190.

[36] Tabeta, K.; Georgel, P.; Janssen, E.; Du, X.; Hoebe, K.; Crozat, K.; Mudd, S.; Shamel, L.; Sovath, S.; Goode, J.; Alexopoulou, L. Flavell, R.; Beutler, B. *Proc. Natl. Acad. Sci. USA* **2004,** *101*, 3516-3521.

[37] Bafica, A.; Santiago, H.; Goldszmid, R.; Ropert, C.; Gazzinelli, R. Sher, A. *J. Immunol*. **2006**, *177*, 3515-3519.

[38] Brown, E.; Shear, J.; Adams, S.; Tsien, R.; Webb, W. *Biophys. J.* **1999**, *76*, 489-499.

[39] Smith, M.; Ellis-Davis, G.; Magee, J. *J. Physiol*. **2003**, *548*, 245-258.

[40] Firer, M. A.; Gellerman, G. *J. Hematol. Oncol*. **2012**, *5*, 1756–8722.

[41] Kurzrock, R.; Gabrail, >; Chandhasin, C.; Moulder, S.; Smith, C.; Brenner, A.; Sankhala, K.; Mita, A.; Elian, K.; Bouchard, D.; Sarantopoulos, *J. Mol. Cancer Ther*. **2012**, *11*, 308-316.

[42] Srinivasaroo, M.; Calliford, C. V.; Low, P. S. *Nat. Rev. Drug Discov*. **2015**, *14*, 203-219.

[43] McNerny, D.; Leroueil, P. R.; Baker, J. R. *Wiley Interdiscip. Rev. Nanomed. Nanobiotechnol*. **2010**, *2*, 249-259.

[44] Allen, T. M.; Cullis, P. R. *Science* **2004**, *303*, 1818-1822.

[45] Kidane, A.; Bhatt, P. P. *Curr. Op. Chem. Biol*. **2005**, *9*, 347-351.

[46] LaVan, D. A.; McGuire, T.; Langer, R. *Nat. Biotechnol*. **2003**, *21*, 1184-1191.

[47] Rautio, J.; Kumpulainen, H.; Heimbach, T.; Oliyai, R.; Oh, D.; Jarvinen, T.; Savolainen, J. *Nat. Rev. Drug Disc.*, **2008**, *7*, 255-270.

CHAPTER 2. Immune Response Modulation with Spatial Control of Agonists

2. 1. Objective of Present Study

Current research in immunotherapies focuses on the function of the innate and adaptive immune system to combat diverse diseases such as malaria, cancer, HIV and Q-fever.[1] Pattern recognition receptors such as Toll-like receptors (TLRs) of innate immune cells recognize a host of chemical species. Thereafter the receptors induce a signaling cascade initiating the production of cytokines and co-stimulatory molecules in innate immune cells, ultimately activating the adaptive immune system.[2] Activating multiple TLRs can lead to synergies that direct the adaptive immune response.[3] Controlling these synergies to enhance and direct immune signals is an ongoing challenge. In addition to using soluble agonists[4-13], nanoparticle encapsulation[14], and conjugation of agonists[15] all increase immune activity. Recently, we found that linking agonists also increases immune activity.[16]

Here we show that altering the distance between agonists can modulate the synergy between two covalently conjugated agonists. We explore this principle for agonists of different molecular weights (500-9,000 Da) and different TLRs (TLR2, 4 and 9). The guidelines governing these linkages change for each agonist pair. We report that the activity of conjugated agonists depends on a combination of the synergistic TLR pair, the linker length, and the agonist size, with size and linker length being most pronounced (**Figure 2. 1**). As a result, for certain TLR pairs and cell types, one can increase agonist activity and potency by controlling the average distance between two conjugated agonists. These data show that a portion of the inflammatory response can be modulated using chemical synthesis of multi-agonist systems to control cytokine levels. This information may be useful as one of the first steps toward developing immunotherapeutics

with application-specific, customized immune responses, as well as informing the design of future polymeric activators of the innate immune system for delivery purposes.

2. 2. Design and Synthesis of TLR Agonist Heterodimer

Previously we showed the increased agonist activity of heterodimeric crosslinked agonist system where lipoteichoic acid (LTA, average MW=6000 Da, a TLR2/6 agonist)[17] and CpG_1826 (MW=7112.7 Da, a TLR 9 agonist)[18] were conjugated to form a heterodimer of two immune agonists (LTA_PEG_6_CpG). To understand the importance of average agonist distance in linked systems, we synthesized a series of heterodimers of covalently-conjugated LTA and CPG_1826 with each agonist separated by a fixed distance *via* a hetero-telechelic polyethylene glycol (PEG) linker. The synergistic agonist complexes were synthesized using a PEG linker bearing a terminal N-hydroxysuccinimide (NHS) ester and maleimide groups (**Figure 2. 1**b). To form the conjugates, the free amines of the side chains of LTA[19] from *Bacillus subtilis* were reacted with the NHS terminal terminus of the PEG linkers in PBS (pH 7.5) for 12 h. 3' thiol, 5'-fluorescein phophoramidite modified CpG_1826 was then conjugated to the maleimide terminus of the LTA_PEG_n (n = 6, 12, or 24) compounds in PBS at room temperature for 12 h (**Figure 2. 1**c). The resulting LTA_PEG_n_CpG heterodimer was purified *via* gel electrophoresis and quantified by the absorbance of the FAM tag of the CpG at 495 nm. The average intermolecular distance varied by changing the length of the PEG linker: PEG_6 (31.7 Å), PEG_{12} (53.3 Å), and PEG_{24} (95.2 Å).

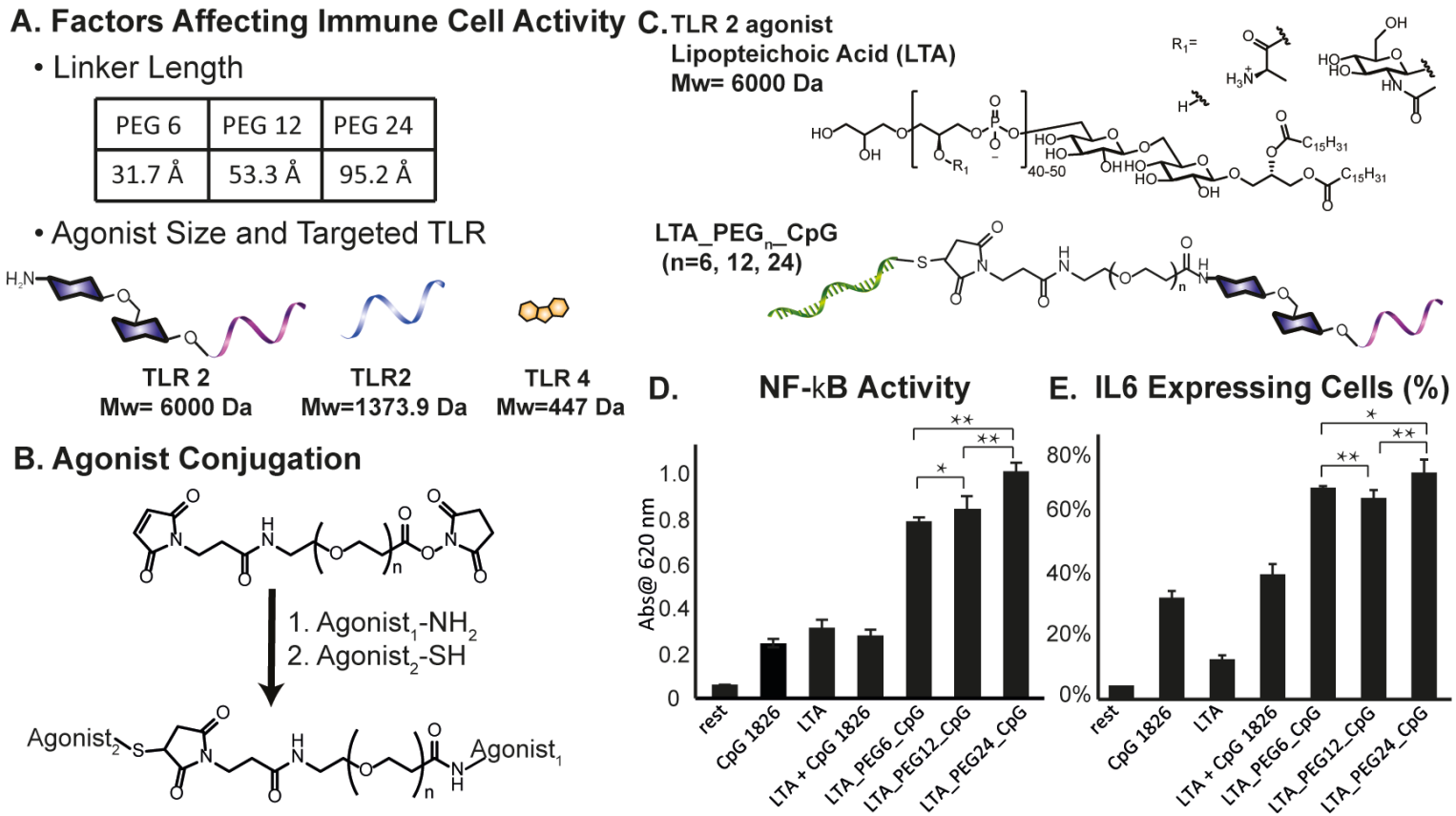

Figure 2. 1. (a) Agonist characteristics affecting immune cell activity when conjugated. (b) Synthesis of agonist conjugation with PEG linker. (c) Molecular structure and average mass of lipoteichoic acid (LTA) and representation of TLR2/TLR9 agonist heterodimer LTA_PEGn_CpG.. Stimulation of 50 nM of LTA, CpG_1826, equimolar LTA and CpG_1826, and LTA_PEGn_CpG measured by (d) RAW-Blue activation *via* NF-κB stimulation after 24 h incubation at 37 °C (e) BMDC intracellular cytokine production when incubated with agonists for 8 h at 37 °C. Cell surface marker and cytokine expression measured *via* flow cytometry. Each result is from three independent experiments. * $p>0.05$, ** $p<0.01$.

2. 3. Immune Response Modulation with TLR Agonist Heterodimer

To determine how linking these agonists changed the response of innate immune cells, we tested the linked agonists on a reporter macrophage cell line (RAW 264.7) to show the change in NF-κB activity. The LTA_PEG_n_CpG agonists (50 nM) showed not only higher NF-κB activity compared to equimolar soluble agonists (50 nM of each agonist), but also increasing linker length increased NF-κB activity (**Figure 2. 1**). In addition, we tested cytokine (IL-6, IL-12, and CD86 (**Figure 2. 13**) production and cell surface marker upregulation of primary bone-marrow derived dendritic cells (BMDCs) induced by the heterodimers. When stimulating BMDCs with LTA-PEG_n-CpG heterodimer, the linked agonists showed a higher immune response, as measured by IL-6, compared to the activation induced by equimolar doses of individual agonists or combined soluble agonists (**Figure 2. 1**). However, when comparing the different lengths of the PEG linkers in BMDCs, we observed no linker length dependent increase in IL-6 levels. The weakest IL-6 production was from PEG_{12}, but there was no significant difference between PEG_6 and PEG_{24}. While there was a clear correlation between linker length and NF-κB activity for reporter macrophages, the lack of a linker length effect for primary cells showed the heterodimers can have different activities depending on the characteristics of the agonists. Therefore, we sought to determine if other agonists of different size or TLR pairing showed an increase in linked agonist activity but a lack of linker length-dependent activity.

To determine if the synergy we observed for the LTA_PEG_6_CpG system was specific to the synergistic TLR agonist pair or depended on the size of the agonists, we synthesized a TLR2/6 and TLR9 pair that varied only by the size of the TLR2/6 agonist. To vary agonist size, we chose Pam_2CSK_4C (PAM, 1373 Da)[20], and covalently coupled it to CpG_1826 (**Figure 2. 2**). The Pam_PEG_n_CpG compounds were synthesized with a 3’ amino terminated CpG_1826 (5’

fluorescein phophoramidite) conjugated to the NHS ester of the PEG linker. The synthetic diacylated lipopeptide, PAM, was modified with the addition of a terminal cysteine for conjugation to the terminal maleimide of the CpG_PEG_n complex. The conjugated heterodimer was purified by gel electrophoresis.

Unlike the LTA_PEG_n_CpG system, linked Pam_2CSK_4C and CpG_1826 (PAM_PEG_n_CpG, 50 nM) agonists did not induce higher NF-κB activity than the equimolar soluble agonists in the RAW 264.7 cells (**Figure 2. 2**b). However, there was a linker length dependent activity where PEG_{12} decreased the level of activity while PEG_6 was the most comparable to the soluble agonists. In primary cells, the PAM_PEG_n_CpG did not show higher IL-6 production or a linker length dependent increase. However, a similar trend in drop of activation with PEG_{12} was observed, congruent with the trends in NF-κB activity. Therefore, the linker length dependent cell stimulation may change NF-κB activity, but this change in transcription factor activity does not translate directly into increased transcription and production of cytokines as measured by IL-6 and IL-12 levels (**Figure 2. 2**c, **Figure 2. 14**).

After comparing both linker length and agonist size with the TLR2/6_TLR9 linked agonists system, we set out to test agonist pairing as a potential influence on linked TLR synergies. We chose TLR4 and TLR9 both to consolidate our synthetic route and because of the similarity in biological activity between TLR4 and TLR2.[21-23] TLR4 is also a membrane-bound TLR with activity at both the cell surface and in endosomes, but stimulated by a small molecule agonist (447 Da). (**Figure 2. 3**a) The TLR4_PEG_n_TLR9 construct was synthesized in an analogous manner to the TLR2_PEG_n_TLR9 molecules. The TLR4 agonist, pyrimidoindole (Ind), was modified from previously reported SAR studies[24] to bear a free amine for conjugation to the heterodimer. The amine handle was conjugated to the NHS ester of the PEG linkers and the

resulting Ind_PEG_n_maleimide was reacted with 3'-thiol CpG_1826. The resulting heterodimer conjugates, Ind_PEG_n_CpG, were quantified by the absorbance of the FAM-labeled CpG_1826. Through the new pairs, we sought to compare the effect of agonist spacing in relation to TLR pair (TLR4+TLR9 vs. TLR2/6+TLR9) and the effect of a small molecule (MW<500 Da) compared to larger molecules (MW>1300) such as Pam_2CSK_4C or LTA.

In Ind_PEG_n_CpG systems, the linked agonists showed higher NF-κB activity in the reporter RAW-Blue cell line than stimulation by equimolar soluble agonists at 100 nM[a] (**Figure 2. 3**b). There was also a distinct linker length dependent increase in activity for the two systems. In the Ind_PEG_n_CpG system, NF-κB activity was highest when the agonists were separated by PEG_{12}. This suggests there is an optimal spatial distance required for conjugating multiple TLR agonists as the NF-κB activity of LTA_PEG_n_CpG and Pam_PEG_n_CpG reached a maximum at different linker lengths. In primary BMDCs, Ind_PEG_n_CPG heterodimers showed higher activity than the indole and CpG_1826 agonists combined as soluble agonists. Further, clear linker length dependence was observed in contrast with the previously described TLR2_TLR9 hetero-dimers. PEG_{12} had higher levels of IL-6 than those observed for PEG_6 and PEG_{24} (**Figure 2. 3**c). PEG_6 had the second most potent activity followed by PEG_{24} with the lowest activity of the three linked agonists.

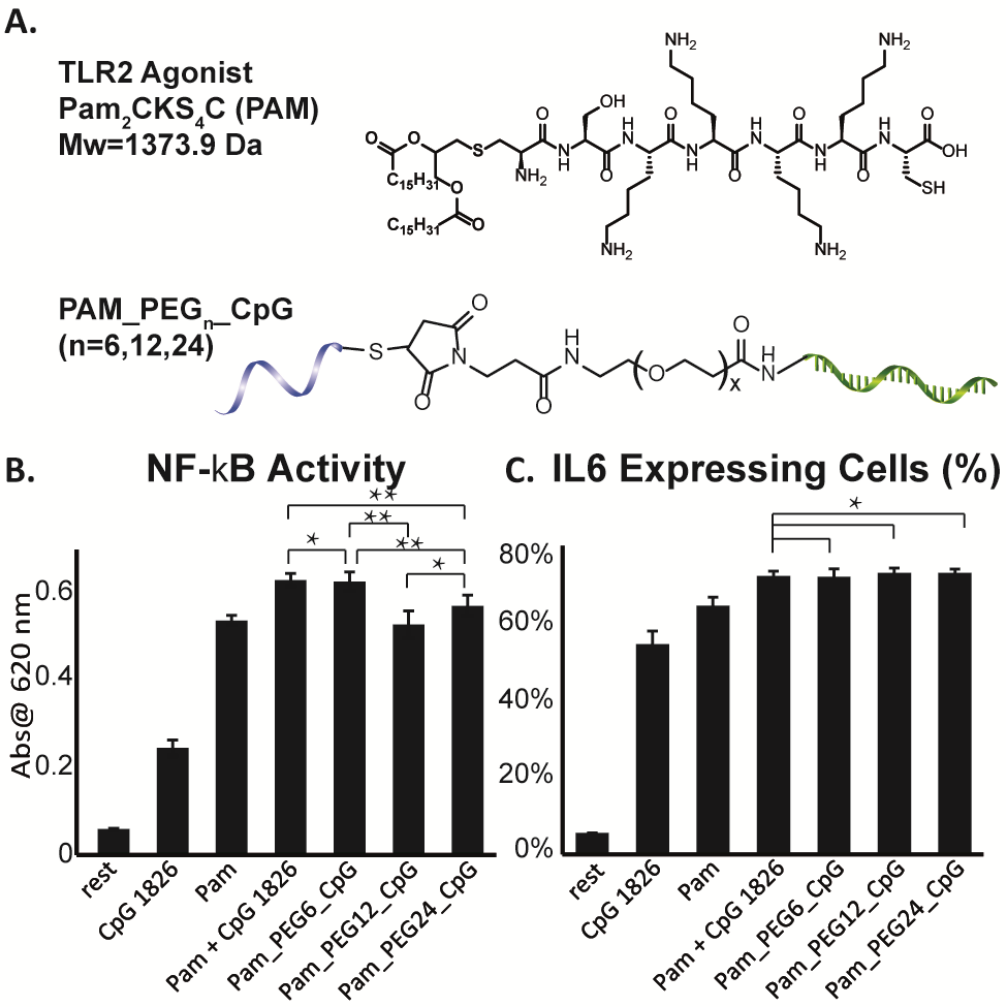

Figure 2. **2.** (a) Molecular structure and mass of Pam_2CSK_4C (PAM) and representation of TLR2/TLR9 agonist heterodimer $Pam\_PEG_n\_CpG$.. Stimulation of 50 nM of Pam_2CSK_4, CpG_1826, equimolar Pam_2CSK_4 and CpG_1826, and $Pam\_PEG_n\_CpG$ measured by (b) RAW-Blue activation *via* NF-κB stimulation after 24 h incubation at 37 °C of (c) BMDC intracellular cytokine production when incubated with agonists for 8 h at 37 °C. Cell surface marker and cytokine expression measured *via* flow cytometry. Each result is from three independent experiments. * $p>0.1$, ** $p<0.02$.

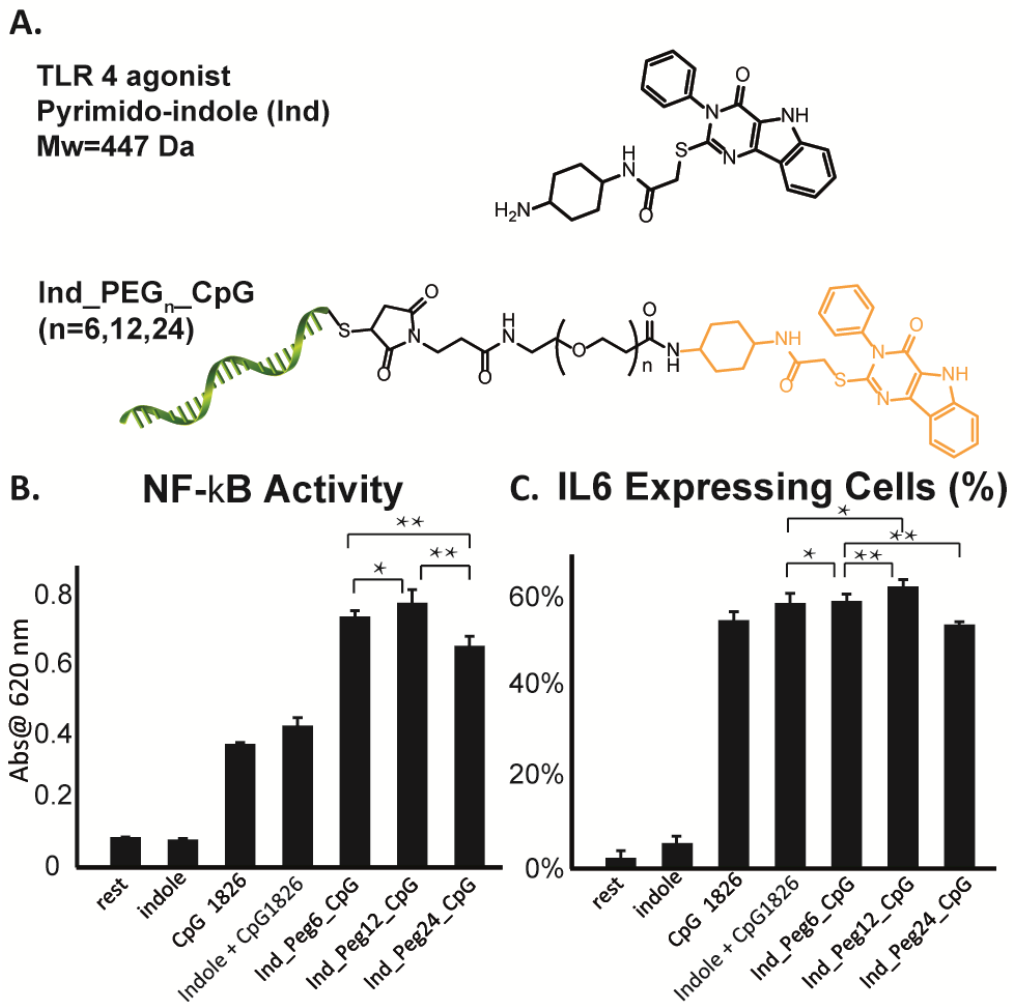

Figure 2. 3. (a) Molecular structure and mass of pyrimido-indole (Ind) and representation of TLR4/TLR9 agonist heterodimer Ind_PEG$_n$_CpG. Stimulation of 100 nM of pyrimido-indole, CpG_1826, equimolar pyrimido-indole and CpG_1826, and Ind_PEG$_n$_CpG measured by (b) RAW-Blue activation *via* NF-κB stimulation after 24 h incubation at 37 °C of (c) BMDC intracellular cytokine production when incubated with agonists for 8 h at 37 °C. Cell surface marker and cytokine expression measured *via* flow cytometry. Each result is from three independent experiments. *p>0.07, **p<0.005

2. 4. Mechanistic Understanding of Heterodimer Activity

To better understand the distinct differences in the synergistic activation between multiple linked TLR agonist pairs, we sought to understand the mechanism through which these different activations were proceeding. TLR 2 knockout (KO), TLR 4 KO and TLR 9 KO cells were used to study the effect of not only covalently conjugating the agonists but also the linker length dependence on immune cell activity to determine how steric constraints of different size molecules balanced with activation of unique receptor pairs. The BMDCs of the KO mice were incubated overnight with the heterodimers at the same concentrations as the wildtype BMDCs and the IL-6 levels were measured *via* flow cytometry and inter-cellular cytokine staining.[b]

For TLR9 KO BMDCs, both the LTA_PEG_n_CPG and PAM_PEG_n_CPG showed reduced cytokine production for all compounds (**Figure 2. 4**d). For LTA_PEG_n_CpG there was a distinct decrease in CpG_1826-dependent cytokine production with increasing linker length (**Figure 2. 4**a). While CPG_1826 had high levels of activation in TLR2 knockout BMDCs, the linked systems had lower activation, and within the heterodimers, the shortest linker length - smallest heterodimer - showed the highest activity. The linker length dependent decrease in activity can be due to the steric bulk of the agonist dimer. Compared to CpG_1826 alone, the additional LTA_PEG_n conjugation on CpG_1826 may be hindering CpG_1826 activation of TLR9. As such, the larger linker length, PEG_{24}, provided the most additional steric bulk to CpG_1826, resulting in lowest immune cell activation. In this case, the increased size of the linker hindered activation of the receptors pointing to a biochemical rationale (i.e. synergistic pathways) for increased activity seen previously from longer linker lengths.

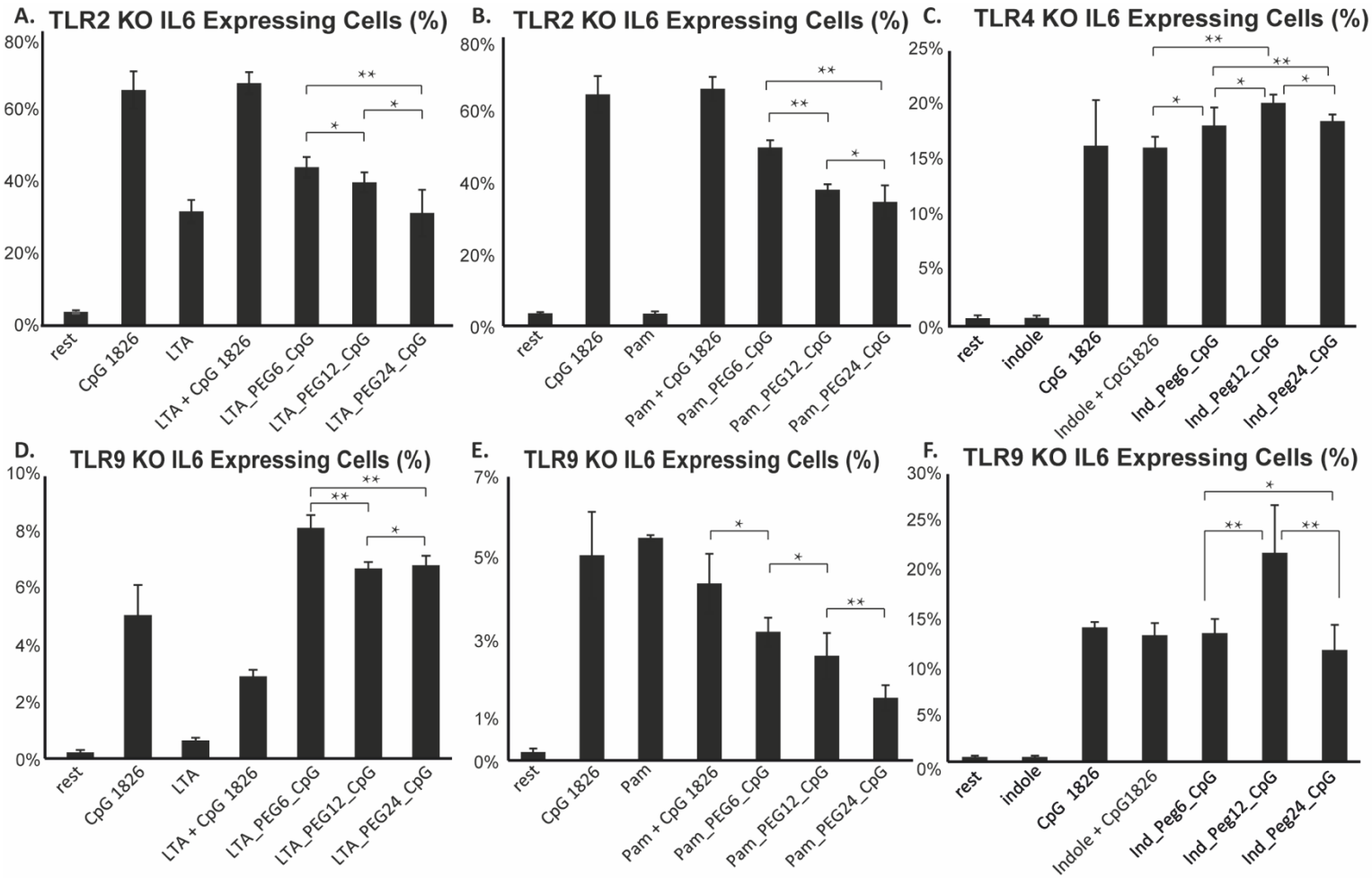

Figure 2. 4. TLR knockout BMDC IL-6 expression measured for each heterodimer. (a,d) 50 nM of LTA, CpG_1826, equimolar LTA and CpG_1826, and LTA_PEG$_n$_CpG (b, e) 50 nM of Pam_2CSK_4, CpG_1826, equimolar Pam_2CSK_4 and CpG_1826, and Pam_PEG$_n$_CpG (c,f) 100 nM of pyrimido-indole, CpG_1826, equimolar pyrimido-indole and CpG_1826, and Ind_PEG$_n$_CpG. *p>0.05, **p<0.05.

The same trend was observed with Pam_PEG_n_CpG (**Figure 2. 4**b, e). Interestingly, Pam_PEG_n_CpG had higher IL-12 production compared to LTA_PEG_n_CpG in TLR 2 KO BMDCs (**Figure 2. 4**b). This result may be explained by the smaller size of Pam (1.3 kDa) compared to LTA (average 6 kDa). The smaller size of PAM_2CSK_4C reduces the steric hindrance in Pam_PEG_n and is therefore less disruptive to CpG_1826 induced TLR9 activation – leading to higher IL-6 production. Thus, synergistic activation of TLRs depends both on the size of the agonist and the increased immune activity of heterodimers depends on the synergistic activity of both TLRs.

Agonist size dependent activation for Ind_PEG_n_CpG had closer agreement with the activation of RAW-Blue 264.7 macrophages and activation of wild type BMDCs (**Figure 2. 4**). For both the TLR 4 KO and TLR9 KO cells, PEG_{12} showed the highest activity. Likely, because the Pyrimido-indole is a small molecule, the additional size added to CpG_1826 is less than that of adding Pam_2CSK_4C or LTA. Therefore, the activity of the CpG is not affected as drastically as was observed for Pam_PEG_n_CpG and LTA_PEG_n_CpG and is similar to the wild type BMDCs.

2. 5. Conclusions

We report examples of linked TLR agonists and the change in immune cell activation with changing linker length. Through the TLR KO BMDC IL-6 presentation, we found the importance of activation of both TLRs in increasing activity through conjugated agonists. The conjugated TLR agonists increased the NF-κB activity. Many heterodimer pairs have an optimal spatial distance between the agonists for effective activation of some innate immune cells. LTA_PEG_n_CpG showed the greatest activity with the largest distance, while PAM_PEG_n_CpG

showed good activity at PEG_6 and PEG_{24} but a decrease in activity with PEG_{12}. Ind_PEG_n_CPG heterodimers had the highest cytokine presentation at PEG_{12}.

Our operating hypothesis of the discrepancies in agonist spacing can be attributed to the size of the paired agonists. As seen in KO BMDC activity, with smaller agonists, the distance between agonists can be shorter and still induce robust immune signaling. In contrast, larger agonists created steric bulk that interfered with single agonist dependent activity. Therefore, depending on the linker length and spatial presentation of two agonists, the activity of the synergistic agonists can be limited by access to the receptor. Additionally, the change in synergistic pairing can add to the changes of the effect of conjugated agonists. Though TLR synergy has been shown for multiple TLR pairs, the effects of synergy are not universal as the changes are subtle, depending on the combination of stimulated TLRs. Therefore, the change in response from one TLR pair to another can be attributed to the mechanism of the TLR synergy involved.

In this study we present evidence that spatial distance between agonists can alter and control innate immune cell activity, but the control depends on TLR agonist, their distance and steric sizes. Contrasting that the spatial organization increased activity, we found that spatially constrained TLR agonists limited their ability to activate individual TLRs in knockout studies. As different agonist pairs require different spatial presentation of agonists, we plan to further explore the direct mechanism of linked agonist and TLR synergy mechanism in future work. As an increasing number of spatially constrained multi-agonists are developed as therapeutic agents and tools for adjuvanting activity *in vivo*, it is important to consider the spatial elements which can allow customized immune responses. Changing the spatial constraint can both enhance or

mitigate the synergistic effects of linked TLR agonists potentially lowering the effective dose or adjusting the downstream activity.

2. 6. Supplementary Experimental Data

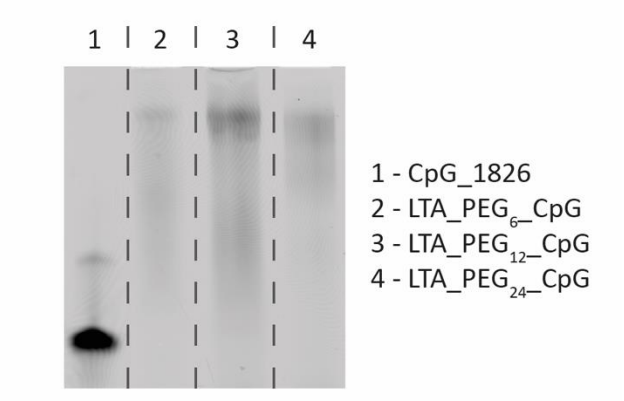

Figure 2. 5. Gel electrophoresis of LTA_PEG$_n$_CpG compounds visualized by 6-fluorescein amidite tag on CpG_1826 for all lanes and compounds shown.

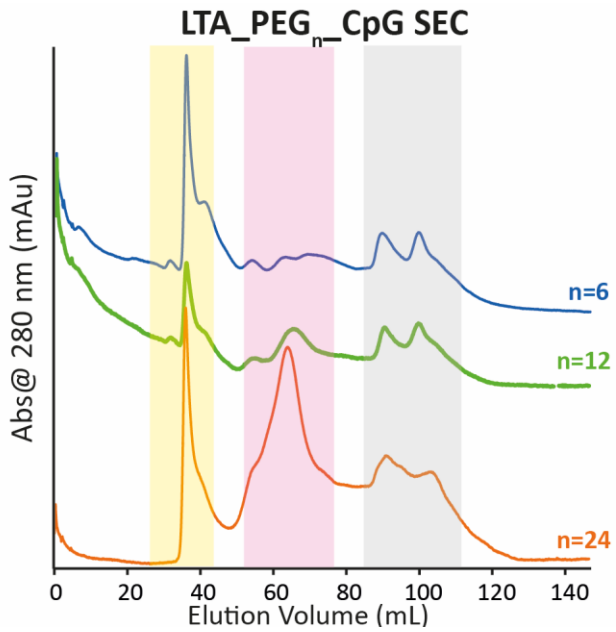

Figure 2. 6. Size exclusion chromatography (SEC) run on fast protein liquid chromatography (FPLC) of crude LTA_PEG$_n$_CpG compounds. SEC shows LTA_PEGn_CpG dimer (yellow region), free CpG_1826 (red region), and free PEG$_n$ (gray region). See SI 8 for CpG_1826 and PEG standard curves.

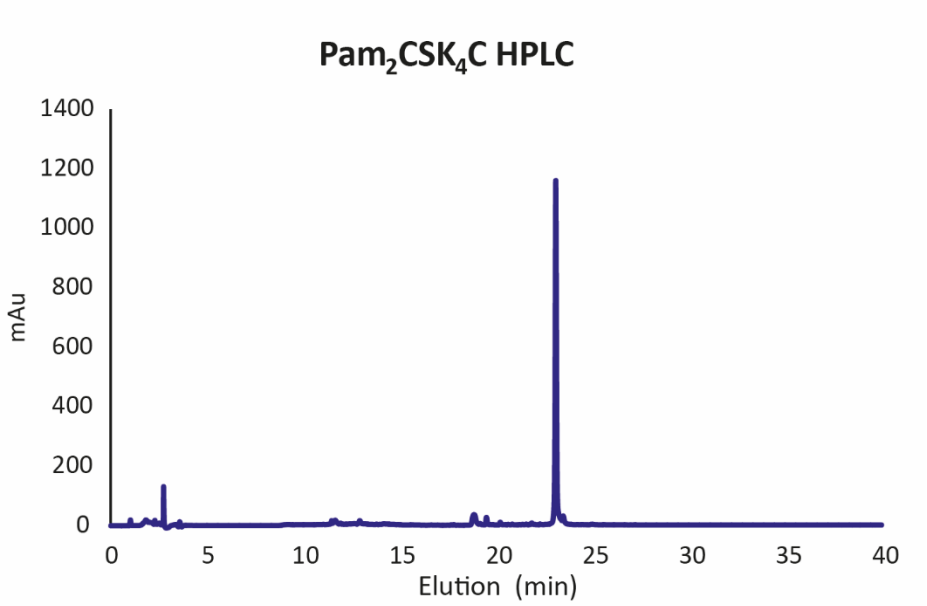

Figure 2. 7. Pam_2CSK_4C purity assessed by HPLC.

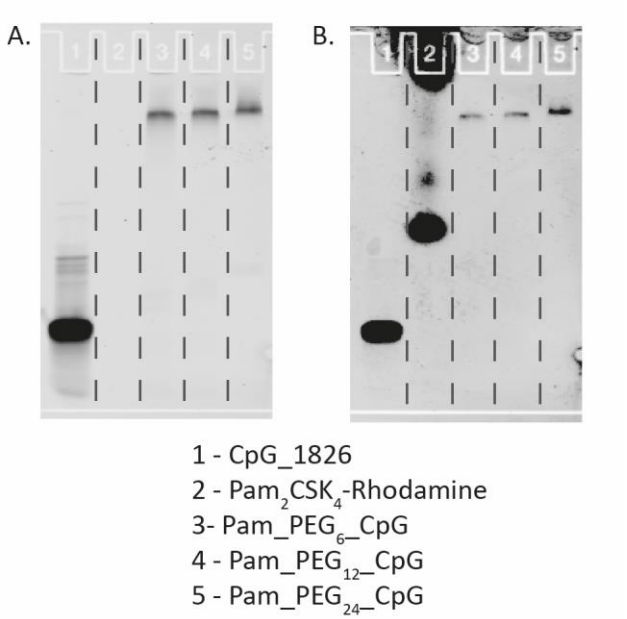

Figure 2. 8. (a) Gel electrophoresis of FAM labeled CpG_1826, Rhodamine labeled Pam_2CSK_4, and FAM labeled Pam_PEG_n_CpG compounds visualized by 6-fluorescein amidite tag (473 nm laser excitation). (b) Gel electrophoresis of FAM labeled CpG_1826, Rhodamine labeled Pam_2CSK_4, and FAM labeled Pam_PEG_n_CpG compounds visualized by 6-fluorescein amidite tag (532 nm laser excitation).

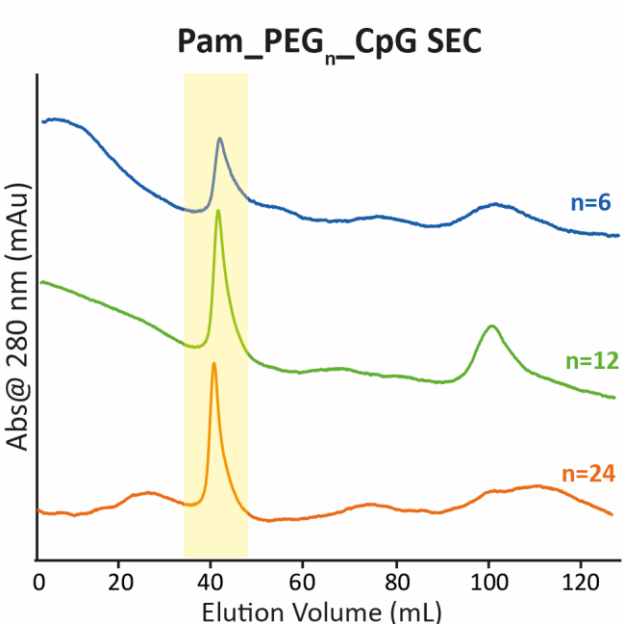

Figure 2. 9. Size exclusion chromatography (SEC) run on fast protein liquid chromatography (FPLC) of crude Pam_PEG$_n$_CpG compounds. SEC shows Pam_PEGn_CpG dimer (yellow region).

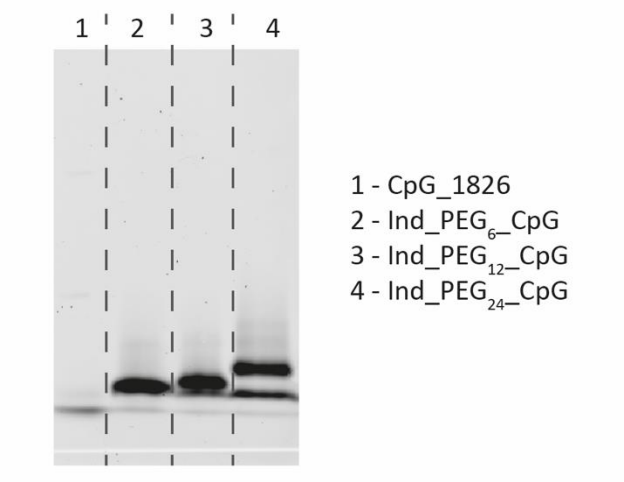

Figure 2. 10. Gel electrophoresis of Ind_PEG$_n$_CpG compounds visualized by 6-fluorescein amidite tag on CpG_1826 for all lanes and compounds shown.

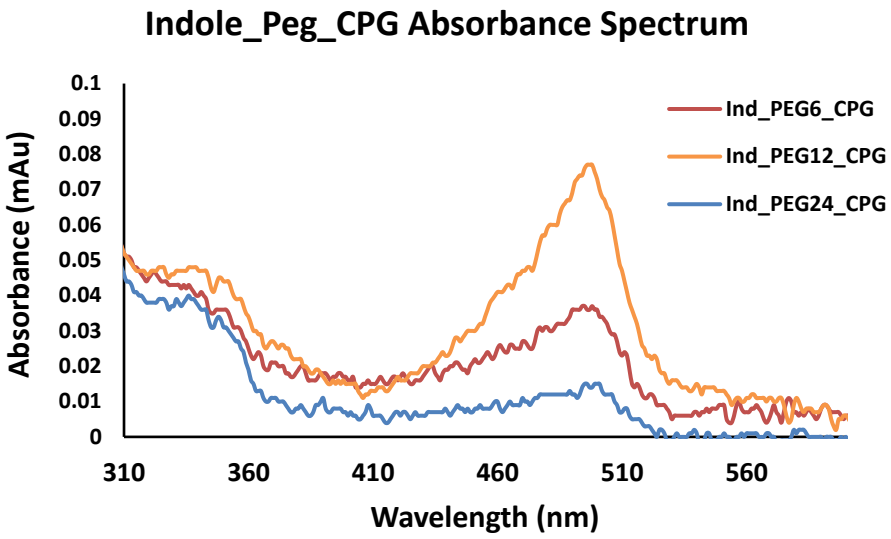

Figure 2. 11. UV-VIS of Ind_PEG$_n$_CpG compounds showing presence of cycloindole with absorbance at 350 nm and FAM tagged CpG with absorbance at 495 nm.

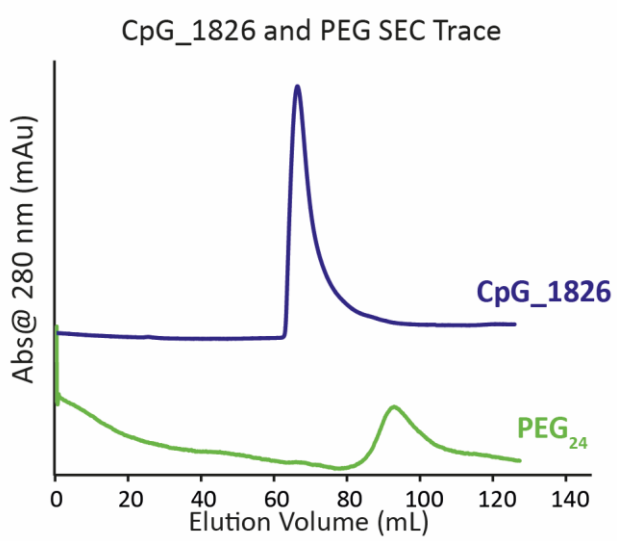

Figure 2. 12. Standard FPLC traces for CpG_1826 and PEG24.

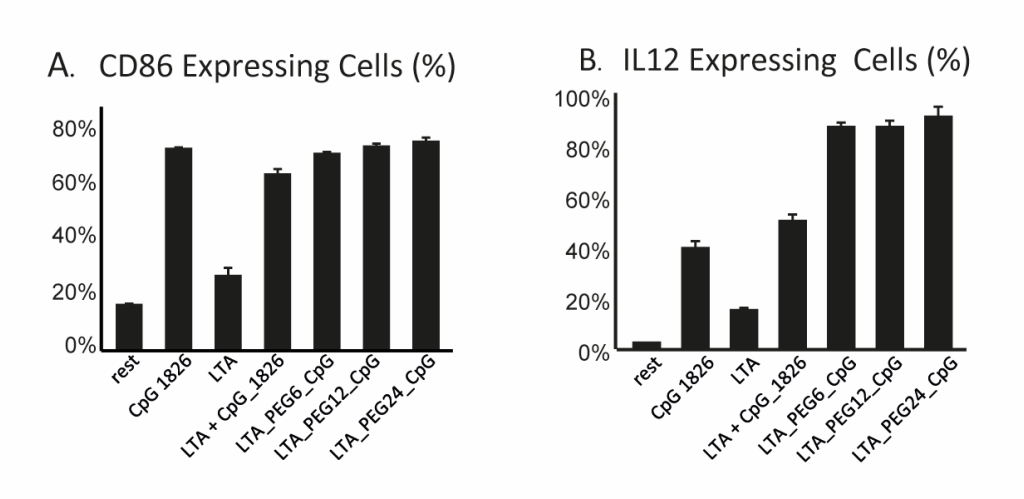

Figure 2. 13. LTA_PEGn_CpG stimulated BMDC IL-12 and CD86 expression levels.

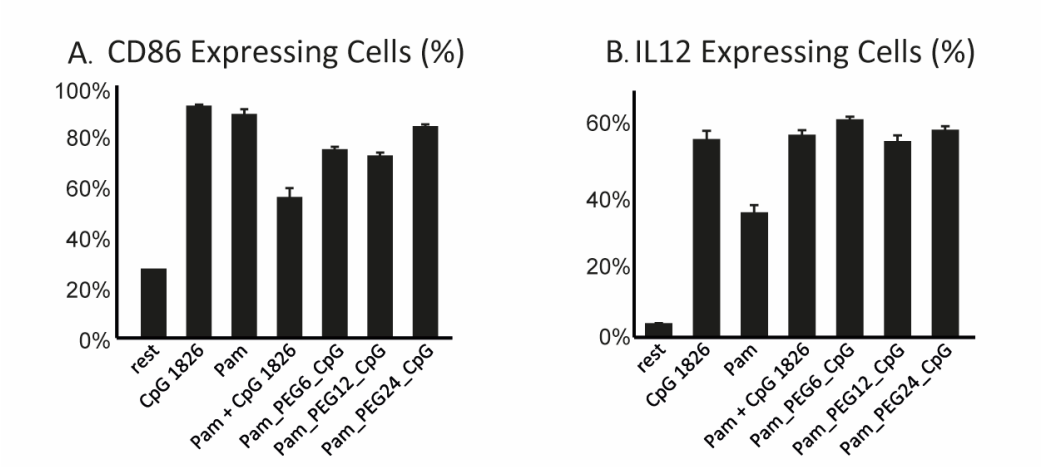

Figure 2. 14. Pam_PEGn_CpG stimulated BMDC IL-12 and CD86 expression levels.

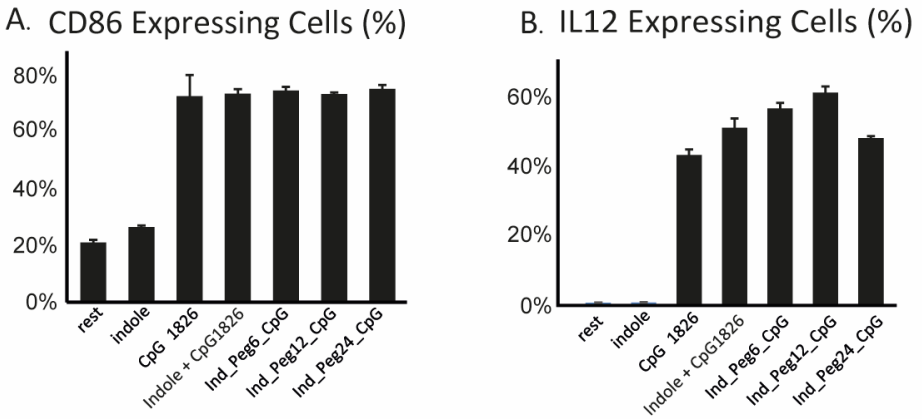

Figure 2. 15. Ind_PEGn_CpG stimulated BMDC IL-12 and CD86 expression levels.

2. 7. Experimental Procedures

2. 7. 1. Materials and Methods

Unless otherwise noted, all reagents were purchased from Sigma-Aldrich and used as received. CPG ODN 1826, was purchased from IDT Tech. Antibodies were purchased from BioLegend. BD Cytofix/Cytoperm Kit for intracellular cytokine flow cytometry and GolgiPlug were purchased from BD Biosciences. Fmoc-Cys((RS)-2,3-di(palmitoyloxy)-propyl)-OH (Pam_2C) was purchased from Bachem. ^{13}C and ^{1}H NMR spectra were taken on an AVANCE500 (500 MHz) spectrometer and analyzed using MestreNova software. Automated solid-phase peptide synthesis was carried out by using a PS3TM Peptide Synthesizer (Protein Technologies, Inc.). Analytical reversed-phase HPLC was performed in an Agilent Zorbax SB-C18 column (50 mm4.6 mm) with a gradient of 5–100% CH_3CN in H_2O with 0.1% TFA and a flow of 1.0 mL/ min over 20 min. Preparative reversed-phase HPLC purification was carried out on a Zorbax SB-C18 PrepHT (21.2250 mm, 7 μm particle size) column from Agilent in conjunction with a Beckmann system and a flow of 15.0 mL/min. UV detection (214 nm) was used for analytical and preparative HPLC. Size exclusion chromatography was performed on a GE superdex G75 in DPBS, pH 7.4 at a flow rate of 1mL/min with a UV/Vis detector set to monitor at 495 nm. Gel electrophoresis samples were analyzed using a GE Healthcare Typhoon Trio+ Variable Mode Imager to observe FITC or FAM fluorescence. UV Vis was measured on Thermo Scientific Nano Drop. Mass spectrum was obtained using AB SCIEX MALDI TOF-TOF. Flow cytometry data was acquired using BD Accuri C6 Flow Cytometer and analyzed using the BD Accuri C6 software. RAW-Blue absorbance was measured on a Bio-Tek Quant microplate spectrophotometer MQX200. C57/BL6 (wild type), B6.129-Tlr2tm1Kir/J (TLR2 KO), C57BL/6J-Tlr9M7Btlr/Mmjax (TLR9 KO), and B6.B10ScN-Tlr4lps-del/JthJ (TLR4 KO) were

purchased from Jackson Laboratories and allowed to equilibrate for a minimum of 48 h. All animal studies and mice maintenance were approved by the Institutional Animal Care and Use Committee (IACUC #2012-3048).

2. 7. 2. Synthetic Procedures

1. LTA_PEG$_n$_CPG Conjugates

i. LTA_PEG$_n$ synthesis

Followed previously published procedures. General Procedure is as follows:

A stock solution of lipoteichoic acid (LTA, 10mg/mL) was prepared in DPBS (pH 7.4). In a typical reaction the PEG linker (n=6, 12, or 24, 12 μL, 100 mg/mL, DMSO) was added to LTA (2 mg, 10 mg/mL, DPBS) and the solution was incubated with agitation at room temperature overnight. The reaction mixture was subjected to centriprep purification (3 kDa MWCO, DPBS, 1 mM EDTA) for removal of excess PEG linker. The resulting LTA_PEG$_n$ conjugate was diluted to a final volume of 200 μL (DPBS, 1 mM EDTA) and was used directly for LTA_PEG$_n$_CPG synthesis.

ii. LTA_PEG$_n$_CPG synthesis

Followed previously published procedures.[c]

General Procedure for DNA reduction and conjugation is as follows:

The DNA sequence 5'-FAM-tccatgacgttcctgacgtt-3'-SS-Et was diluted to 1 mM in endotoxin free water. The 5'-FAM-tccatgacgttcctgacgtt-3'-SS-Et (100 μL, 1 mM, H2O) was added to 300 μL of a 3% aqueous TCEP solution and the reaction was incubated at room temperature overnight (15 h). The DNA was precipitated by adding 100□L of 3 M sodium acetate, and 1.5 mL of anhydrous EtOH to the reaction mixture, and the solution was cooled to -78°C for 30 min.

The frozen solution was centrifuged for 20 min at 4°C, the supernatant was removed. This procedure was repeated 3 times. The resulting CpG pellet was dried and then diluted to 1 mM (DPBS, 1 mM EDTA) and added to LTA_PEG_n. The reaction mixture was incubated at 40 °C overnight (15 h) with constant shaking. The crude reaction mixture was passed through a 0.2 μm filter and directly purified by gel extraction (Bio-Rad, 10% Mini Protean TBE-Urea Gel).

2. Pam_PEG_n_CPG Conjugates

i. Pam_2C synthesis

Linear peptide SK_4C was synthesized on an automated synthesizer and Pam_2C was coupled *via* hand coupling following modified procedures previously published.[d] General procedure listed below.

ii. SK_4C linear peptide Synthesis

Loading of the resin: 2-Chlorotrityl chloride resin (300 mg, 1.12 mmol/g) was added to a Bio-Rad Poly-Prep chromatography column (10 mL, 0.84.0 cm) and allowed to swell in dry CH_2Cl_2 (10 mL) for 30 min. The solution was drained from the resin and a solution of Cysteine (0.50 equiv., 70 mg, 0.17 mmol) in 20% 2,4,6-collidine in dry DMF (5 mL) was added. The solution was then drained after 2 h of agitation. The resin was capped with a mixture of CH_2Cl_2/MeOH/DIPEA (17:2:1, 10 mL) and agitated for 1 h to cap the unreacted 2- chlorotrityl chloride sites. The resin was then washed with DMF (twice) and dried by passing nitrogen through the vessel.

Peptide Coupling: The PS-2-chlorotrityl-Cys(Fmoc)-tBu generated from the previous step was transferred to a solid-phase peptide synthesizer reaction vessel. The linear peptide was

constructed from the C terminus to the N terminus. Automated peptide coupling steps includes a) fmoc-deprotection with 20% piperidine in amine free DMF for 5 min, b) washing with DMF for 30 sec three times, c) coupling of the amino acid (0.5 mmol, 4 equiv.) in the presence of [2-(6-chloro-1H-benzotriazol-1-yl)-1,1,3,3-tetramethylaminium hexafluorophosphate] (HCTU, 199 mg, 0.50 mmol, 4 equiv.) for 20 min, and d) washing with 3X with DMF for 30 s.

Hand coupling on Pam2Cys peptide to NH2-SK4C-Resin: The resin from the automated synthesis procedure was transferred in to a Bio-Rad Poly-Prep chromatography column. The terminal Fmoc group was removed with 20% piperidine in DMF for 5 min, and the resin was washed with DMF. The fmoc-Pam_2C (0.5 mmol, 4 equiv.) was dissolved in 20% 2,4,6-collidine in DMF with HCTU (199 mg, 0.50 mmol, 4 equiv) and agitated for 20 min. The suspension was drained thoroughly and washed with DMF followed by dry CH_2Cl_2 twice.

Cleavage of the Peptide from the Resin: The peptide was cleaved from the resin by agitating the resin for 60 min with a solution of hexafluoroisopropanol (HFIP) in CH_2Cl_2 (1:4, 5 mL). The suspension was drained and the filtrate collected. The resin was washed with additional hexafluoroisopropanol (HFIP) in CH_2Cl_2 (1:4, 5 mL) for 30 min and washed with CH_2Cl_2 (2 10 mL). The combined filtrates were concentrated under vacuum to give a white solid.

Global Deprotection and Purification: The cleaved peptide was dissolved in TFA/triisopropylsilane (TIPS)/H_2O (18:1:1, 10 mL) and the solution was stirred for 1.5 h. The reaction mixture was then concentrated under vacuum resulting in a white solid. The solid was dissolved in 20% ACN in H_2O (5 mL) and the solution was filtered through a 0.45 μm syringe

filter and purified by reversed-phase HPLC (gradient elution with 20–50% CH_3CN over 40 min). The pure fractions were lyophilized to afford peptide. ESI (*m/z*) calc'd for $C_{68}H_{131}N_{11}O_{13}S_2$, $[M+H]^+$1373.94; found, 1374.9823 $[M+H]^+$, 687.99 $[M+2H]^{2+}$.

3. Pam_PEG$_n$_CPG synthesis

5'-FAM-tccatgacgttcctgacgtt-3'-NH_2 (50 μL, 1mM in PBS) was incubated with PEG_n (12 □L, 100 mg/mL) overnight. The reaction mixture was purified with a spin column 5X to remove excess PEG. PAM_2CSK_4C was added to the purified mixture and incubated overnight with agitation. The resulting mixture was purified by gel extraction (Bio-Rad, 10% Mini Protean TBE-Urea Gel).

4. Ind_PEG$_n$_CpG Conjugates

i. Indole synthesis

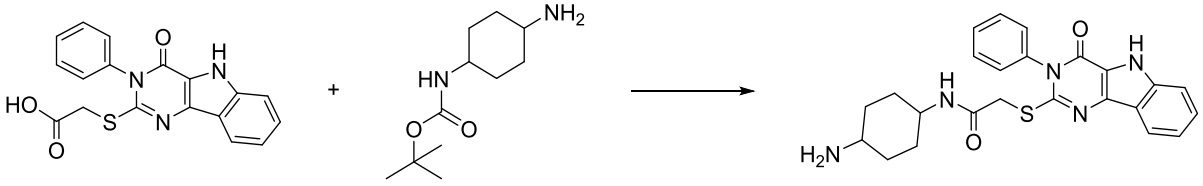

1[e] (1 g, 3.4 mmol) was stirred with N-boc-1, 4-cyclohexyldiamine (1.2 g, 5.5 mmol) in DMF (15 mL) and trimethylamine (1 mL) at 0°C. HATU (1.2 g) was added and the resulting solution was warmed to room temperature overnight. The solution was concentrated under vacuum and deprotected with 50% TFA in CH_2Cl_2 for 1 hour. The resulting product was concentrated under vacuum and dried. The resulting solid was purified by solid loaded column chromatography in a gradient of 10% MeOH in CH_2Cl_2. Affording product **2** as a pale pink solid in 60% yield over two steps. ^{1}H NMR (500 MHz, d-DMSO) δ 1.22 (dt, *J*=24.2, 11.5 Hz, 4H), 1.75 (s, 4H), 3.42 (s, 2H), 3.88 (s, 2H), 7.29 (d, *J*=7.8, 2H), 7.52-7.46 (m, 5H), 7.62 (d, *J*=6.8 Hz, 2H), 8.07 (d, *J*=

8.0Hz, 1H), 8.25 (d, *J*=8.2 Hz, 1H), 12.10 (s, 1H);^{13}C NMR (500MHz, d-DMSO) δ 166.59, 155.41, 152.93, 139.41, 136.52, 130.36, 130.04, 129.34, 127.79, 120.81, 120.55, 119.74, 113.32, 48.94, 47.66, 37.14, 30.36, 29.50; HRMS (*m/z*) calc'd for $C_{24}H_{25}N_5O_2S$, 448.1807 $[M+H]^+$; found (ESI), 448.1797 $[M+H]^+$.

ii. Indole_PEG$_n$_CPG synthesis

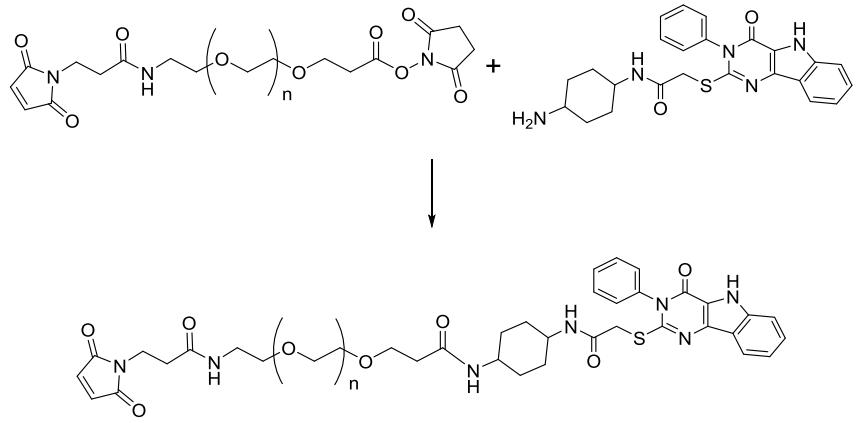

2 (5 eq) was stirred with PEG$_n$ in DMF for 3 h. The reaction was concentrated under vacuum and the resulting crude product was purified with column chromatography (10% MeOH in DCM). The resulting product was concentrated and dried under vacuum. Reduced CpG (50 μL) was added to the Ind_PEG$_n$ and left to stir overnight. The reaction mixture was further purified by gel extraction (Bio-Rad, 10% Mini Protean TBE-Urea Gel).

2. 7. 3. General Procedure for RAW264.7 Macrophage (RAW-Blue) NF-κB assay.[f]

RAW264.7 macrophage cells (RAW-Blue, Invivogen) were grown in complete culture media composed of Dulbecco's Modified Eagle's Medium (DMEM) with 4.5 g/L glucose (Life Technologies), 2 mM L-glutamine, 10,000 U/mL penicillin, 10 mg/mL streptomycin, 25 μg/mL amphotericin B, supplemented with 10% fetal bovine serum (FBS, Sigma). For the NF-κB assay,

RAW-Blue cells (passage 3-8) were plated at $1x10^5$ cells/mL in 96-well optically clear bottomed, black-walled microplates cells in complete media supplemented with 10% heat-inactivated FBS (Sigma) with addition of agonist at the specified concentrations. The cells were incubated for 18 h at 37 °C with 5% CO_2. Cell media (50 μL) from the wells was transferred to a new 96- well plate and incubated with QUANTI-Blue reagent (150 μL, Invivogen) for 1 h at 37 °C with 5% CO2. The absorbance (620 nm) was measured using a Bio-Tek Quant microplate spectrophotometer.

2. 7. 4. Bone Marrow-Derived Dendritic Cell Harvest and Culture.

Bone marrow-derived dendritic cells (BMDCs) were harvested from 6-week-old C57Bl/6 mice (Jackson Laboratory). Femur bones were removed from mice and the bone marrow was extracted into PBS buffer and pelleted. ACK Lysing Buffer (3 mL, Lonza) was added to the cell pellet and incubated for 2 min at RT. PBS buffer (13 mL) was then added to the cell suspension, and the cell solution was centrifuged at 300 RCF for 10 min at RT. Thereafter, the cell pellet was resuspended in BMDC complete media composed of RPMI 1640, 10% heat inactivated FBS, 20 ng/mL granulocyte-macrophage colony-stimulating factor (GM-CSF), 2 mM L-glutamine (Life Technologies), 10,000 U/mL penicillin, 10 mg/mL streptomycin, 25 μg/mL amphotericin B, and 50 μM beta-mercaptoethanol. Harvested cells were plated at $1x10^6$ cells/mL in 100 mm petri dishes (10 mL total media) and incubated at 37 °C in a CO_2 incubator (day 0 of cell culture). On day 3, 10 mL of fresh BMDC primary media was added to each petri dish. On day 5, BMDCs were released and plated in 24-well plates at $5x10^5$ cells/mL for cell surface marker activation, cytokine profile flow cytometry experiments.

2. 7. 5. General Procedure for Flow Cytometry for Cell Surface Marker Upregulation.

BMDCs were incubated in individual wells with each agonist (9:1 BMDC:agonist) in 0.5 mL culture media) for 18 h at 37 °C with 5% CO_2. The cells were released from the plate and centrifuged at 2500 RPM at 4 °C for 10 min. The cell pellet was resuspended in cold FACS (composed of PBS (1x), 10% FBS, and 0.1% sodium azide) buffer (100 μL) and incubated with CD16/32 FcR blocking antibodies (1.0 μg/1x10^6 cells) on ice for 10 min. The cell suspension was pelleted and the supernatant was removed. The cell pellet was resuspended in cold FACS buffer (100 μL) and incubated with FITC-CD11c (1.0μg/1x10^6 cells) and PE-CD86 (1.0 μg/1x10^6 cells), -CD40 (1.0 μg/1x10^6 cells), -MHCII (0.25 μg/1x10^6 cells), or -CD80 (0.5 μg/1x10^6 cells) on ice and removed from light for 30 min. Each sample was washed twice with 300 μL cold fluorescence-activated cell sorting (FACS) buffer. The dendritic cells were resuspended in cold FACS buffer (150 μL) and kept on ice until being loaded onto the flow cytometer.

2. 7. 6. General Procedure for Intracellular Cytokine Flow Cytometry Staining.

BMDCs were incubated individually with a solution of agonist (9:1 BMDCs : agonist in 0.5 mL culture media for 8 h at 37 °C with 5% CO2. GolgiPlug (BD Biosciences), containing Brefeldin was added to cell culture (following BD Biosciences protocol) for the final 4 h of culture. After 12 h, stimulated BMDCs were released from the plate and centrifuged at 2500 RPM at 4 °C for 10 min. The cell pellet was resuspended in cold FACS buffer (100 μL) and CD16/32 FcR blocking antibodies (1.0 μg/1*10^6 cells). Cells were incubated on ice for 10 min, then centrifuged at 2500 RPM at 4 °C for 10 min. The supernatant was removed and the cell pellet was resuspended in cold FACS buffer (100 μL) and FITC-CD11c (1.0 μg/1x106 cells). Cells

were incubated on ice for 10 min. Each sample was washed twice with 300 μL cold FACS buffer. The supernatant was removed and the cell pellet was resuspended in 100 μL BD Cytofix/Cytoperm solution. Cells were incubated on ice, removed from light for 20 min. BMDCs were washed twice with BD Perm/Wash solution and the supernatant removed. The cell pellet was resuspended in cold FACS buffer (100 μL) and incubated with APC-IFN-γ (1.0 μg/1x10^6 cells), -TNF-α (0.25 μg/1x10^6 cells), -IL-6 (0.25 μg/1x10^6 cells), or -IL-12 (0.25 μg/1x10^6 cells) on ice, removed from light for 30 min. The cells were rinsed with cold FACS buffer (300 μL) twice. BMDCs were resuspended in cold FACS buffer (200 μL) and kept on ice until analysis *via* flow cytometry.

2. 8. References and Notes

[1]TLR7 Agonist GS-9620 Activates HIV-1 in PBMCs From HIV-Infected Patients on cART | CROI Conference http://www.croiconference.org/sessions/tlr7-agonist-gs-9620-activates-hiv-1-pbmcs-hiv-infected-patients-cart (accessed Jul 12, 2016).

[2] Mancini, R. J., Stutts, L., Ryu, K. A., Tom, J. K., and Esser-Kahn, A. P. *ACS Chem. Biol.* **2014**, *9*, 1075–1085.

[3] Ozinsky, A., Underhill, D. M., Fontenot, J. D., Hajjar, A. M., Smith, K. D., Wilson, C. B., Schroeder, L., and Aderem, A. *Proc. Natl. Acad. Sci.* **2000**, *97*, 13766–13771.

[4] Querec, T.; Bennouna, S.; Alkan, S.; Laouar, Y.; Gorden, K.; Flavell, R.; Akira, S.; Ahmed, R.; Pulendran, B. *J. Exp. Med.* **2006**, *203* (2), 413–424.

[5] Duggan, J. M.; You, D.; Cleaver, J. O.; Larson, D. T.; Garza, R. J.; Guzmán Pruneda, F. A.; Tuvim, M. J.; Zhang, J.; Dickey, B. F.; Evans, S. E. *J. Immunol.* **2011**, *186* (10), 5916–5926.

[6] Theiner, G.; Rössner, S.; Dalpke, A.; Bode, K.; Berger, T.; Gessner, A.; Lutz, M. B. *Mol. Immunol.* **2008**, *45* (1), 244–252.

[7] Moody, M. A.; Santra, S.; Vandergrift, N. A.; Sutherland, L. L.; Gurley, T. C.; Drinker, M. S.; Allen, A. A.; Xia, S.-M.; Meyerhoff, R. R.; Parks, R.; Lloyd, K. E.; Easterhoff, D.; Alam, S. M.; Liao, H.-X.; Ward, B. M.; Ferrari, G.; Montefiori, D. C.; Tomaras, G. D.; Seder, R. A.; Letvin, N. L.; Haynes, B. F. *J. Virol.* **2014**, *88* (6), 3329–3339.

[8] Trinchieri, G.; Sher, A. *Nat. Rev. Immunol.* **2007**, *7* (3), 179–190.

[9] Warger, T.; Osterloh, P.; Rechtsteiner, G.; Fassbender, M.; Heib, V.; Schmid, B.; Schmitt, E.; Schild, H.; Radsak, M. P. *Blood* **2006**, *108* (2), 544–550.

[10] Goff, P. H.; Hayashi, T.; Martínez-Gil, L.; Corr, M.; Crain, B.; Yao, S.; Cottam, H. B.; Chan, M.; Ramos, I.; Eggink, D.; Heshmati, M.; Krammer, F.; Messer, K.; Pu, M.; Fernandez-Sesma, A.; Palese, P.; Carson, D. A. *J. Virol.* **2015**, *89* (6), 3221–3235.

[11] Fox, C. B.; Sivananthan, S. J.; Duthie, M. S.; Vergara, J.; Guderian, J. A.; Moon, E.; Coblentz, D.; Reed, S. G.; Carter, D. *J. Nanobiotechnology* **2014**, *12* (1), 17.

[12] Bergmann-Leitner, E. S.; Leitner, W. W. *Vaccines* **2014**, *2* (2), 252–296.

[13] Siefert, A. L.; Caplan, M. J.; Fahmy, T. M. *Biomaterials* **2016**, *97*, 85–96.

[14] Kasturi, S. P., Skountzou, I., Albrecht, R. A., Koutsonanos, D., Hua, T., Nakaya, H. I., Ravindran, R., Stewart, S., Alam, M., Kwissa, M., Villinger, F., Murthy, N., Steel, J., Jacob, J., Hogan, R. J., García-Sastre, A., Compans, R., and Pulendran, B. *Nature* **2011**, *470*, 543–547.

[15] Shukla, N. M., Mutz, C. A., Malladi, S. S., Warshakoon, H. J., Balakrishna, R., and David, S. A. *J. Med. Chem.* **2012**, *55*, 1106–1116.

[16] Mancini, R. J., Tom, J. K., and Esser-Kahn, A. P. *Angew. Chem. Int. Ed.* **2014**, *53*, 189–192.

[17] Ginsburg, I. *Lancet Infect. Dis.* **2002**, *2*, 171–179.

[18.] Klinman, D. M., Currie, D., Gursel, I., and Verthelyi, D. *Immunol. Rev.* **2004**, *199*, 201–216.

[19] Fischer, W., Mannsfeld, T., and Hagen, G. *Biochem. Cell Biol.* **1990**, *68*, 33–43.

[20] (1) Spohn, R., Buwitt-Beckmann, U., Brock, R., Jung, G., Ulmer, A. J., and Wiesmüller, K.-H. *Vaccine* **2004**, *22*, 2494–2499. (2) Buwitt-Beckmann, U., Heine, H., Wiesmüller, K.-H., Jung, G., Brock, R., and Ulmer, A. J. *FEBS Journal* **2005**, *272*, 6354–6364.

[21] Iwasaki, A.; Medzhitov, R. *Nat Immunol* **2004**, *5* (10), 987–995.

[22] Kagan, J. C. *Cell* **2012**, *151* (6), 1168–1178.

[23] Maisonneuve, C.; Bertholet, S.; Philpott, D. J.; Gregorio, E. D. *Proc. Natl. Acad. Sci.* **2014**, 201400478.

[24] Chan, M., Hayashi, T., Mathewson, R. D., Nour, A., Hayashi, Y., Yao, S., Tawatao, R. I., Crain, B., Tsigelny, I. F., Kouznetsova, V. L., Messer, K., Pu, M., Corr, M., Carson, D. A., and Cottam, H. B. *J. Med. Chem.* **2013**, *56*, 4206–4223.

a. Molarity used is different from LTA_PEG$_n$_CpG and Pam_PEG$_n$_CpG due to the weak potency of the pyrimido-indole agonist.

b. As the changes we were expecting might be subtle, in each case, we included a corresponding dose of CpG1826as a guide for differences from experiment in base-level cytokine production. Dosage of CpG varied between LTA and PAM2 (50 nM) and Pyrimido-indole (100 nM).

c. Mancini, R. J., *et. al. Angew. Chem. Int. Ed.* **2014**, *53*, 189–192.

d. Spencer, R. *et. al. Eur. J. Org. Chem*., **2013**, *2013*, 3523–3528.

e. Chan, M. *et. al. J. Med. Chem*., **2013**, *56*, 4206-4223.

f. http://www.invivogen.com/PDF/RAW_Blue_TDS.pdf

CHAPTER 3. Photoactivation of TLR7/8 on Immune Cells

3. 1. Objective of Present Study

The innate immune response plays a large role in determining self from non-self.[1] It is guided, in part, by the interaction of chemical agonists with Toll-like receptors (TLRs).[2] TLRs recognize distinct chemical species leading to the activation of the innate and adaptive immune system, influencing everything from vaccines to atherosclerosis.[3] The spatial and temporal responses of these receptors are critical for understanding their activity,[4] yet few techniques exist to control the spatial activity of TLR agonists. Here we show a photo-caging method[5] to control the activity of TLRs. Understanding the signaling of TLRs using photo-controlled agonists can aid understanding of how the innate immune system determines non-self - potentially, leading to better vaccine design and understanding of inflammatory responses.

TLR7/8 are TLRs for which a small molecule agonist and its binding interaction have been defined. The imidazoquinoline and thiazoquinoline family, of which the potent anti-tumor drug imiquimod is a member, are widely used TLR7/8 agonists.[6] Here we report a photo-controlled agonist of TLR7/8 (**Figure 3. 1**). We designed this photo-controlled agonist based on the recently published crystal structure of TLR8.[7] We present results on the photo-activation of two molecules, a TLR7 agonist, Imiquimod (R837),[8] and a TLR 7 and TLR 8 agonist, Resiquimod (R848).[9] Activating both of these compounds with UV light led to stimulation of NF-κB[10] in model cell lines and primary cells. In addition, we selected and activated antigen-presenting cells (APCs) within a population of cells using light.

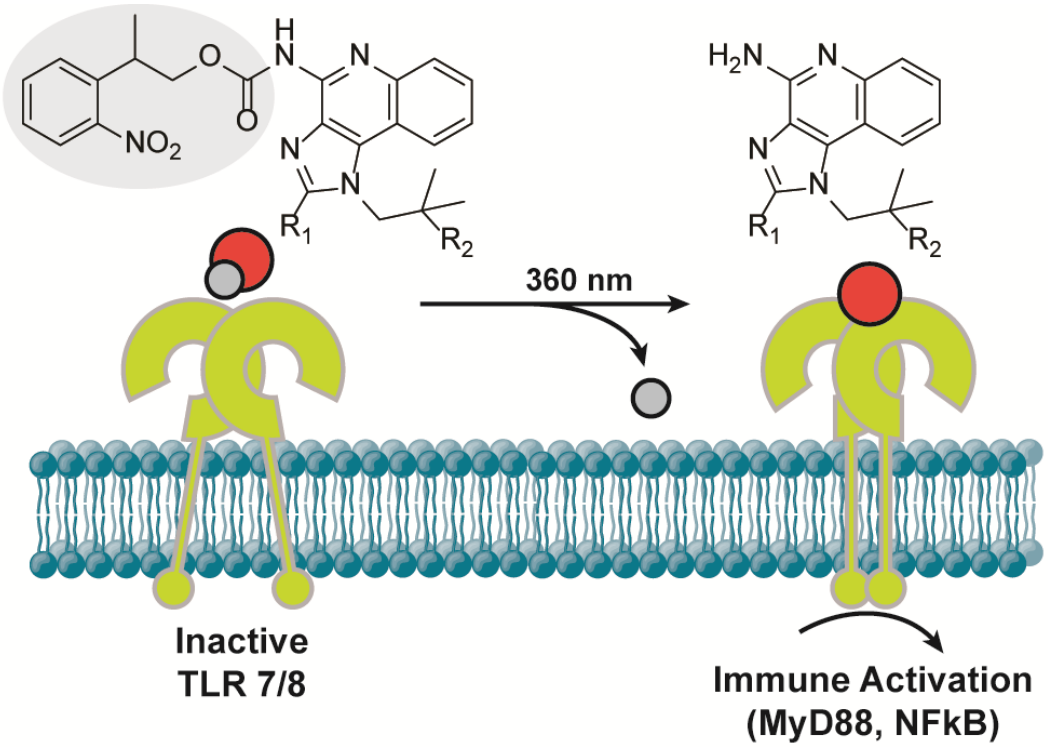

Figure 3. 1. TLR 7/8 activation and subsequent MyD88 signaling cascade following deprotection of photocaged small molecule agonist.

3. 2. Design of Photocaged Agonist

In creating photo-caged agonists, we sought to control the signaling of TLRs. In the crystal structure as reported by Tanji and coworkers, TLR 8 exists as a homo-dimeric pair. The C-terminus of each monomer is separated by 53 Å. Once the agonist is bound, the C termini are brought together to 30 Å initiating downstream signaling. In addition to the alanine scanning studies of Tanji, previous SAR studies[11] showed the critical role of the C4 amine on the imidazoquinoline molecules and its binding to D543 and V573.

Based on the crystal structure of TLR 8, we proposed that the C4 amine of the imidazoquinolines was critical for activity (**Figure 3. 2)**. We predicted that caging the amine would block activity by inhibiting those same interactions. To protect the C4 amine, we created a carbamate of 2-(2-nitrophenyl)propyloxycarbonyl (NPPOC), a well-studied photo-protecting group[12], on both Resiquimod (Resiq) and Imiquimod (Imiq). The agonist was reacted with NPPOC-Cl in dioxane, heated to 50 °C, and then purified to yield the protected agonist.

We first examined the kinetics of uncaging of both derivatives. The deprotection and retrieval of the original agonist along with the half-life was determined through UV absorbance and LC-MS. Initially, the maximum absorbances of NPPOC-Imiq and NPPOC-Resiq were 335 nm and 320 nm, respectively. During an hour of continued UV exposure (4 W, 360 nm), these peaks decrease, indicating deprotection (**Figure 3. 6**). The increase in released imidazoquinoline agonist concentration following UV exposure was also confirmed by LC-MS where aliquots of the NPPOC-agonist in DMSO were analyzed *via* LC-MS from 0 to 60 mins. After 1 min of UV exposure, 30-40% of the agonist was deprotected reaching up to 88% after 60 mins (**Figure 3. 3**). These results confirmed that Resiquimod and Imiquimod are recovered after short exposures to UV-light.

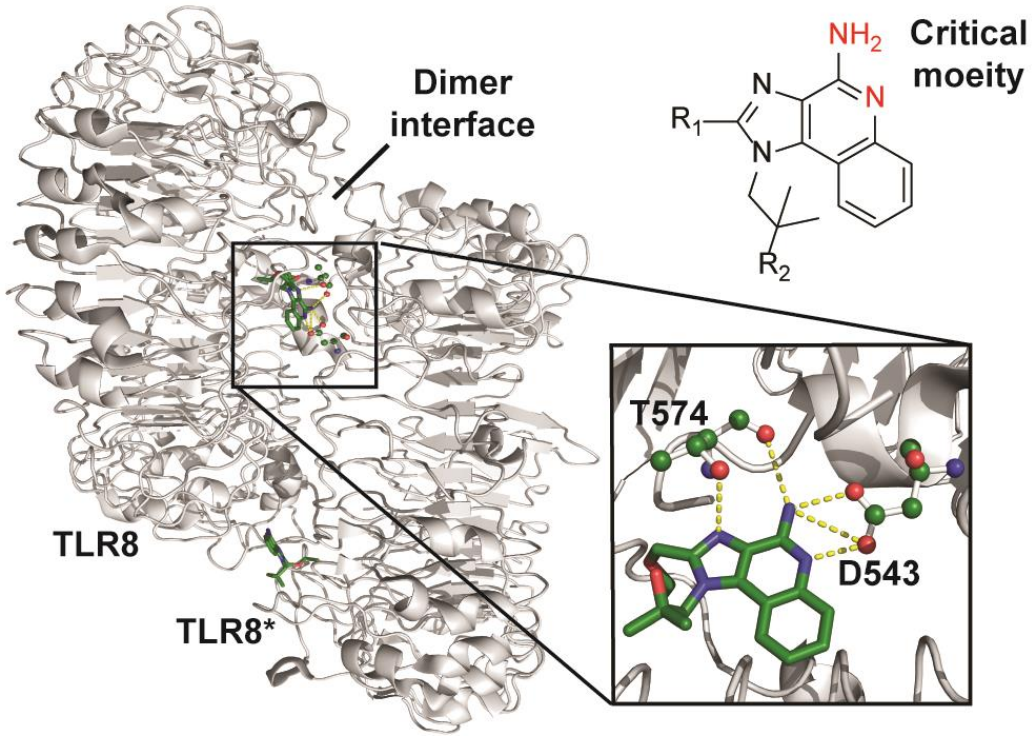

Figure 3. 2. Crystal structure of TLR 8 dimer and key binding sites of agonist (Resiquimod) upon activation. D543 and T573 knockout studies showed a decrease in NF-κB activity, demonstrating the importance of hydrogen bonding in activation.

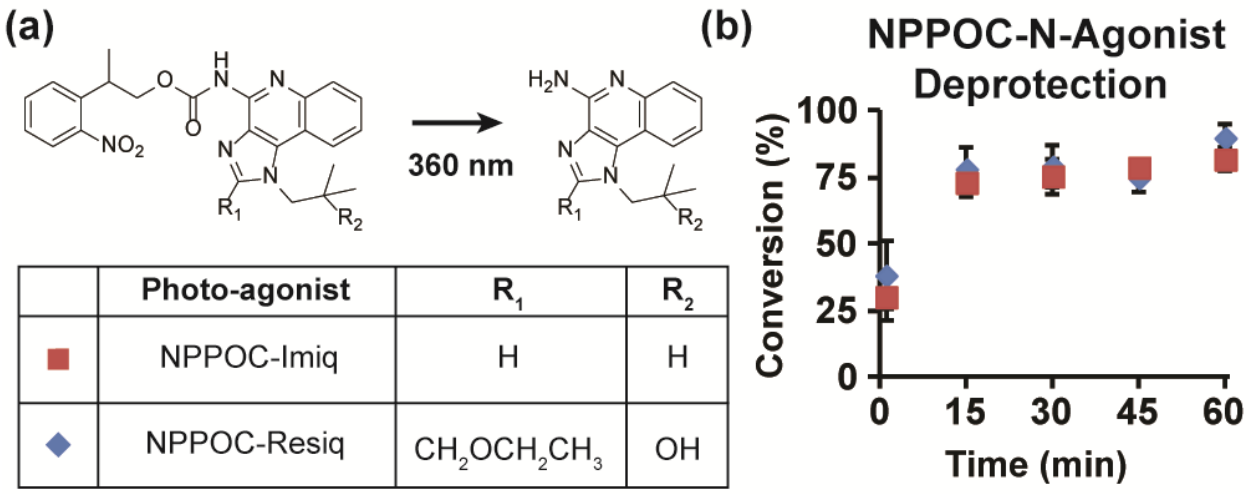

	Photo-agonist	R_1	R_2
■	NPPOC-Imiq	H	H
◆	NPPOC-Resiq	$CH_2OCH_2CH_3$	OH

Figure 3. 3. (a) Deprotection of Imiquimod and Resiquimod with 360 nm light. (b) Percent conversion of protected agonists to Imiquimod (■) and Resiquimod (♦) measured by LC-MS. After 20 minutes of activation, the deprotection reaches 80% conversion. The first data points represent t = 1 min.

3. 3. Photoactivation of RAW-Blue Cells and Primary Dendritic Cells

Next, we confirmed that photo-deprotection translated into activation of TLRs and a cellular response. We determined the effect of caging on TLR activity and innate immune stimulation using a reporter cell-line; RAW 264.7 (RAW-Blue).[13] The protected agonists were added to RAW-Blue cells, half the samples were exposed to UV light for 20 mins. Without UV exposure, samples with protected agonist yielded no NF-κB activity. With UV exposure, NF-κB activity increased, as the protecting group is removed from the C4 amine and the TLR can dimerize to initiate signaling. Activation with uncaged agonists was comparable to the activation with either Imiquimod or Resiquimod (**Figure 3. 4**).[a] As Imiquimod is a weaker agonist[14], only Resiquimod and NPPOC-Resiq were used in subsequent experiments.

Protected agonists were also tested against bone marrow-derived dendritic cells (BMDCs). The photo-activation of BMDCs was confirmed *via* flow cytometry by measuring secretion of cytokines; IL-6, IL-12, and TNF-α and the increase in the expression of a costimulatory molecule, CD40. As observed in **4c** and **4d**, NPPOC-Resiq with no exposure to UV shows no activation compared to the Resiquimod control. After deprotection, the cytokine production and cell surface marker expression values of the NPPOC-Resiq are comparable to the Resiqumod control.[b]

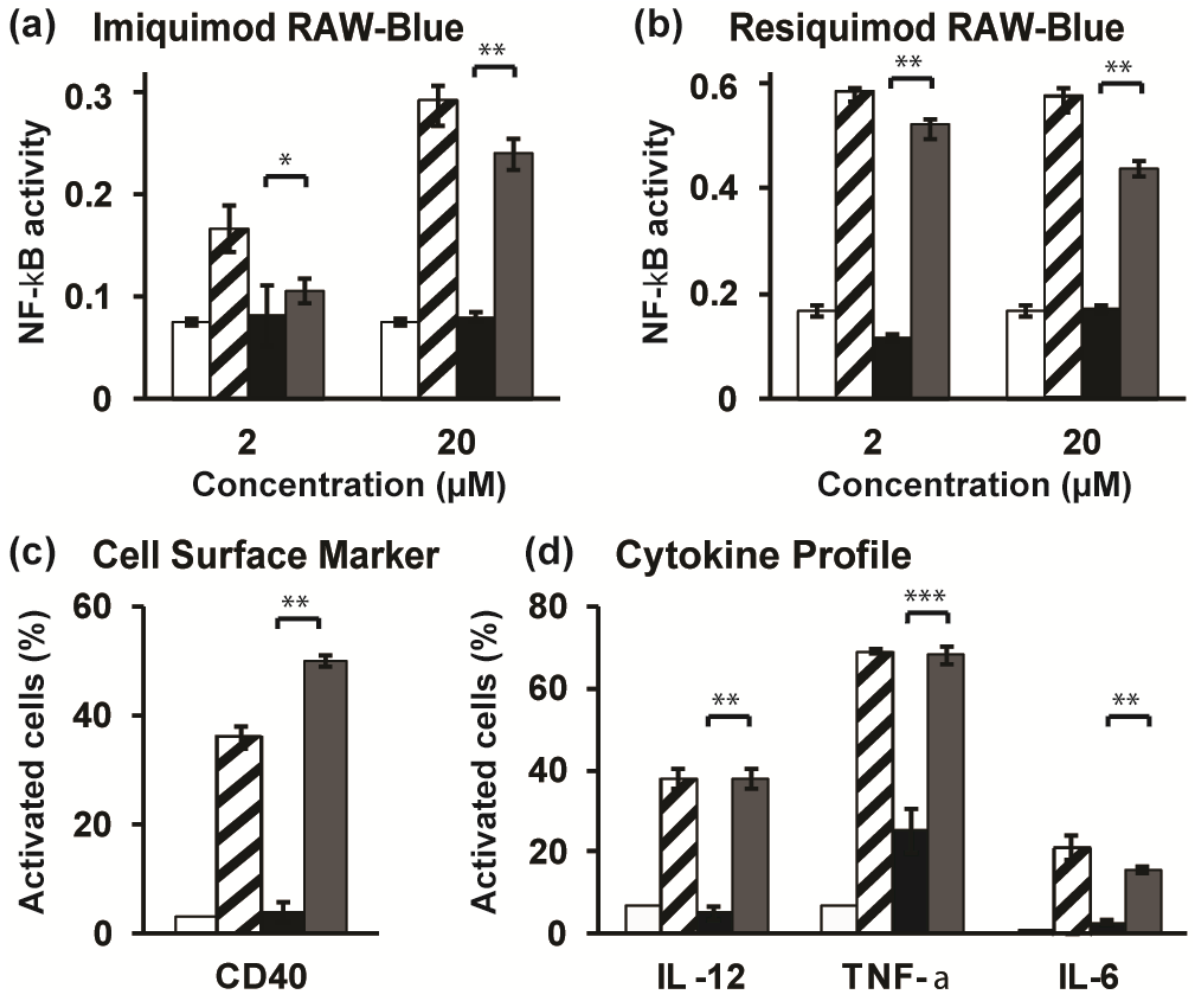

Figure 3. 4. (a) RAW-Blue activation *via* NF-κB stimulation after 24 hr incubation at 37 °C of Imiquimod (dashed), NPPOC-Imiq (black), in-situ deprotected NPPOC-Imiq (grey), and resting (unfilled). (b) RAW-Blue activation *via* NF-κB stimulation after 24 hr incubation at 37 °C of Resiquimod (dashed), NPPOC-Resiq (black), in-situ deprotected NPPOC-Resiq (grey), and resting (unfilled). (c) BMDC activation *via* cell surface marker expression when incubated with agonists for 18 hr at 37 °C. (d) BMDC intracellular cytokine production measurement when incubated with agonists for 8 hr at 37 °C. For flow cytometry experiments, Resting (unfilled), Resiquimod (dashed), NPPOC-Resiq (black), in situ deprotected NPPOC-Resiq (grey). Each result is from three independent experiments where *$p<0.047$, **$p<0.0001$, and ***$p<0.0002$.

3. 4. Spatially Controlled Activation of Dendritic Cells

The photo-activation of BMDCs was also observed using confocal microscopy. Dendritic cells, when stimulated, initiate macropinocytosis within 15 minutes.[15] Cells treated with Resiquimod dendronize and engulf FITC-labeled dextran (**Figure 3. 5**a). To confirm that agonist protection inhibits activity, cells were treated with NPPOC-Resiq, without (**5b**) and with (**5c**) exposure to UV light. Without UV exposure, BMDCs remain spherical and limited endocytosis occurs. Following 2 min of UV exposure using a Hg lamp (120 W), the cells become activated, comparable to cells treated with unmodified Resiquimod. While activation of BMDCs showed spatial selectivity, upon activation, BMDCs rapidly migrated outside the activation area making quantification difficult. To test spatial constraints, we instead used the less mobile DC 2.4s and a circular photo-mask of 3 mm diameter to activate a portion of the cells in a 14 mm diameter well. After 1 min of photo-activation, we visualized intracellular expression levels of IL-12. (**Figure 3. 5**f) Comparing the circular zone of activation versus the periphery, revealed that only cells that were exposed to UV light were activated, with much higher levels of IL-12, while the remaining cells in the culture did not activate (**Figure 3. 5**e). From this, we conclude that activation of specific cellular populations is possible using a photo-caging approach.

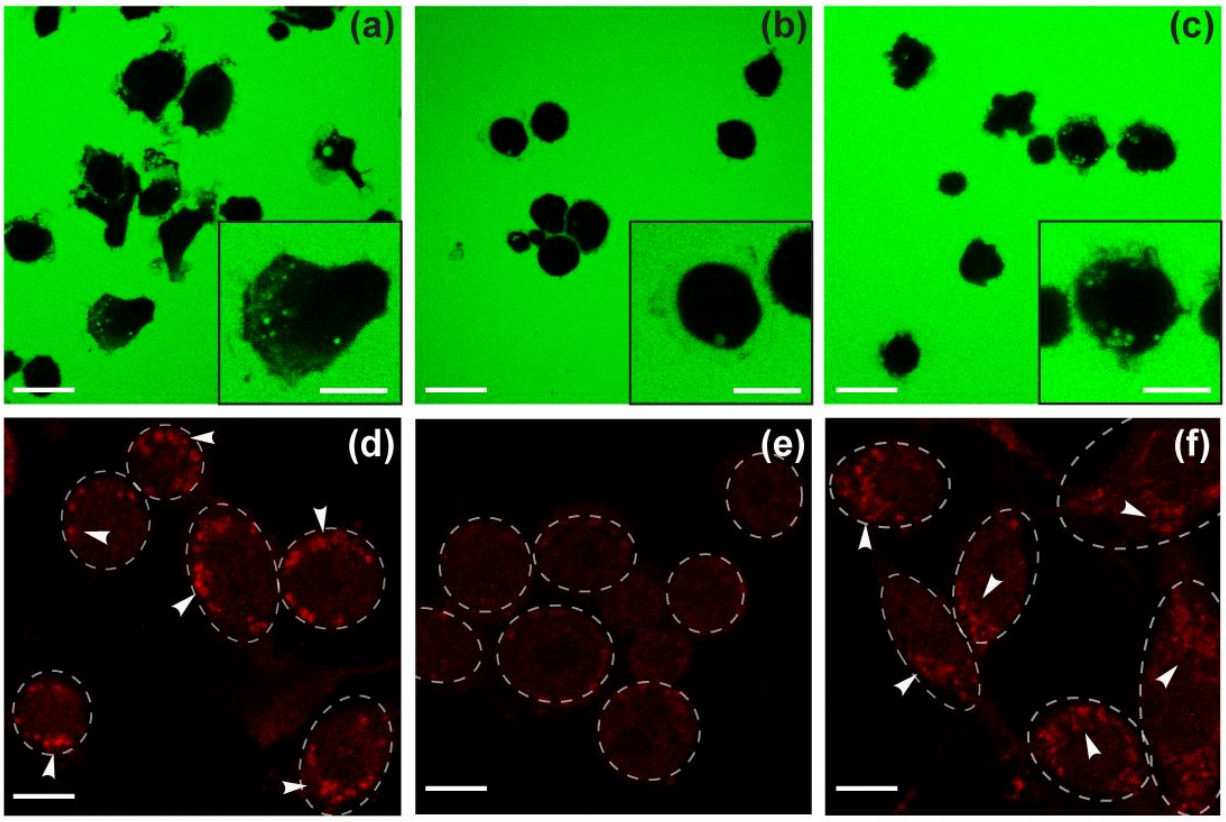

Figure 3. 5. Confocal images of BMDCs in FITC-labeled dextran 10 minutes after treatment with (a) Resiquimod, (b) NPPOC-Resiq, and (c) NPPOC-Resiq and UV exposure. Scale bar is equal to 20 μm and 10 μm for inlaid images. (d-e) Visualization of spatially activated DC 2.4 *via* IL-12 staining. Individual cells are highlighted by dashed lines. (d) DC 2.4s treated with resiquimod, (e-f) Selections of a single cell culture containing DC 2.4 treated with NPPOC-Resiq. (e) location at edge of culture with no activation (f) location at center of culture with activated DCs exposed to UV light. Scale bar is equal to 10 μm. See Supplemental Information for videos of BMDC activation and experimental set up of spatial control of DC 2.4 activation.

3. 5. Conclusions

In this work, we have successfully developed a technique to control immune cell activation through photolysis of a caging group. We found that the designed, protected agonist removes TLR activity and selectively stimulates activity when exposed to UV light. This has been tested on both a model cell line, as well as primary dendritic cells. In the future, we plan to develop a series of caged agonists for different TLRs with selective deprotection at different wavelengths using two-photon excitation. These molecules can be used in conjunction to probe TLR signaling in a spatio-temporal manner.

3. 6. Supplementary Experimental Data

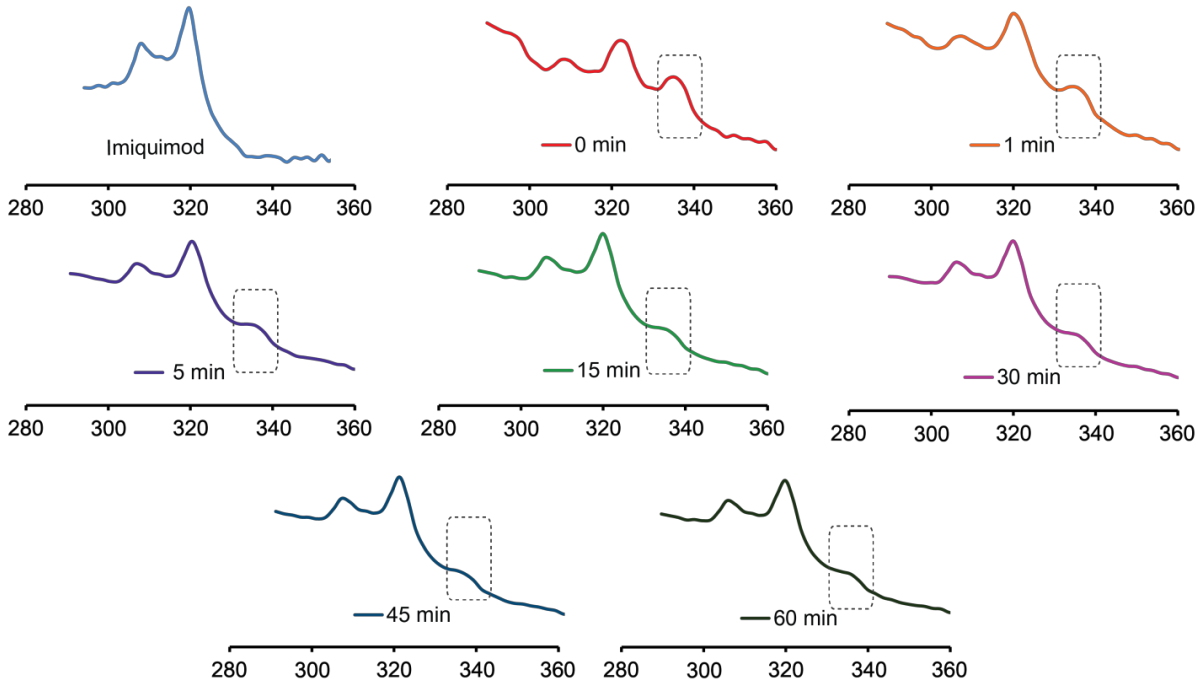

Figure 3. 6. UV-Vis trace of NPPOC-Imiq deprotection with 4 W hand lamp. A stock solution (1 mg/mL) was deprotected and aliquots were taken at various time points. The absorption at 335 nm of NPPOC-Imiq which decreases with the time of UV exposure.

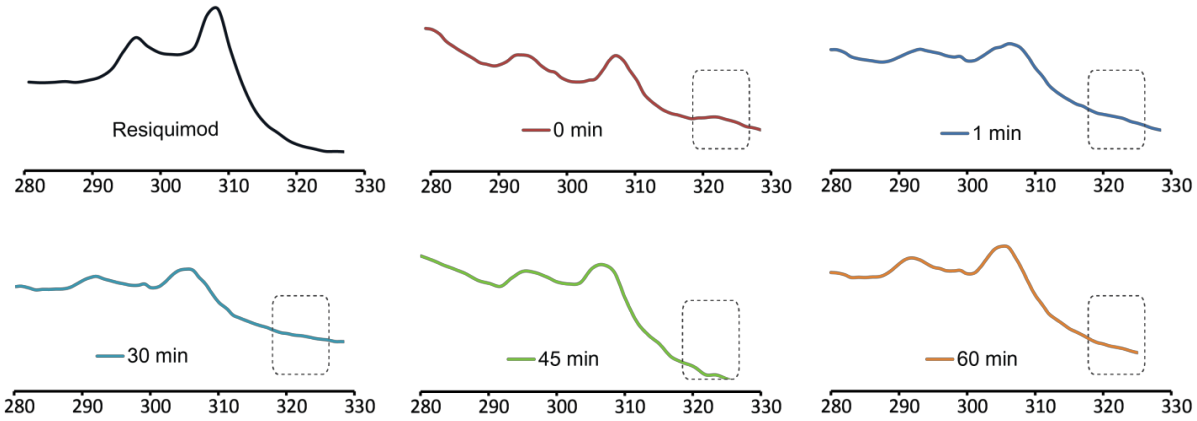

Figure 3. 7. UV-Vis trace of NPPOC-Resiq deprotection with 4 W hand lamp. A stock solution (1 mg/mL) was deprotected and 50 µg/mL aliquots were taken at various time points. The absorption at 325 nm of NPPOC-Resiq which decreases with the time of UV exposure.

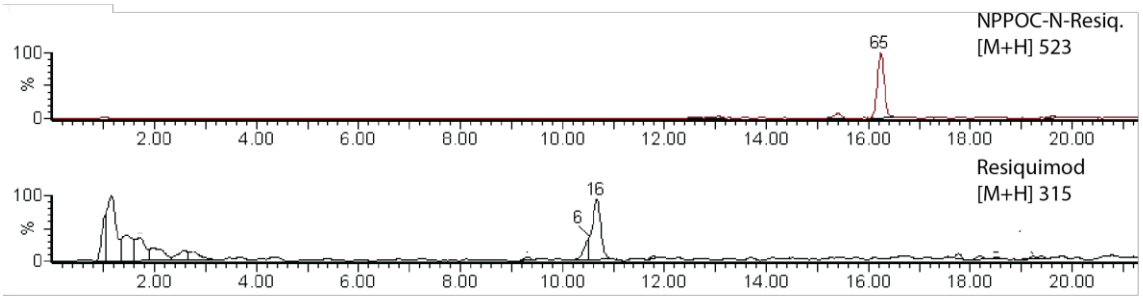

Figure 3. 8. A 1 mg/mL stock solution was deprotected and 100 µg/mL aliquots (diluted in water) were measured by positive ion LC/MS (200-1000, 30 min). After integrating the amount of NPPOC-N-agonist (16 min) and agonist (11 min), the ratio of agonist in the total amount of agonist in solution was plotted as seen in Fig. 3.

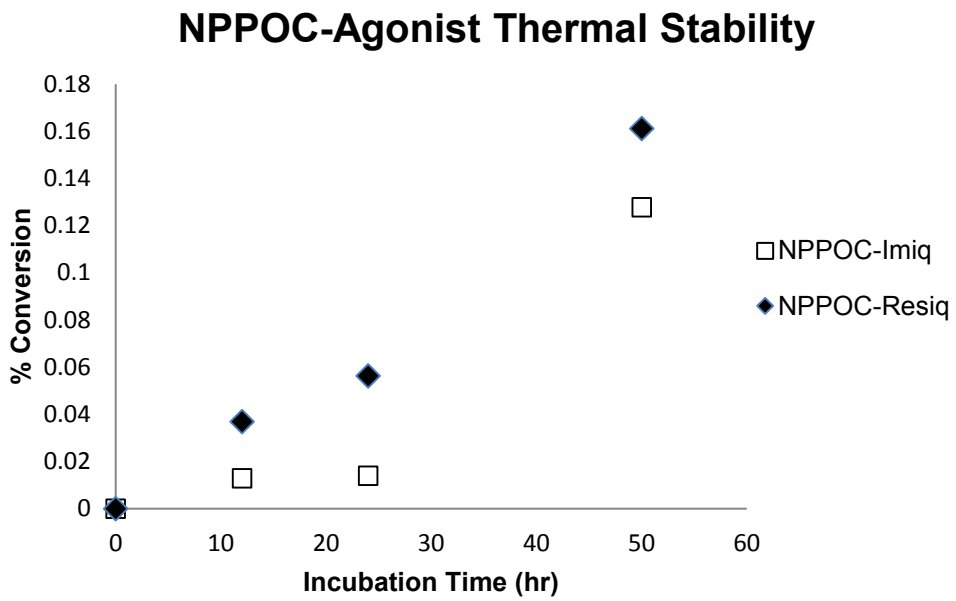

Figure 3. 9. Thermal stabilities of the protected agonists were assessed *via* LC/MS (200-1000, 30min). The protected agonists were heated to 37 °C in the cell incubator to reenact the incubation conditions of the cells. Minimal conversion was observed after 12 hrs of incubation**.**

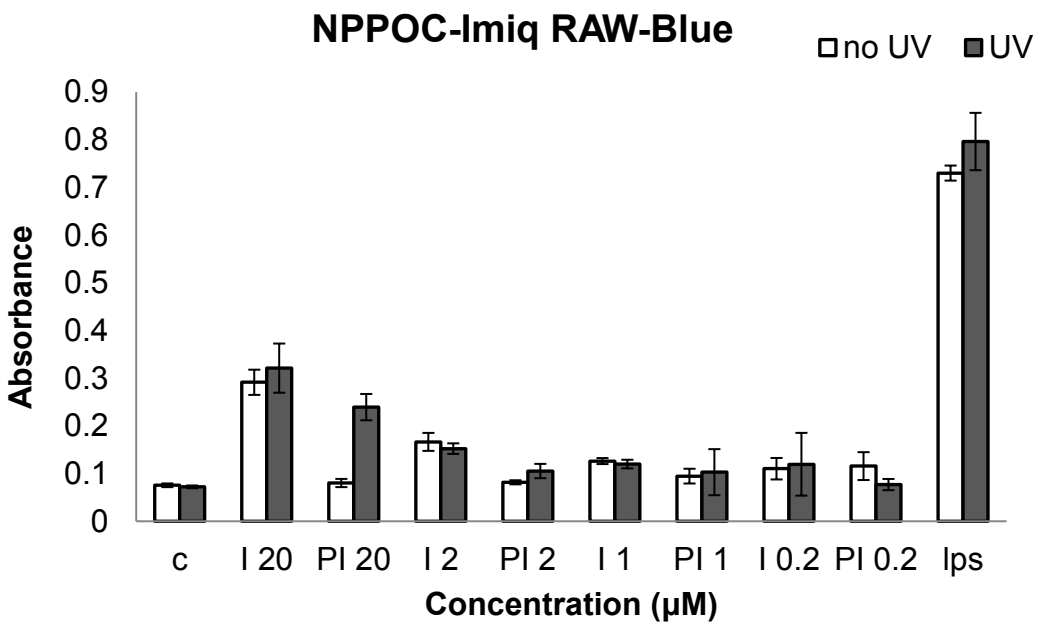

Figure 3. 10. RAW264.7 macrophage NF-κB stimulation *via* alkaline phosphatase secretion. Data displays absorbance (620 nm) caused by macrophage cell incubation with agonists for 19 h at 37 °C, which correlates to NF-κB stimulation. Various concentrations of both Imiquimod (positive control) and NPPOC-Imiq before (unfilled) and after (filled) UV exposure with 4 W, 360 nm hand lamp for 15 min. P values represent that for NPPOC-Imiq relative to deprotected NPPOC-Imiq where $p < 0.0001$ (20 μM), $p<0.047$ (2 μM), $p<0.04$ (1 μM, 0.2 μM) over four independent experiments.

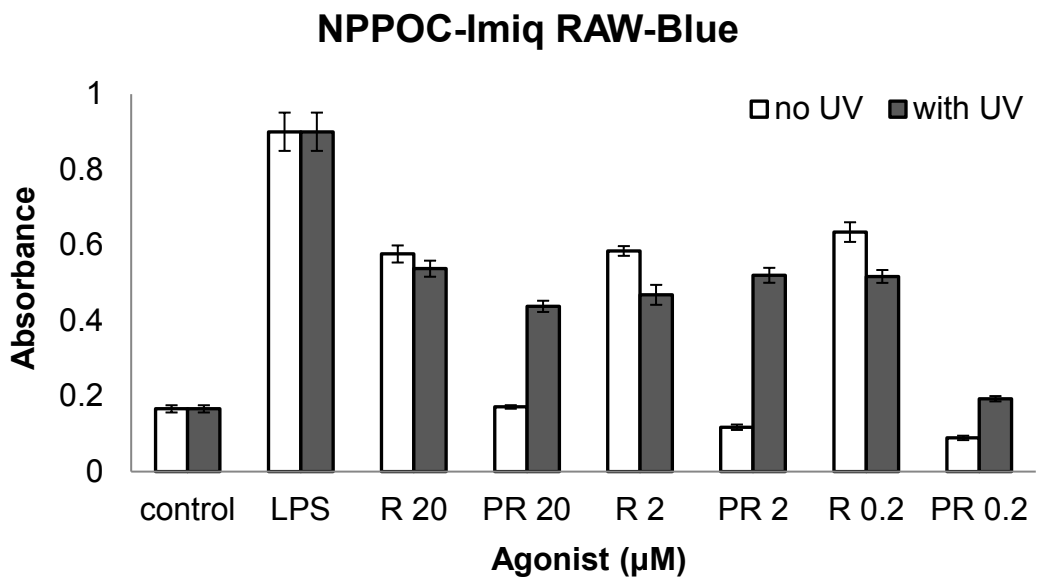

Figure 3. 11. RAW264.7 macrophage NF-κB stimulation *via* alkaline phosphatase secretion. Data displays absorbance (620 nm) caused by macrophage cell incubation with agonists for 19 h at 37 °C, which correlates to NF-κB stimulation. Various concentrations of both Resiquimod (positive control) and NPPOC-Resiq before (unfilled) and after (filled) UV exposure with 4 W, 360 nm hand lamp for 15 min. P values represent that for NPPOC-Resiq relative to deprotected NPPOC-Resiq where $p < 0.0001$ (20 μM, 2 μM), and $p<0.0002$ (0.2 μM) over four independent experiments.

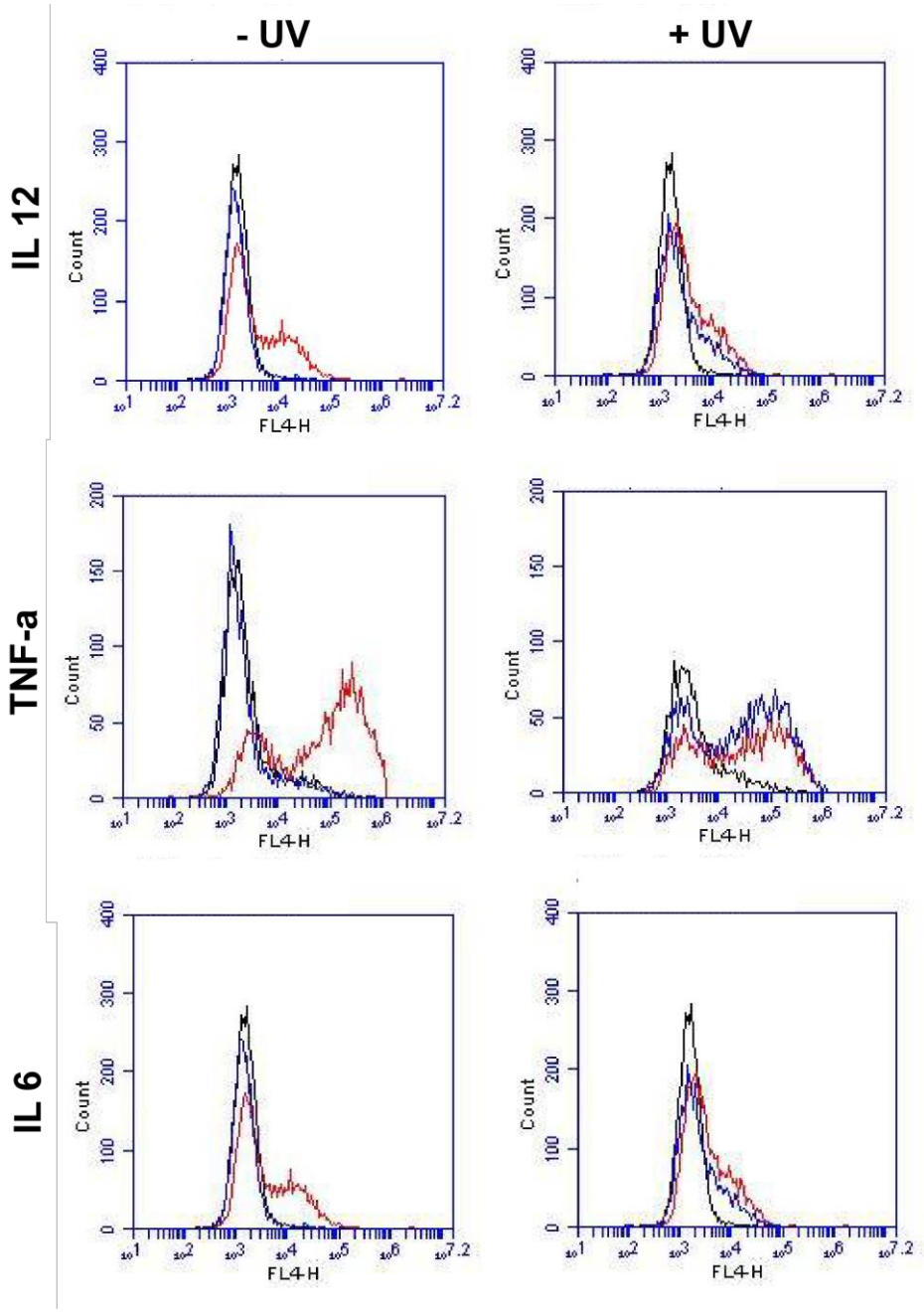

Figure 3. 12. Activation of BMDCs using protected agonist. TNF-α and IL-12 cytokine production was analyzed *via* flow cytometry. Two separate sets of control values were measured due to the effect of UV on the sensitive BMDCs. Consequently, the post UV exposure values are presented separate from the pre- exposure. However, it is clear that there is no cytokine activity before UV exposure and that there is a gain of activity after deprotection. Resting (black), Resiquimod (red), NPPOC-Resiq (blue). Agonist concentrations are 2 μM.

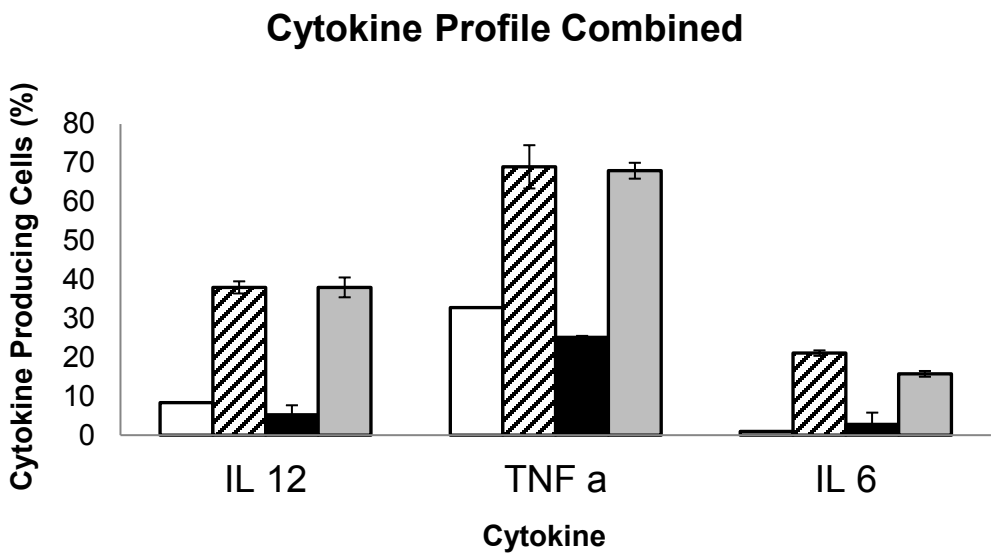

Figure 3. 13. BMDC intracellular cytokine flow cytometry analysis. Resting (white), Resiquimod with 15 minute UV exposure (dashed), NPPOC-Resiq (black), in situ deprotected NPPOC-Resiq (grey). P values represent that for NPPOC-Resiq relative to deprotected NPPOC-Resiq where $p < 0.0001$ (IL-12, IL-6) and $p < 0.0002$ (TNF-α) over three independent experiments. Agonist concentrations are 2 μM.

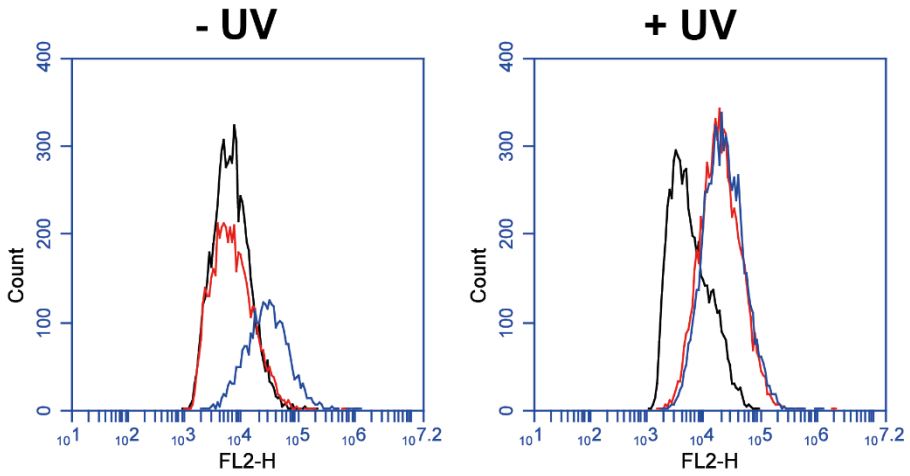

Figure 3. 14. Activation of BMDCs using protected agonist. CD40 cell surface marker activation was analyzed *via* flow cytometry. Two separate sets of control values were measured due to the effect of UV on the sensitive BMDCs. Consequently, the post UV exposure values (resting (black), resiquimod (red), NPPOC-Resiq (blue)) are presented separate from the pre- exposure (resting (black), resiquimod (blue), NPPOC-Resiq (red)). However, it is clear that there is no CD40 activity before UV exposure and that there is a gain of activity after deprotection. Agonist concentrations are 2 μM.

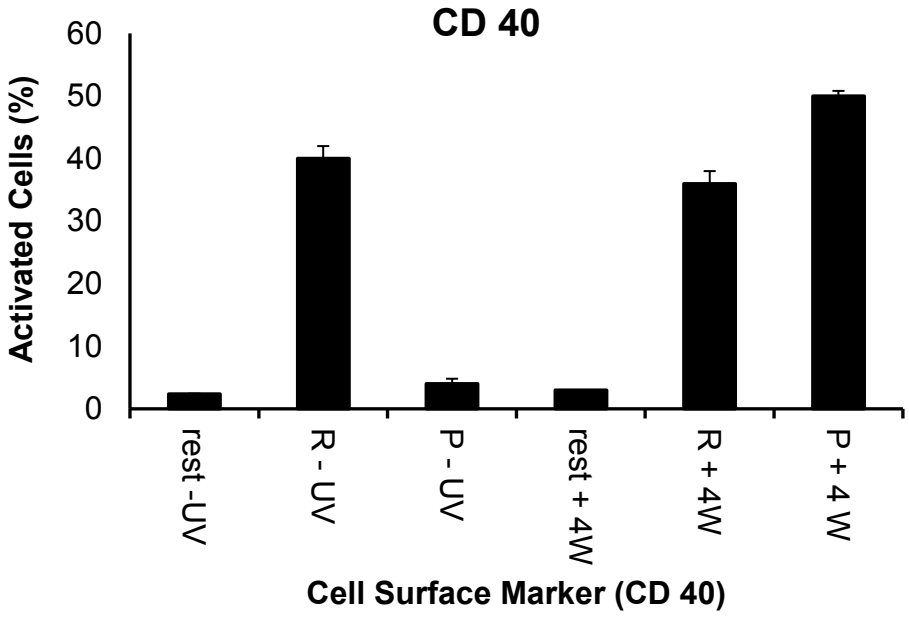

Figure 3. 15. BMDC cell surface marker (CD40) analysis after 10 min of UV exposure. P values represent a comparison of NPPOC-Resiq relative to deprotected NPPOC-Resiq where $p < 0.0001$ was measured over three independent experiments. Agonist concentrations are 2 μM.

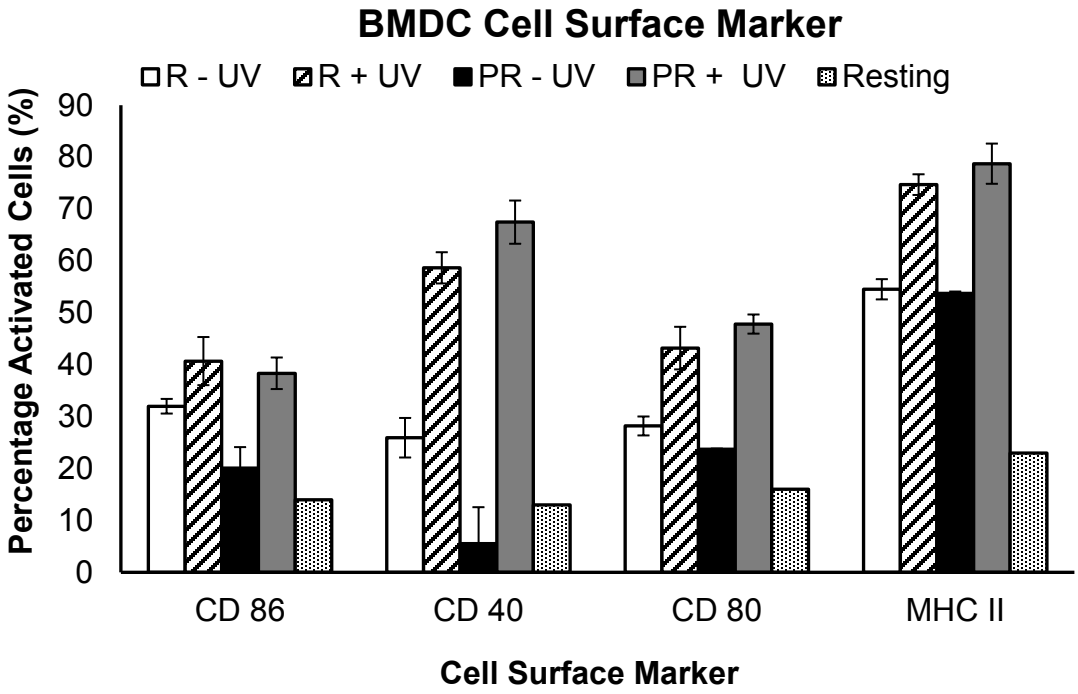

Figure 3. 16. Additional BMDC cell surface marker (CD 86, CD 40, CD 80, MHC II) flow cytometry analysis. Resiquimod (white), resiquimod with 15 minute UV exposure (dashed), NPPOC-Resiq (black), in situ deprotected NPPOC-Resiq (grey), Resting (dotted). A decrease in CD 86, CD 40, and CD 80 activity was observed, however, data points were in duplicate and no p values were calculated. Agonist concentrations are 2 μM.

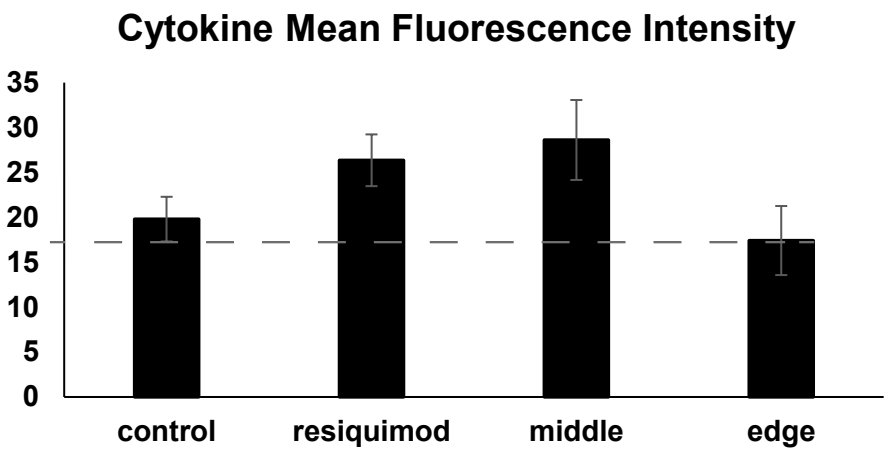

Figure 3. 17. Quantified mean fluorescence intensity values of stained cytokine (IL-12) in DC 2.4 after incubation with 20 μM NPPOC-Resiq and spatially selective deprotection. P values represent a comparison of control (no agonist) and resiquimod (positive control), $p<0.0001$ and the middle of the well plate (UV exposed) and the edge of the well plate (no UV) with $p<0.0001$. Each bar represents measurements from a minimum of 50 cells.

3. 7. Experimental Procedures

3. 7. 1. Materials and Methods

Unless otherwise noted, all reagents were purchased from Sigma-Aldrich and used as received. Imiquimod was purchased from LKT Technologies. Antibodies were purchased from BioLegend. BD Cytofix/Cytoperm Kit for intracellular cytokine flow cytometry and GolgiPlug were purchased from BD Biosciences. ^{13}C and ^{1}H NMR spectra were taken on an AVANCE500 (500 MHz) spectrometer and analyzed using MestreNova software. Mass spectrum was obtained using ESI LC-TOF Micromass LCT 1. Flow cytometry data was acquired using BD Accuri C6 Flow Cytometer and analyzed using the BD Accuri C6 software. RAW-Blue absorbances were measured on a Bio-Tek Quant microplate spectrophotometer MQX200. All animal studies and mice maintenance were approved by the Institutional Animal Care and Use Committee (IACUC #2012-3048).

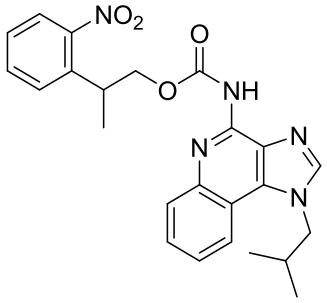

3. 7. 2. NPPOC-Imiq

Imiquimod (0.03 g, 0.2 mmol) was stirred with 3 mL of anhydrous 1,4 dioxane and the solution was cooled to 10 °C. 2-(2-nitrophenyl)propyloxycarbonyl chloride (NPPOC-Cl, 0.0608 g, 0.4 mmol) was diluted with 1 mL of anhydrous 1, 4 dioxane (2 mL). The NPPOC-Cl solution was added dropwise to the agonist solution. The resulting solution was heated to 50 °C for 6 hr. Reaction was monitored *via* TLC. The resulting products were purified by column

chromatography (10% MeOH/DCM) and concentrated under vacuum. Resulted in 0.020g (38 % yield) as yellow oil. R_f 0.67; ^{1}H NMR ($CDCl_3$, 500MHz) δ 8.15 (s, 1H), 8.12 (d, *J* = 8.1 Hz, 1H), 7.92 (d, *J* = 7.8 Hz, 1H), 7.75 (s, 1H), 7.71 (d, *J* = 8.0 Hz, 1H), 7.59 – 7.47 (m, 3H), 7.45 (t, *J* = 7.3 Hz, 1H), 7.26 (t, *J* =7.4 Hz, 1H), 4.38 (dd, *J* = 17.3, 8.0 Hz, 2H), 4.25 (d, *J* = 6.6 Hz, 2H), 3.74 (dd, *J* = 12.7, 6.2 Hz, 1H), 2.30 (m, 1H), 1.37 (d, *J* = 6.9 Hz, 3H), 0.97 (d, *J* = 6.4, 6H). ; ^{13}C (CDCl3, 500MHz) δ 151.45, 150.50, 144.12, 144.02, 142.86, 137.36, 133.32, 132.78, 130.24, 129.45, 128.33, 127.57, 127.48, 125.03, 124.30, 119.76, 116.65, 109.99, 69.14, 55.23, 33.33, 29.76, 28.88, 19.86, 17.92; MS m/z calc'd for $C_{24}H_{25}N_5O_4$ [M+Na] 470.18; Observed [M+Na] 470.1.

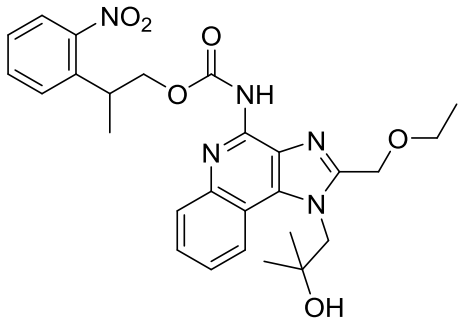

3. 7. 3. NPPOC-Resiq

Resiquimod (0.03 g, 0.1 mmol) was stirred with 3 mL of anhydrous 1,4 dioxane and the solution was cooled to 10 °C. 2-(2-nitrophenyl)propyloxycarbonyl chloride (NPPOC-Cl, 0.0465 g, 0.19 mmol) was diluted with 1 mL of anhydrous 1, 4 dioxane (2 mL). The NPPOC-Cl solution was added dropwise to the agonist solution. The resulting solution was heated to 50 °C for 6 hr. Reaction was monitored *via* TLC. The resulting products were purified by column chromatography (10% MeOH/DCM) and concentrated under vacuum. Resulted in 0.005g (16 % yield) as yellow oil. R_f 0.65; ^{1}H NMR ($CDCl_3$, 500MHz) ^{1}H NMR (500 MHz, $CDCl_3$) δ 8.31 (s, 1H), 8.22 (d, *J* = 8.4 Hz, 1H), 8.18 (d, *J* = 8.1 Hz, 1H), 7.84 (d, *J* = 8.0 Hz, 1H), 7.71 – 7.61 (m,

4H), 7.53 (t, *J* = 5 Hz, 1H), 7.42 (t, *J*= 5 Hz, 1H), 4.96 (s, 3H), 4.84 (s, 2H), 4.52 (d, *J* = 6.5 Hz, 2H), 3.85 (dd, *J* = 13.3, 6.7 Hz, 1H), 3.72 (d, *J* = 7.1 Hz, 2H), 1.50 (d, *J* = 6.9 Hz, 3H), 1.38 (s, 6H), 1.32 (d, *J* = 6.8 Hz, 3H). ^{13}C (CDCl3, 500MHz) δ 151.49, 150.68, 150.36, 144.52, 143.96, 137.40, 135.43, 132.85, 130.40, 128.39, 127.49, 126.99, 124.57, 124.33, 119.87, 116.83, 71.51, 69.04, 67.12, 66.74, 64.98, 56.41, 33.44, 28.01, 18.16, 14.97; MS m/z calc'd for $C_{27}H_{31}N_5O_6$ [M+Na] 544.21; Observed [M+Na] 544.21.

3. 7. 4. General Procedure for RAW264.7 Macrophage (RAW-Blue) NF-κB assay.[c]

RAW264.7 macrophage cells (RAW-Blue, Invivogen) were grown in complete culture media composed of Dulbecco's Modified Eagle's Medium (DMEM) with 4.5 g/L glucose (Life Technologies), 2 mM L-glutamine, 10,000 U/mL penicillin, 10 mg/mL streptomycin, 25 μg/mL amphotericin B, supplemented with 10% fetal bovine serum (FBS, Sigma).

For the NF-κB assay, RAW-Blue cells (passage 3-8) were plated at $1x10^5$ cells/mL in 96-well optically clear bottomed, black-walled microplates cells in complete media supplemented with 10% heat-inactivated FBS (Sigma) with addition of agonist at the specified concentrations. A hand held UV lamp (4 W) was employed for UV exposure; the optically-clear bottom of the well plate was exposed with long wave UV light (360 nm) for 20 min. The cells were incubated for 18 h at 37 °C with 5% CO_2. Cell media (50 μL) from the wells was transferred to a new 96-well plate and incubated with QUANTI-Blue reagent (150 μL, Invivogen) for 1 h at 37 °C with 5% CO_2. The absorbance (620 nm) was measured using a Bio-Tek Quant microplate spectrophotometer.

3. 7. 5. Bone Marrow-Derived Dendritic Cell Harvest and Culture.

Bone marrow-derived dendritic cells (BMDCs) were harvested from 6-week-old C57Bl/6 mice

(Jackson Laboratory). Femur bones were removed from mice according to protocols describes by Matheu[d], and the bone marrow was extracted into PBS buffer. The cell suspension was made into a homogeneous solution using a pipette and subsequently filtered through a 70 μm cell strainer. The cell solution was centrifuged at 300 RCF for 10 min at RT. The supernatant was removed, and ACK Lysing Buffer (3 mL, Lonza) was added to the cell pellet and incubated for 2 min at RT. PBS buffer (13 mL) was then added to the cell suspension, and the cell solution was centrifuged at 300 RCF for 10 min at RT. In a washing step, the cell pellet was resuspended in RPMI 1640 (Fisher Scientific) and centrifuged at 300 RCF for 10 min at RT. Thereafter, the cell pellet was resuspended in BMDC complete media composed of RPMI 1640, 10% heat-inactivated FBS, 20 ng/mL granulocyte-macrophage colony-stimulating factor (GM-CSF, donated by the Cahalan Lab), 2 mM L-glutamine (Life Technologies), 10,000 U/mL penicillin, 10 mg/mL streptomycin, 25 μg/mL amphotericin B, and 50 μM beta-mercaptoethanol. Harvested cells were plated at $1x10^6$ cells/mL in 100 mm petri dishes (10 mL total media) and incubated at 37 °C in a CO_2 incubator (day 0 of cell culture). On day 3, 10 mL of fresh BMDC primary media was added to each petri dish. On day 5, BMDCs were released by repeated pipetting, centrifuged at 300 RCF for 10 min at RT, and plated in 24-well plates at $1.2x10^6$ cells/mL for cell surface marker activation, cytokine profile flow cytometry, and confocal microscopy experiments.

3. 7. 6. General Procedure for Flow Cytometry for Cell Surface Marker Upregulation.

BMDCs were incubated in individual wells with each agonist (9:1 BMDC:agonist) in 0.5 mL culture media) for 18 h at 37 °C with 5% CO_2. Cells exposed to UV with 4 W hand lamp (15 min) on top of separate 24 well plate sealed with optically clear tape and incubated for 18 h at 37 °C with 5% CO_2. The cells were released from the plate and transferred to microcentrifuge

tubes. The cells were centrifuged at 2500 RPM at 4 °C for 10 min. The supernatant was removed and the cell pellet was resuspended in cold FACS (composed of PBS (1x), 10% FBS, and 0.1% sodium azide) buffer (100 µL) and incubated with CD16/32 FcR blocking antibodies (1.0 µg/1x10^6 cells) on ice for 10 min. The cell suspension was centrifuged at 2500 RPM for 10 min at 4 °C. Then the supernatant was removed and the cell pellet was resuspended in cold FACS buffer (100 µL) and incubated with FITC-CD11c (1.0µg/1x106 cells) and PE-CD86 (1.0 µg/1x10^6 cells), -CD40 (1.0 µg/1x10^6 cells), -MHCII (0.25 µg/1x10^6 cells), or -CD80 (0.5 µg/1x10^6 cells) on ice and removed from light for 30 min. Each sample was washed twice with 300 µL cold fluorescence-activated cell sorting (FACS) buffer. The dendritic cells were resuspended in cold FACS buffer (200 µL) and kept on ice until being loaded onto the flow cytometer.

3. 7. 7. General Procedure for Intracellular Cytokine Flow Cytometry Staining.

BMDCs were incubated individually with a solution of agonist (9:1 BMDCs : agonist in 0.5 mL culture media for 8 h at 37 °C with 5% CO_2. Cells exposed to UV with 4 W hand lamp (15 min) on top of separate 24 well plate sealed with optically clear tape and incubated for 18 h at 37 °C with 5% CO_2. GolgiPlug (BD Biosciences), containing Brefeldin was added to cell culture (following BD Biosciences protocol) for the final 4 h of culture. After 8 h, stimulated BMDCs were released from the plate and transferred to 1 mL microcentrifuge tubes. The cells were centrifuged at 2500 RPM at 4 °C for 10 min. The supernatant was removed and the cell pellet was resuspended in cold FACS buffer (100 µL) and CD16/32 FcR blocking antibodies (1.0 µg/1*10^6 cells). Cells were incubated on ice for 10 min, then centrifuged at 2500 RPM at 4 °C for 10 min. The supernatant was removed and the cell pellet was resuspended in cold FACS

buffer (100 µL) and FITC-CD11c (1.0 µg/1x10^6 cells). Cells were incubated on ice for 10 min and protected from light for 30 min, then centrifuged at 2500 RPM at 4 °C for 10 min. The supernatant was removed and each sample was washed twice with 300 µL cold fluorescence-activated cell sorting (FACS) buffer. The supernatant was removed and the cell pellet was resuspended in 100 µL BD Cytofix/Cytoperm solution. Cells were incubated on ice, removed from light for 20 min. The cell suspension was centrifuged at 2500 RPM and 4 °C for 10 min and the supernatant removed. BMDCs were washed twice with BD Perm/Wash solution and the supernatant removed. The cell pellet was resuspended in cold FACS buffer (100 µL) and incubated with APC-IFN-γ (1.0 µg/1x10^6 cells), -TNF-α (0.25 µg/1x10^6 cells), -IL-6 (0.25 µg/1x10^6 cells), or -IL-12 (0.25 µg/1x10^6 cells) on ice, removed from light for 30 min. Cold FACS buffer (300 µL) was added to each sample. The cell suspension was centrifuged at 2500 RPM and 4 °C for 10 min and the supernatant removed. The cells were rinsed with cold FACS buffer (300 µL) one more time. BMDCs were resuspended in cold FACS buffer (200 µL) and kept on ice until analysis *via* flow cytometry.

3. 7. 8. General Procedure for Cytokine Staining for Microscopy

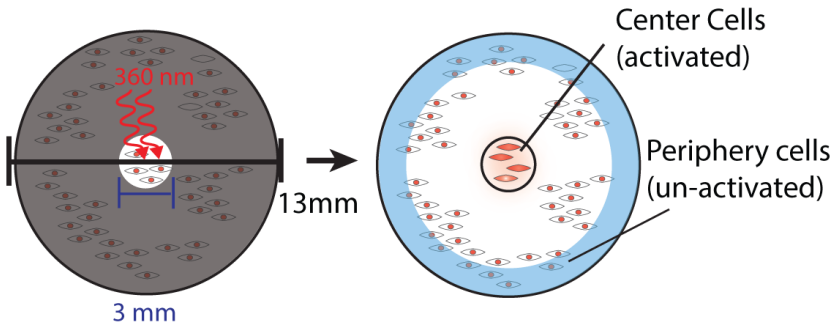

DC 2.4s were incubated individually in Mattek 35 mm dishes (14 mm glass) with a solution of agonist (9:1 v/v media : agonist to a reach a final concentration of 20 µM NPPOC-Resiq) in 2

mL culture media (DMEM, 10% HI FBS) for 8 h at 37 °C with 5% CO_2. The area of UV exposure was controlled by exposing only the middle of the well plate using a laser-machined photo-mask consisting of black-plastic with a circular hole (3 mm) placed in the center of the well plate. Cells were exposed to 360 nm UV light for 1 min, after which the culture media was removed and exchanged for media containing no NPPOC-Resiq.

To measure the activation, we used an intracellular cytokine staining assay to measure the expression levels of IL-12 in activated cells. GolgiPlug (BD Biosciences), containing Brefeldin was added to cell culture (according to BD Biosciences protocol) for the final 4 h of culture. After 8 h, the BMDCs were fixed with -78ºC acetone for 5 min. The cells were then rinsed with FACS buffer (1 mL) three times. The cells were incubated with rat anti-mouse APC IL-12 (0.25 μg/1x10^6 cells) in 1 mL of FACS buffer on ice, removed from light for 30 min. Each sample was rinsed with cold FACS buffer. The cells were subsequently incubated with donkey anti-rat alexa fluor 594 (1 μg/1x10^6 cells) in 1 mL of FACS buffer for 30 min removed from the light, on ice. The cells were rinsed with cold FACS buffer (1 mL) and kept on ice until analysis *via* confocal microscope of the activated area (red) and inactivated areas (blue).

3. 7. 9. General Procedure for Confocal Microscopy

BMDCs were washed with RPMI. The cell pellet was resuspended at approximately 2x10^4 cells/μL complete media supplemented with 10% heat-inactivated FBS. Agonist and protected agonist solutions were prepared in FITC-dextran-containing complete media supplemented with 10% heat-inactivated FBS.

To visualize endocytosis following activation by an agonist, cells were imaged as time series (100 frames, 3.15 µs pixel dwell) on a Zeiss 780 confocal microscope using a 63x oil immersion. The BMDC suspension was combined with the agonist solution containing FITC-dextran 1:1 by volume, sandwiched between glass coverslips, and imaged without further incubation. For deprotection of NPPOC-Resiq, the samples were exposed to UV light by opening the mercury lamp (120 W) shutter for 2 min.

3. 7. 10. Image Quantification Procedure

Image J was used to quantify the fluorescence intensities of the IL-12 cytokine staining. Images were quantified using using the red channel image. The image was filtered with a Gaussian blur and median filter. Subsequently, the brightness and contrast of the image was set to a minimum of 10 and maximum of 27 for all images. The modified image was then converted to a binary image. After setting the measurement to the original red channel image, the particles selected were analyzed and graphed to find the mean fluorescence intensities.

Step by step procedure for Image J analysis

1. Import image into Image J
2. Split color and select red channel
3. Duplicate image
4. Filter duplicate with Gaussian blur (4) and median (5)
5. Adjust the brightness/contrast (Min: 10; Max: 27)

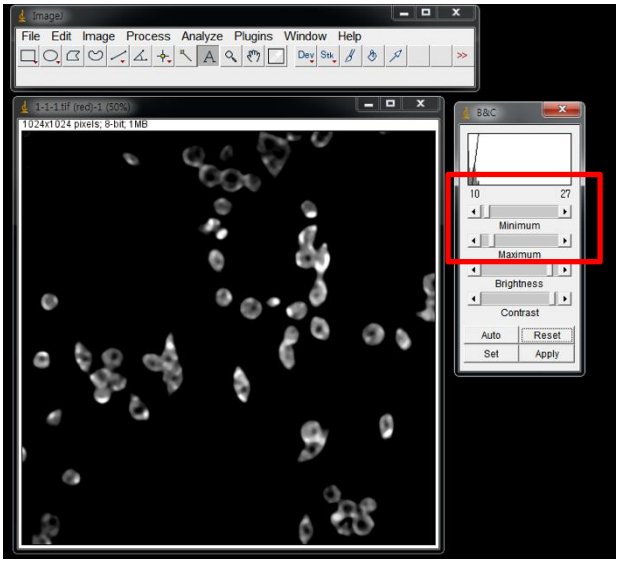

6. Convert into binary image

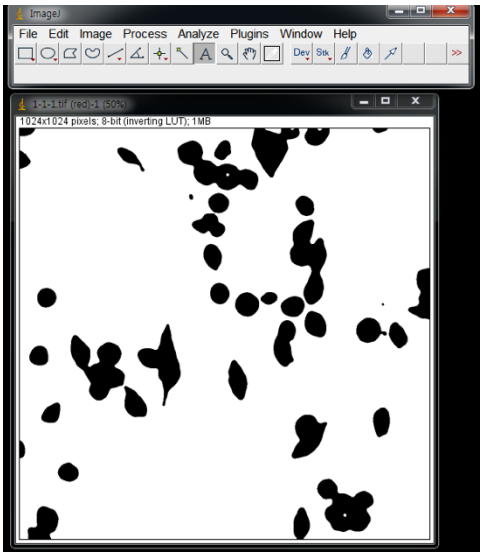

7. Set measurement to redirect to original image

8. Analyze particle

9. Graph average of mean intensities of 60-100 cells

3. 8. References and Notes

(1) (a) Iwasaki, A.; Medzhitov, R. *Nat. Immunol*. **2004**, *5*, 987-995. (b) Janeway, C. A.; Medzhitov, R. *Annu. Rev. Immunol.* **2002**, *20*, 197–216. (c) Medzhitov, R. *J. Immunol* **2013**, *191*, 4473–4474. (d) Beutler, B.; Rietschel, E. T. *Nat. Rev. Immunol.* **2003**, *3*, 169–176.

(2) Ozinski, A.; Underhill, D.; Fontenot, J.; Hajjar, A.; Smith, K.; Wilson, C.; Schroeder, L.; Aderem, A. *Proc. Natl. Acad. Sci. U. S. A.* **2000**, *97*, 13766-13771.

(3) Akira, S.; Takeda, K.; Kaisho, T. *Nat. Immunol*. **2001**, *2*, 675-680.

(4) (a) Kagan, J.; Medzhitov, R. *Cell* **2006**, *125*, 943-955. (b) Spiegel, D. A. *Nat. Chem. Biol.* **2010**, *6*, 871–872.

(5) (a) Lee, H.; Larson, D.; Lawrence, D. *ACS Chem. Biol*. **2009**, *4*, 409-427. (b) Dore, T. M. In *Dynamic Studies in Biology*; Goeldner, urice; Givens, R. S., Eds.; Wiley-VCH Verlag GmbH & Co. KGaA, 2005; pp. 435–459. (c) Brown, E. B.; Shear, J. B.; Adams, S. R.; Tsien, R. Y.; Webb, W. W. *Biophys. J.* **1999**, *76*, 489–499. (d) Wöll, D.; Smirnova, J.; Galetskaya, M.; Prykota, T.; Bühler, J.; Stengele, K.-P.; Pfleiderer, W.; Steiner, U. E. *Chemistry – A European Journal* **2008**, *14*, 6490–6497. (e) Olson, J. P.; Kwon, H.-B.; Takasaki, K. T.; Chiu, C. Q.; Higley, M. J.; Sabatini, B. L.; Ellis-Davies, G. C. R. *J. Am. Chem. Soc.* **2013**, *135*, 5954–5957. (f) Lee, H.-M.; Larson, D. R.; Lawrence, D. S. *ACS Chem. Biol.* **2009**, *4*, 409–427.

(6) (a) Sidky, Y.; Borden, E.; Weeks, C.; Reiter, M.; Hatcher, J.; Bryan, G. *Cancer Res*. **1992**, *52*, 3528-3533. (b) Wierenga, W.; Skulnick, H.; Stringfellow, D.; Weed, S.; Renis, H.; Eidson, E. *J. Med. Chem*. **1980**, *23*, 237-239. (c) Li, H.; Wallace, T.; Wierenga, W.; Skulnick, H.; DeKoning, T. *J. Biol. Response Mod*., **1987**, *6*, 44-55. (d) Shukla, N. M.; Mutz, C. A.; Malladi, S. S.; Warshakoon, H. J.; Balakrishna, R.; David, S. A. *J. Med. Chem.* **2012**, *55*, 1106–1116. (e) Shukla, N. M.; Salunke, D. B.; Balakrishna, R.; Mutz, C. A.; Malladi, S. S.; David, S. A. *PLoS*

ONE **2012**, *7*, e43612. (f) Shukla, N. M.; Mutz, C. A.; Malladi, S. S.; Warshakoon, H. J.; Balakrishna, R.; David, S. A. *J. Med. Chem.* **2012**, *55*, 1106–1116. (g) Shukla, N. M.; Malladi, S. S.; Day, V.; David, S. A. *Bioorg. Med. Chem.* **2011**, *19*, 3801–3811. (h) Shukla, N. M.; Mutz, C. A.; Ukani, R.; Warshakoon, H. J.; Moore, D. S.; David, S. A. *Bioorg. Med. Chem. Lett.* **2010**, *20*, 6384–6386.

(7) Tanji, H.; Ohto, U.; Shibata, T.; Miyake, K.; Shimizu, T. *Science* **2013**, *339*, 1426-1429.

(8) Hemmi, H.; Kaisho, T.; Takeuchi, O.; Sato, S.; Sanjo, H.; Hoshino, K.; Horiuchi, T.; Tomizawa, H.; Takeda, K.; Akira, S. *Nat. Immunol*. **2002**, *3*, 196-200. (9) Jurk, M.; Heil, F.; Vollmer, J.; Schetter, C.; Krieg, A.; Wagner, H.; Lipford, G.; Bauer, S. *Nat. Immunol*. **2002**, *3*, 499.

(10) (a) Baltimore, D. *Cold Spring Harb Perspect Biol* **2009**, *1*, a000026. (b) Schreck, R.; Albermann, K.; Baeuerle, P. A. *Free Radic. Res. Commun*. **1992**, *17*, 221-237.

(11) Yoo, E.; Crall, B.; Balakrishna, R.; Malladi, S.; Fox, L.; Hermanson, A.; David, S. *Org. Biomol. Chem*., **2013**, *11*, 6526–6545.

(12) Bhushan, K.; DeLisi, C.; Laursen, R. *Tet. Lett*. **2003**, *44*, 8585-8588.

(13) Ralph, P.; Nakoniz, I. *J. Immunol*. **1977**, *119*, 950-954.

(b) Lee, J.; Chuang, T.; Redecke, V.; She, L.; Pitha, P.; Carson, D.; Raz, E.; Cottam, H. *Proc. Natl. Acad. Sci. U.S.A*. **2003**, *100*, 6646-6651.

(14) Burns, R.; Ferbel, B.; Tomai, M.; Miller, R.; Gaspari, A. *Clin Immunol.* **2000***, 94*: 13–23.

(15) West, M.; Wallin, M.; Matthews, S.; Svensson, H.; Zaru, R.; Ljunggren, H.; Rescottm A.; Watts, C. *Science*, **2004**, *305*, 1153-1157.

a. Higher levels of NF-κB at 2 μm for resiquimod are thought to be specific to the agonist. The discrepancy between the concentrations may be due to incomplete deprotection of NPPOC-Resiq

leading to lower RAW-Blue stimulation.

b. During the experiment, a signal decrease after UV exposure was observed; therefore, results were compared to UV-exposed resiquimod.

c. http://www.invivogen.com/PDF/RAW_Blue_TDS.pdf

d. M. P. Matheu, D. Sen, M. D. Cahalan, and I. Parker, *J. Vis. Exp*., **2008**, *17*, 773.

CHAPTER 4. *In-vivo* Applications of Photoactivation

4. 1. Objective of Present Study

Harnessing the innate and adaptive immune response has led to the development of vaccines and therapeutics.[1-3] However, as the immune system "rivals the nervous system in complexity,[4]" understanding how to design better responses and therapies remains a challenge. One area of complexity is the presentation of antigens by the innate system to the adaptive system – including chemical signaling, spatial migration and cell-cell signaling. During this process, dendritic cells, activated by Toll-like receptors (TLRs) convey pathogenic information to the cells of the adaptive immune systems through the production of cytokines and cell surface markers.[5, 6] This process involves the migration of activated DCs into lymphatics to present antigens to T-cells.[7-10] However, understanding this complex system by manipulating sets of cells within it has been a challenge. Chemical control of various innate and adaptive immune cellular processes has been a burgeoning area of interest.[11-15] Recently, we developed a method to tag and remotely induce a guided immune response (TRIGIR) with a photo-caged TLR2/6 agonist.[16] TRIGIR allows for selective labeling of cells, followed by remote light activation. Here we use the TRIGIR method for *in vivo* light-based activation to control the migration of dendritic cells. We validate our *in vivo* activation by monitoring DC migration using adoptively transferred bioluminescent DCs (Luc-DCs) that bear the TRIGIR compound.

Further, to confirm that the migrating cells were presenting antigens and further priming adaptive immune cells[17, 18], we performed RNA analysis on the target lymph-node. Reported herein is a general procedure where adoptively transferred immune cells can be remotely activated using a UV light source. Though this methodology calls for a TLR2/6 bearing cell type

and has limited tissue penetration of UV light used to activate the cells, it may find use in controlling activation of skin or subcutaneous DCs and for studying effects of inflammation within different spatiotemporal parameters. We expect that improvements in both optogenetic techniques, longer wavelength photo-cages, and light delivery methods will help expand the technique to answer many different immunological questions.

4. 2. Cell labeling with NPPOC-Pam_2CSK_4

Previous work from our lab showed that photo-caging of the N-terminus of the TLR2/6 agonist, Pam_2CSK_4[19], can inhibit its activity to activate TLR2/6. Upon light exposure and subsequent uncaging of the N-terminus, TLR2/6 is activated by the TRIGIR compound. The intercalation of the TRIGIR compound's palmityl chains[20] on TLR2 of dendritic cells allows labelling of the agonists to quiescent innate immune cells without activating TLR2/6. These labelled cells can then be used in adoptive transfer experiments to achieve remote control of inflammatory processes *via* TLR2.

We sought to adapt this technique *in vivo* by labeling cells, performing subcutaneous injection and then activating of the cells in their local environment. As the agonist stays co-localized, we can have the spatial control of agonist presentation and immune cell activation.[16]

In initial experiments, we observed that high concentration of the TRIGIR compound, NPPOC- Pam_2CSK_4 (**1**, **Figure 4. 1**a), incubation overnight resulted in higher amount of labeling of the agonist (**Figure 4. 1**d). However, this also resulted in higher background activation of the cells (**Figure 4. *1***e). Therefore, labeling the Luc-DCs at 0.1 μM (**Figure 4. 1**c) showed both good labeling and did not elicit a background immune response. (**Figure 4. 1**d, e)

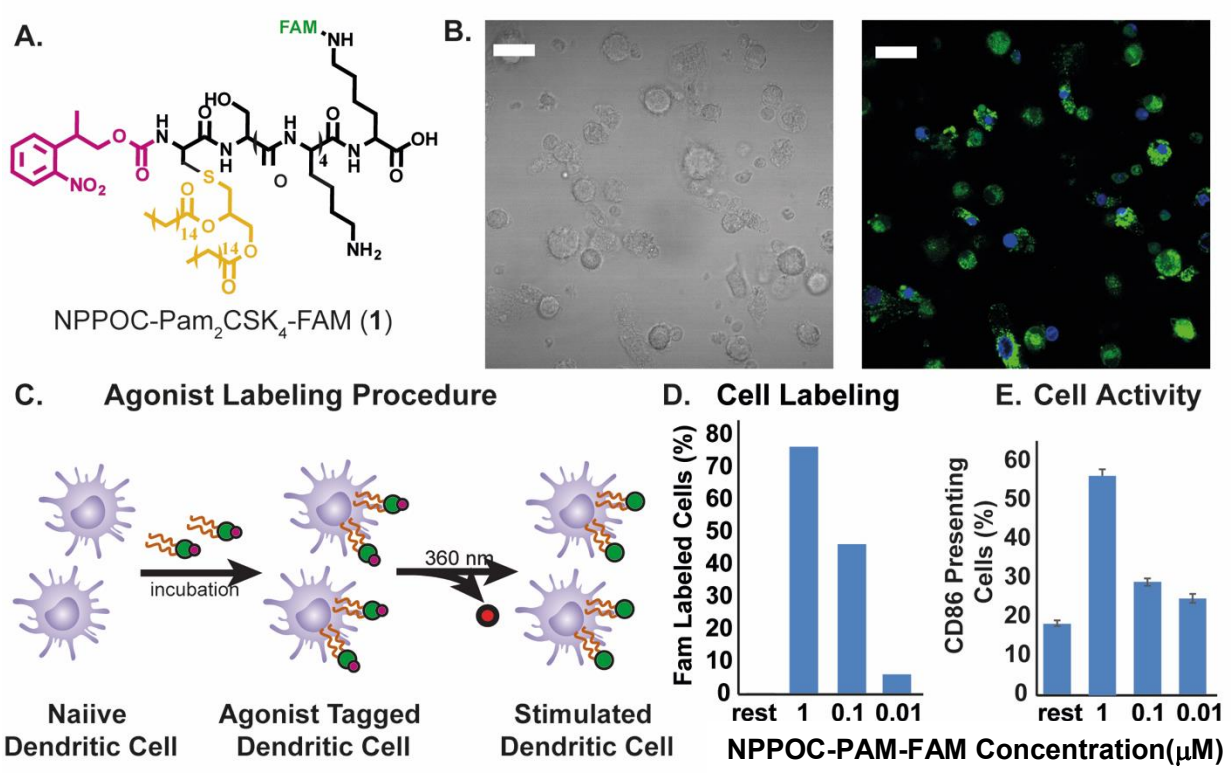

Figure 4. 1. (a) Structure of photo-caged TLR 2/6 agonist NPPOC-Pam_2CSK_4 (**1**) with fluorescein tag, (b) bright field and fluorescent microscopic image of labeled DCs (green-**1**, blue-DAPI, scale bar 10 μm), (c) NPPOC-Pam-FAM labeling procedure (d) Efficiency of agonist labeling, (e) background CD86 presentation induced by labeling DCs.

4. 3. Photo-activation of Transferred Dendritic Cells

Before adoptive transfer, the DCs were incubated with **1** over-night. The cells were then washed to remove excess **1** in the supernatant. The labeled cells were then injected into the footpad of mouse at 1 million cells/30 μL. To activate the cells with light, the injected footpad of mice was then irradiated with 360 nm light for 15 mins. To determine the limit of activity due to the limit of UV light tissue penetration, we irradiated labelled cells with 360 nm light for 15 min *in vitro* before injection. This experiment served as a "pre-activated" control and served as an upper limit for what might be achieved with photo-activated DCs *in vivo*. During the imaging process, following previously reported procedures,[21] we blocked the bioluminescence occurring from the injected foot with black tape to enhance the signal from the popliteal lymph node (**Figure 4. 2**).

To understand the activity of mature DCs, we compared the migration of the Pam_2CSK_4 stimulated DCs and non-stimulated DCs that were adoptively transferred into the footpad of a mouse over a period of 96 hrs. We found the Pam_2CSK_4 stimulated Luc-DCs migrate faster than the unstimulated Luc-DCs, where we observed migration activity as early as 24 h in Pam_2CSK_4 stimulated Luc-DCs with a slow migration, over 96 hrs, of the unstimulated DCs into the draining lymph node at later time points. (**Figure 4. 3**a, b) Because activation of dendritic cells leads to upregulation of cell surface receptors that aid in the migration and translocation of DCs into the lymph node[22], we theorize that a shorter time is required for the activated cell to migrate into the lymph node compared to the unstimulated DCs.

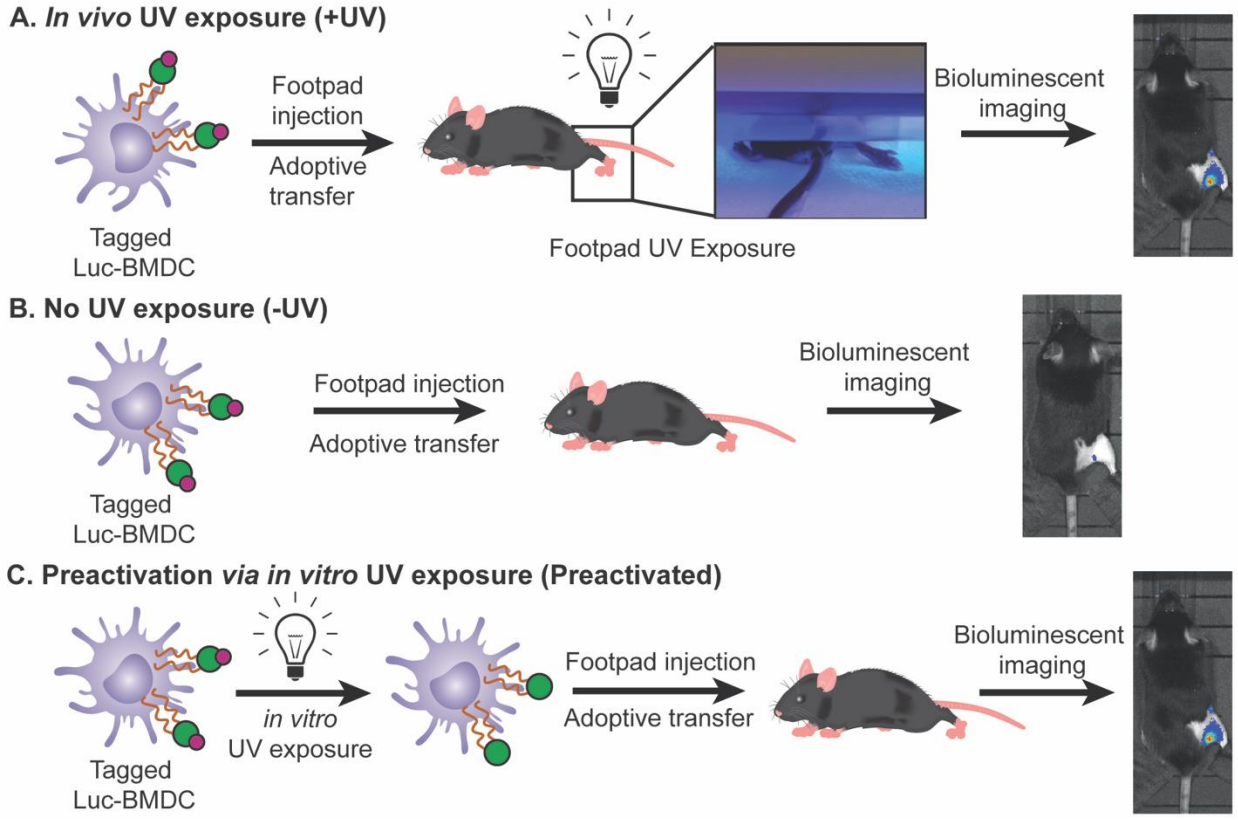

Figure 4. 2. TRIGIR DC adoptive transfer procedures for (a) footpad UV irradiated mouse following adoptive transfer, (b) mouse with no UV irradiation, and (c) Mice injected with pre-irradiated tagged DCs.

We sought to determine if light-activation of TLR2 *via* **1** *in vivo* recapitulated the migration of activated DCs. We imaged the migration of the Luc-DC in mice whose footpads were exposed to UV light (+UV) or not exposed to UV (-UV). Following the trends seen in the Pam_2CSK_4 stimulated cells, the footpads which were directly exposed to UV showed migration of Luc-DCs into the popliteal lymph node much sooner than that of the non-exposed footpads. (**Figure 4. 3**a, c) Additionally, the cells that were exposed to UV migrate at a similar rate as the cells that were photo-activated before being transferred into a mouse. From this data, we conclude that TRIGIR labelled cells can be activated with light in a non-invasive manner and recapitulate the timing and quantity of their migration to the lymph node.

4. 4 Confirmation of Systemic Activation *via* Gene Expression Analysis of Popliteal Lymph Node

To further confirm the inflammatory state of TRIGIR activated DCs *in vivo* by light, we harvested popliteal lymph nodes from the mice and analyzed the RNA levels. This measurement also helped us determine if the activated DCs were enacting their antigen presenting role. If the cells were activated following light exposure, the migrated cells will elicit a systemic response as recruitment and maturation of adaptive immune cells occurs in the lymph node. We harvested lymph nodes from both light irradiated and non-irradiated animals which all contained TRIGIR-labeled DCs identical to our previous experiments. To determine differences, we plotted the changes as a relative fold-change of the from irradiated:non-irradiated at each time point (**Figure 4. 4**). Using this measurement, we determined how irradiation and TLR stimulation changed activity in the lymph node.

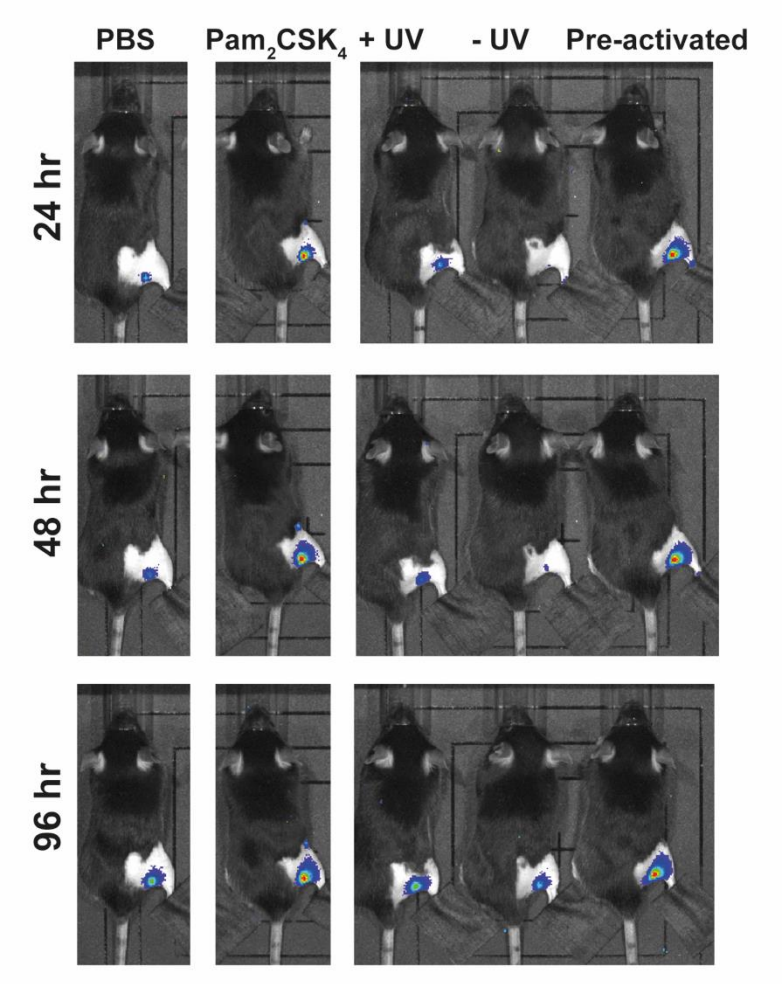

Figure 4. 3. Bioluminescent image of mice taken every 24 h, over 96 h. Control mice include a set of 6 mice injected with DCs preconditioned with Pam_2CSK_4, and a set of 6 mice injected with DCs with no preconditioning. The test set includes a set of 6 mice with TRIGIR labeled DCs followed by light exposure (+ UV), one with no light exposure (-UV), and a mouse injected with TRIGIR labeled DCs exposed to light before footpad injection (pre-activated).

First, we observed that upon TRIGIR activation, there is a gradual increase in ccr7 which is upregulated by immune cells that enter the lymph node through recognition of CCL19 and CCL21 on the lymph node (**Figure 4. 4**a).[23-25] From this we conclude there are more ccr7 producing cells recruited into the lymph node. These cells are likely the TRIGIR activated dendritic cells which we observed migrate to the lymph node as well as T cells that have been recruited into the lymph node within the first 72 h after UV exposure as a result of DC activation.

We saw further evidence for T cell recruitment upon TRIGIR activation with an increase of *cd34* and *cd28* within the same period. CD34 is required for T cells to enter the lymph node while blocking DC migration into the lymph node.[26] The downregulation of cd34 at early time points matches the increased migration of the stimulated DCs from the footpad into the lymph node (**Figure 4. 4**b). The gradual increase suggests the increase of T cell trafficking into the lymph node and decrease in DC migration from the footpad.

Similar to the *cd34* trends, we saw a gradual increase in *cd28*, a T cell receptor that recognizes CD80 and CD86.[27], reaching a maximum after 72hrs (**Figure 4. 4**c). This gradual rise indicates the increase in T cell population in the popliteal lymph node. These trends follow known T cell maturation and migration following mature DC contact in the lymph node.[28]

In comparison, there is a general upregulation of *nfkb1*[29, 30] starting as early as 48 hours, which could be due to the inflammatory signaling from the activated dendritic cells that have migrated into the popliteal lymph node (**Figure 4. 4**d).

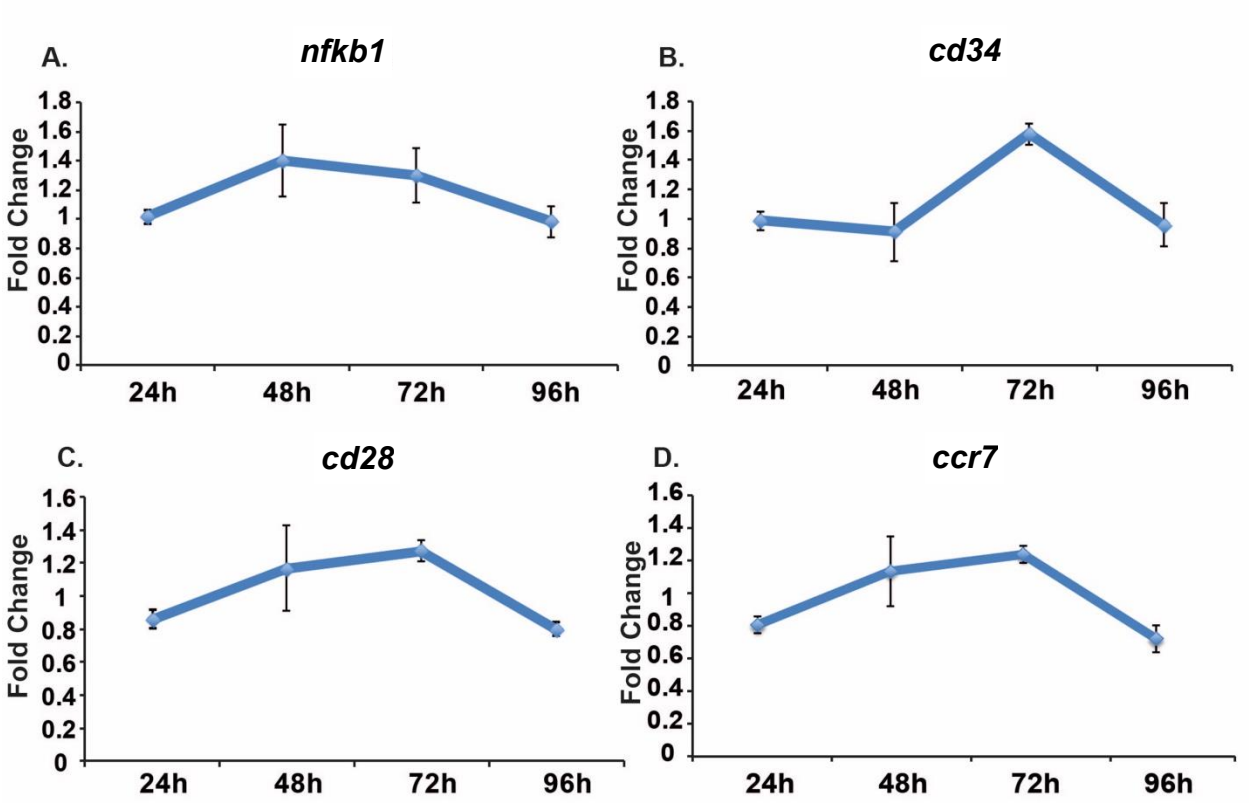

Figure 4. 4. Change in gene profile in harvested lymph node of tested mice. Fold change determined by the ratio of UV irradiated and non-irradiated mice at each time point (n=6) of *nfkb1* (a), *cd34* (b), *cd28* (c), and *ccr7* (d).

4. 5. Effect of Multiple Irradiation and Adoptive Transfer

After confirming the antigen presenting function of the migrated DCs in the lymph node, we wanted to measure if we can get a dose dependent change in immune response from multiple irradiations. Additionally, we explored the systemic effect of light induced immune cell activation by harvesting the draining lymph node (popliteal lymph node) and analyzing the change in cell population within the lymph node. In this study, we analyzed $CD4^+$, $CD8^+$ T cells and $B220^+$ cells through fluorescent antibody staining.

The experimental set up is parallel to the initial irradiation experiment (**Figure 4. 2**) with the addition of a double exposure group. The mice in the double exposure group are irradiated 24 h following the first exposure at the time of adoptive transfer. In designing the experiment, we incorporated two no irradiation controls. These controls are to normalize the amount of time after the adoptive transfer which effects the time the cells reside in the footpad. The mice were sacrificed at 1, 3, and 7 days following the last irradiation step and the draining lymph nodes and spleens were harvested (**Figure 4. 5**).

The harvested tissues were subsequently dissociated *in vitro* and $CD4^+$, $CD8^+$, and $B220^+$ cells were analyzed through fluorescence assisted cell sorting. The cell population for the adoptive immune cells in the spleen showed no difference of any of the irradiation conditions tested (**Figure 4. 5**). This was concurrent with the lack of change in the cytokine production analyzed from the collected serum from each mouse (**Figure 4. 16**). Therefore, we did not see a prevalent systemic change induced from the light induced immune cell activation procedure.

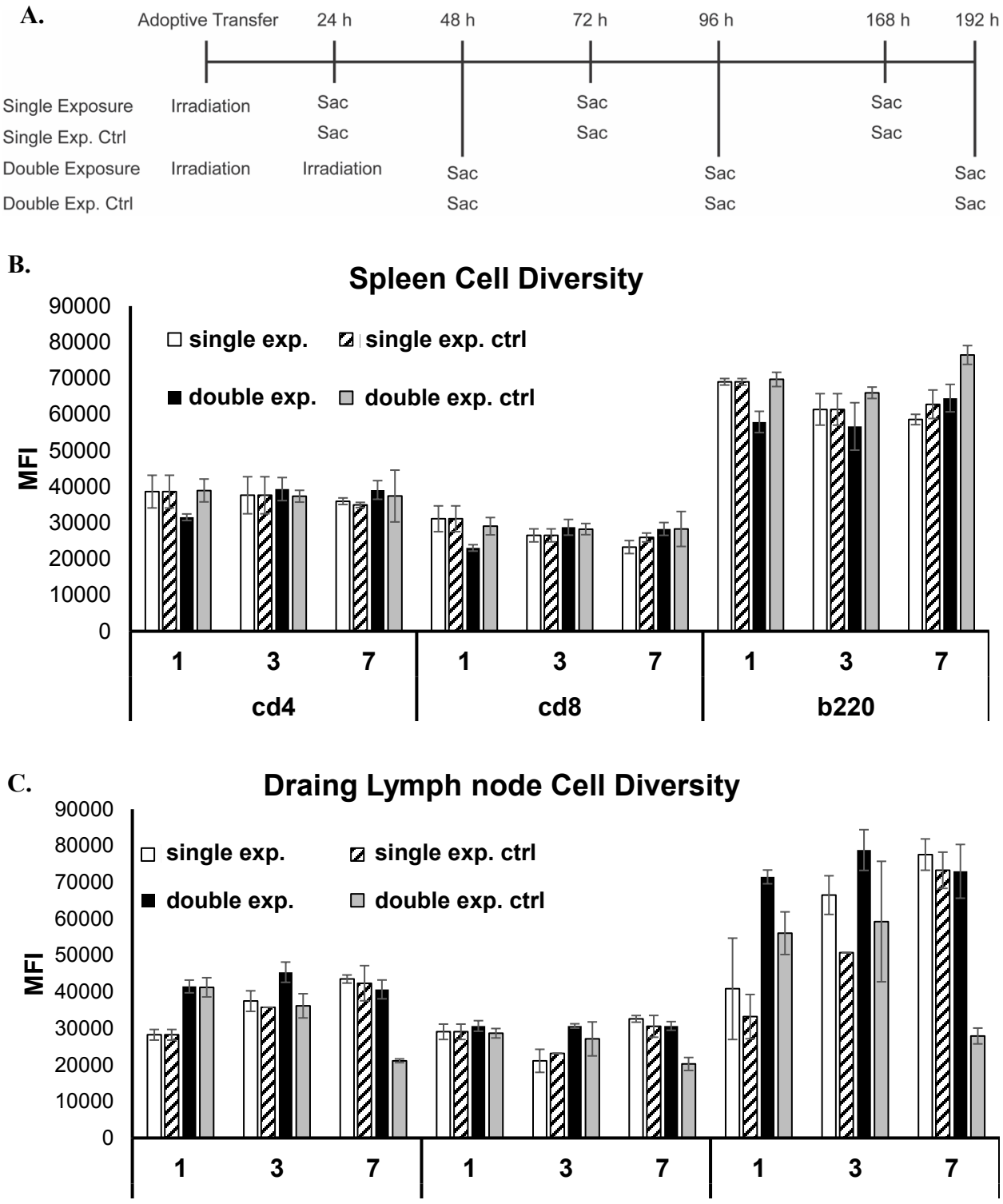

Figure 4. 5. Understanding the effect of multiple irradiation. (a) Experimental procedure. Analysis of change in cell diversity ($CD4^+$, $CD8^+$ T cells and $B220^+$ cells) in the (b) spleen and (c) draining lymph node.

At a more local level we analyzed the population of the adoptive transfer cells in the harvested draining lymph node. Similar to the observations from the spleen, for the $CD4^+$, $CD8^+$ T cells, we did not observe a difference between the irradiated, non-irradiated, or double exposure mice. Interestingly, we observed a difference between the single exposed and double exposed populations $B220^+$ cells (**Figure 4. 5**). The double exposure induced an increase in $B220^+$ cells compared to both the single irradiation control and non-irradiated controls.

Moving forward, we aimed to optimize the amount of time between each irradiation. We shortened the irradiation to 1 hr intervals based on findings reporting Pam_2CSK_4 stimulated TLR2 activation induces NF-κB activation within 45 mins (**Figure 4. 6**).[31] We hypothesized an additional irradiation following the activation of NF-κB. In this study, we also added an additional triple irradiation group. Additionally, the irradiations were performed on the same day as the adoptive transfer due to the increase in cell population observed from background migration of DCs. Following adoptive transfer and irradiation, we harvested the draining lymph node 1 and 3 days after the activation event. The 7-day time point was excluded due to the lack of change in cell population at time points longer than 72 h.

However, we did not observe difference among the different irradiations at shorter intervals (**Figure 4. 6**). A slight increase in $B220^+$ cells after triple exposure can be observed, however, there is no significant change in the T cell populations. Therefore, 1 h irradiation interval may be too short. Though we maybe prompting light mediated NF-κB activation, we are not considering the time for the activated cell to produce the chemical signals necessary to direct the necessary immune response.

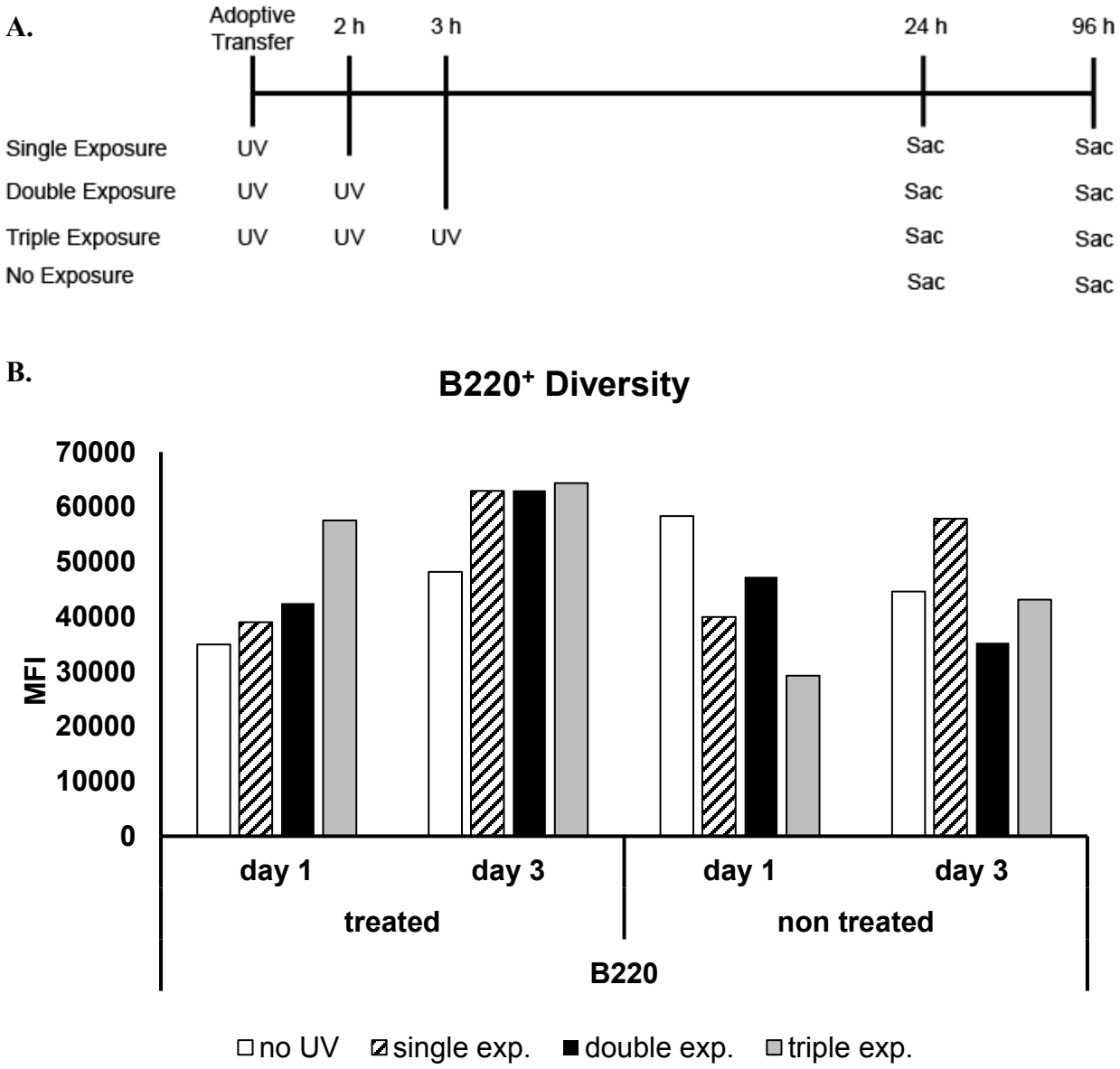

Figure 4. 6. Effect of short irradiation intervals in multiple irradiation. (a) Experimental setup. (b) Change in $B220^+$ in the harvested draining lymph node. See **Figure 4. 20** for T cell change.

4. 6. Antigen Administration

Due to the consistent change in $B220^+$ cells in the draining lymph node we co-administered Ovalbumin (OVA) with the TRIGIR labeled DCs in the footpad. This experiment would allow us to analyze anti-OVA antibodies which should correlate with the change in $B220^+$ cells. With the increase in antibody generating cells due to irradiation, we expect an increase in immune activity against the administered antigen. Additionally, the anti-OVA would offer a better systemic readout compared to analyzing the cytokines circulating in the blood.

The OVA was administered in PBS at 100 μg per mouse with the TRIGIR labeled cells. In this study we also included naive DCs and Pam_2CSK_4 stimulated DCs administered with OVA to fully understand the effect of Pam_2CSK_4 activated DC on OVA immunization as well as the effect of the adoptive transfer procedure, injection of cells into footpad, itself. Serum was collected 1 and 14 days following adoptive transfer.

From the anti-OVA titer (IgG, IgA, IgM) we can see a marked difference in anti-OVA production following adoptive transfer. The mice immunized with OVA only, produced less anti-OVA at both time points compared to mice co-administered with dendritic cells. Within the adoptive transfer groups, we can see that the addition of Pam_2CSK_4 activated cells with OVA induces a robust anti-OVA compared to that of naïve DCs as well as TRIGIR labeled and non-irradiated groups. Within the irradiated groups, through the single exposure groups did not show a difference in anti-OVA production, the double exposure groups showed increased anti-OVA production (**Figure 4. 7**).

However, due to the variability of the anti-OVA levels detected from mouse to mouse within the same test group, more test subjects are needed for a more definitive effect of light induced cell activation and adoptive transfer procedure.

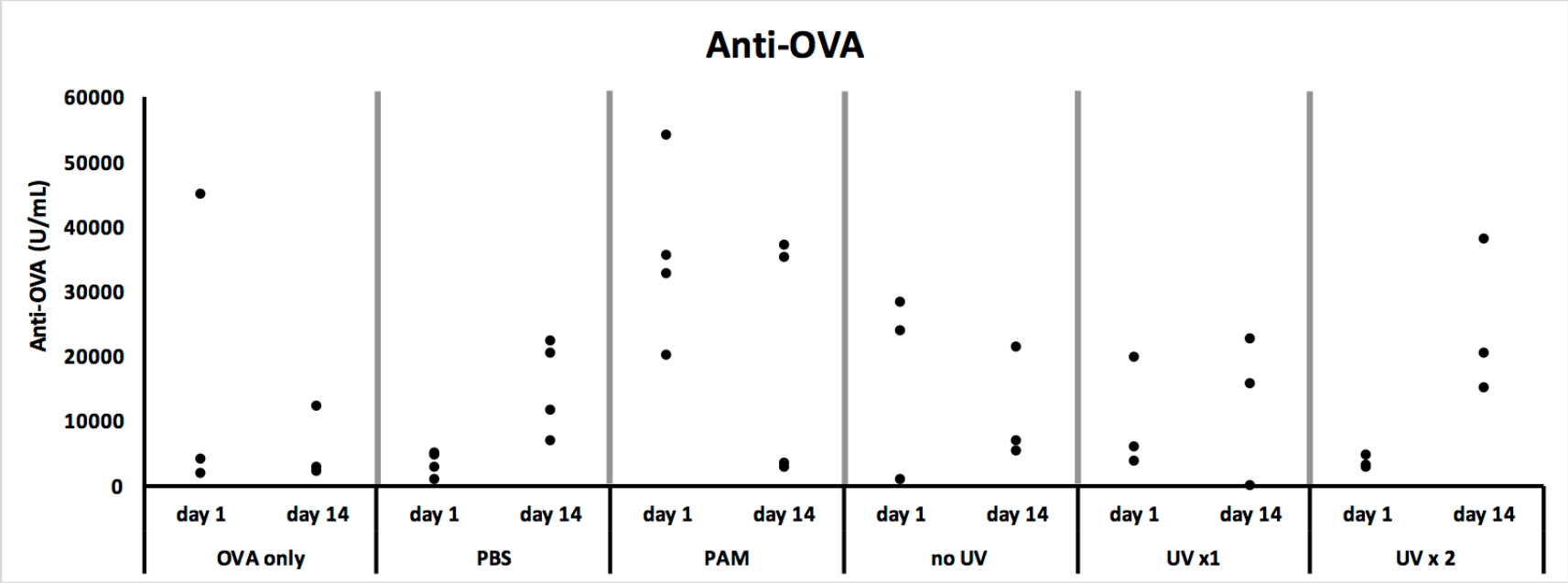

Figure 4. 7. Production of Anti-OVA (IgG, IgM, and IgA) of OVA immunized mice. Test groups include, OVA immunized only (n =3), naïve DC +OVA (n=4), Pam2CSK4 stimulation DC +OVA (n=4), TRIGIR labeled and non-irradiated cells +OVA (n=3), labeled and single exposure (n=3) and double exposure (n=3) mice.

4. 7. Lymphocyte Cytokine Production

In addition to the anti-OVA titer, we were interested in investigating the local production of cytokines within the lymph node. Because cytokine production seems to be more concentrated in the vicinity of the adoptive transfer and irradiation, we performed *ex-vivo* cell culture of the harvested lymph nodes.[32, 33] Cytokine analysis includes Th1 polarizing (IFNγ) and Th2 polarizing cytokines (IL-4, IL-10). This will confirm the change in immune response from the light activated immune cells against the administration of an antigen.

In conjunction with the serum collection, draining lymph nodes were harvested 1 and 14 days following OVA immunization and adoptive transfer. The lymph nodes were then digested with collagenase and the remaining lymphocytes were rinsed and cultured in a 12 well plate. Supernatant was collected after 48 h of culture to detect IL-4, as well as 72 h for the detection of IL-10 and IFNγ.

For Th1 polarizing IFNγ levels were detected from Pam_2CSK_4 activated DCs as well as irradiated DCs as early as 24 h following adoptive transfer procedure while naïve DCs and non-irradiated DCs produced no IFNγ (**Figure 4. 10**). After 14 days of adoptive transfer and immunization, there is a general increase in IFNγ production from all test groups.

Th2 polarizing cytokines, IL-4 and IL-10 were not produced from any of the test groups after one day of immunization and adoptive transfer. After 14 days of immunization, there is an increase in IL-4 production from all test groups excluding the non-irradiated group. A similar trend is also observed in the change in IL-10 production (**Figure 4. 8**, **Figure 4. 9**). Though there is variability in the data, the non-irradiated group, there is more IL-10 production from the other groups. This may indicate an inhibitory role of the TRIGIR label on the DCs over a long period (14 days).

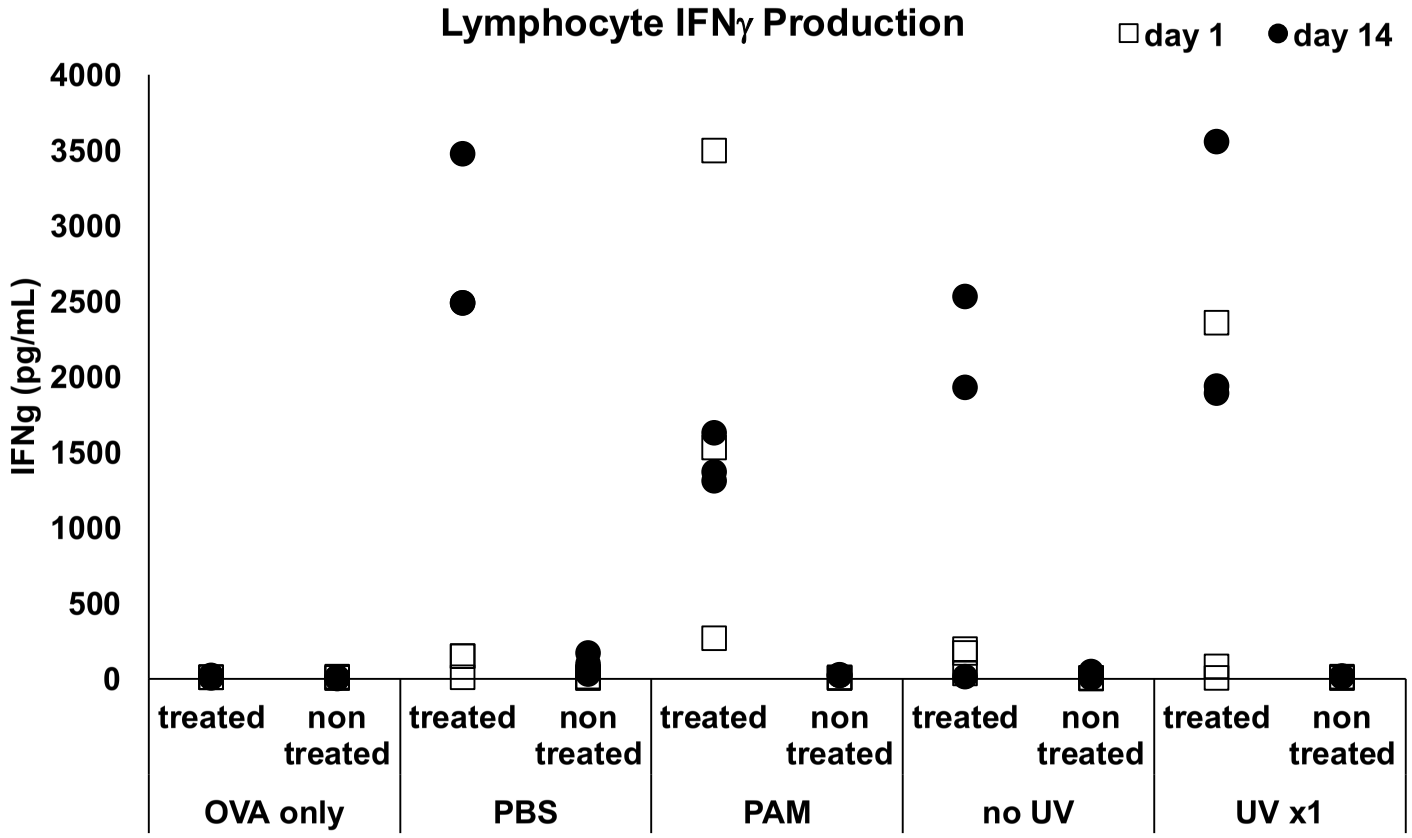

Figure 4. 8. IFNγ production of harvested draining lymph nodes following OVA immunization and adoptive transfer of labeled DCs. The lymph nodes were harvested after 1 (□) and 14 days (•) of adoptive transfer cultured ex-vivo. Test groups include, OVA immunized only, naïve DC +OVA, Pam_2CSK_4 stimulation DC +OVA, TRIGIR labeled and non irradiated cells +OVA, labeled and single exposure, and double exposure with 3 mice per group.

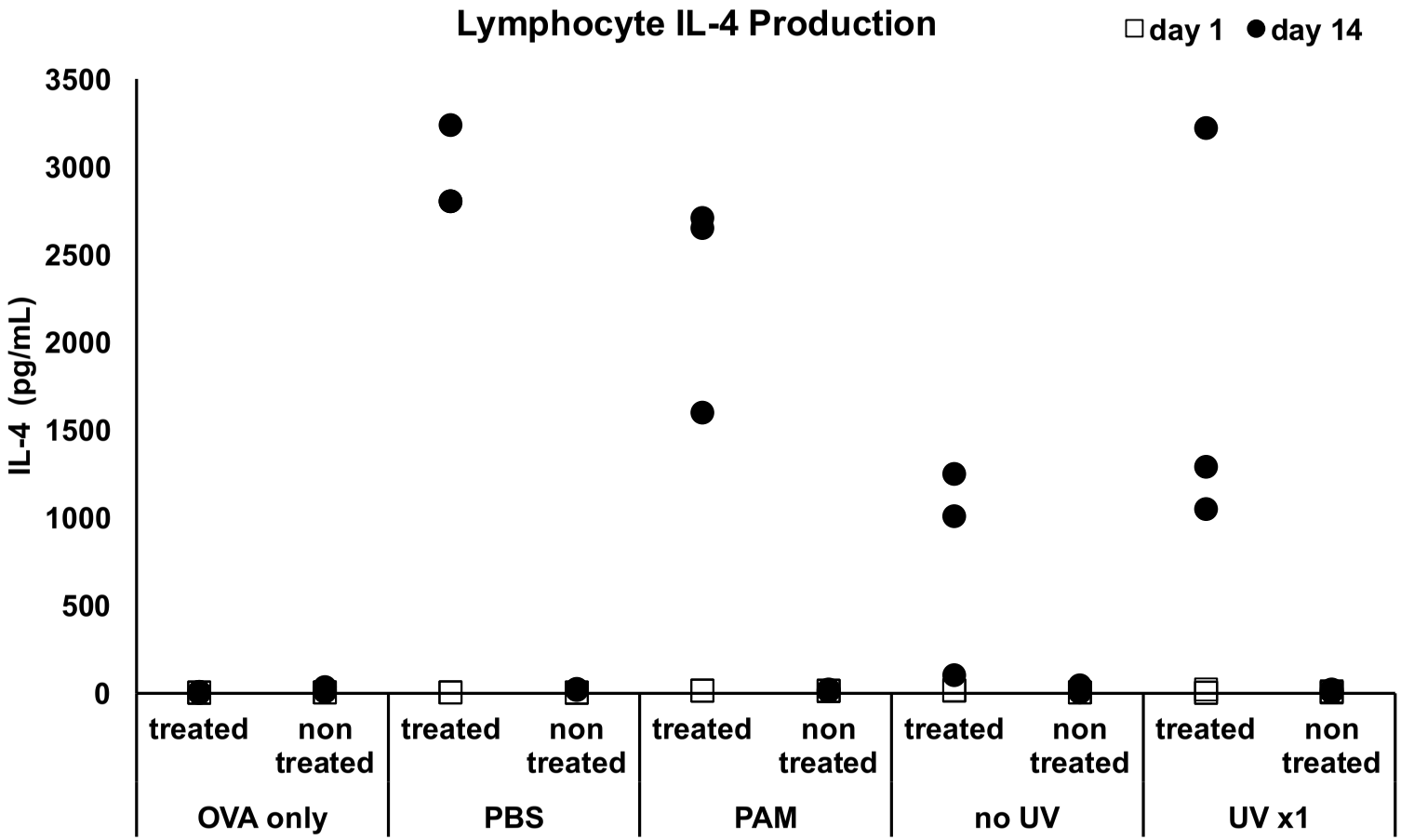

Figure 4. 9. IL-4 production of harvested draining lymph nodes following OVA immunization and adoptive transfer of labeled DCs. The lymph nodes were harvested after 1 (□) and 14 days (•) of adoptive transfer cultured ex-vivo. Test groups include, OVA immunized only, naïve DC +OVA, Pam_2CSK_4 stimulation DC +OVA, TRIGIR labeled and non irradiated cells +OVA, labeled and single exposure, and double exposure with 3 mice per group.

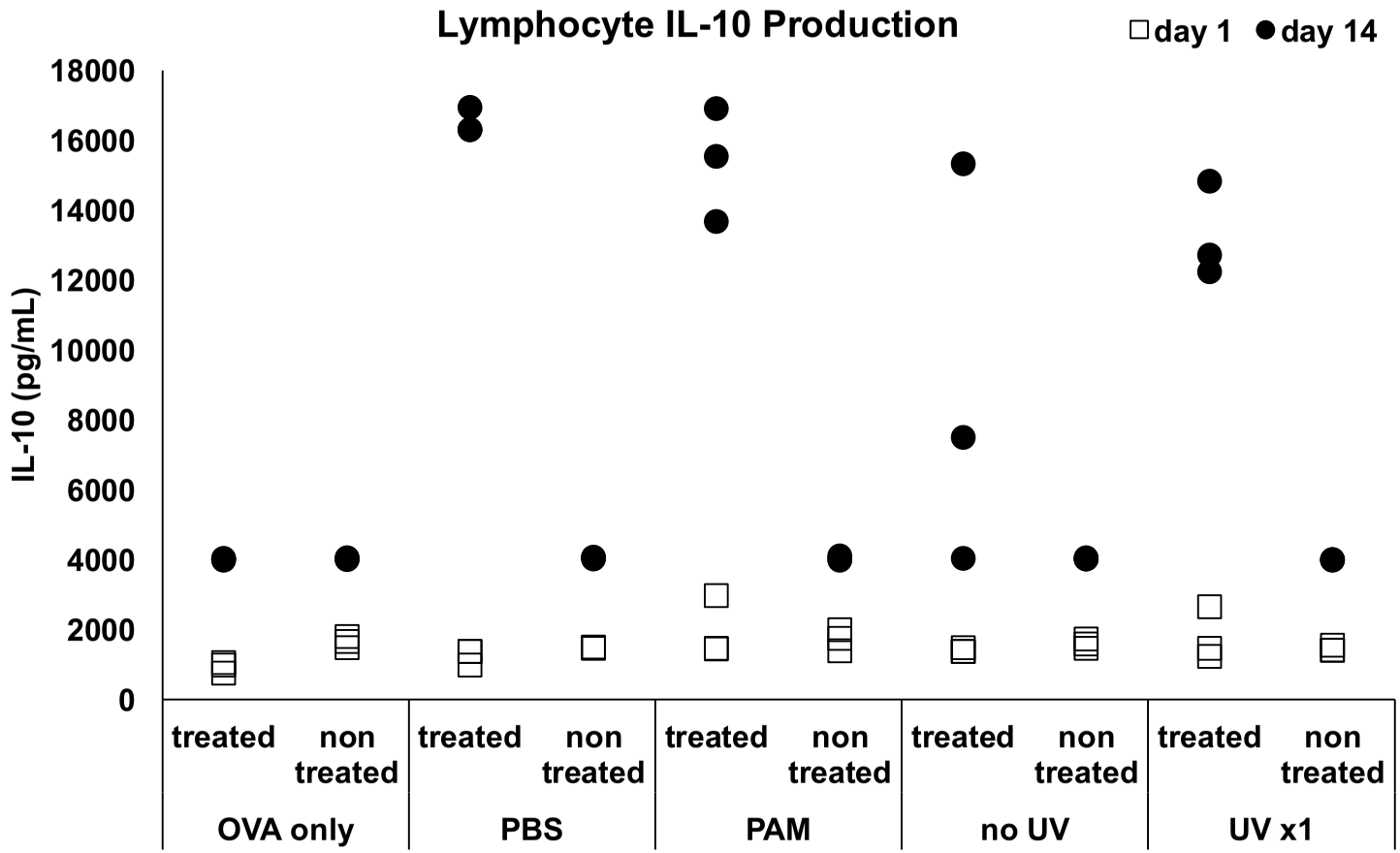

Figure 4. 10. IL-10 production of harvested draining lymph nodes following OVA immunization and adoptive transfer of labeled DCs. The lymph nodes were harvested after 1 (□) and 14 days (•) of adoptive transfer cultured ex-vivo. Test groups include, OVA immunized only, naïve DC +OVA, Pam_2CSK_4 stimulation DC +OVA, TRIGIR labeled and non irradiated cells +OVA, labeled and single exposure, and double exposure with 3 mice per group.

As observed in the anti-OVA studies, there is also marked variability within each test group. Therefore, more test subjects are needed for a more definitive effect of light induced cell activation and adoptive transfer procedure. Additionally, the lymph culture protocol can be enhanced to optimize the viability of the cells that are cultured for multiple days at a time. This can help reduce the variability of the amount of cytokine detected.

4. 8. Conclusion

With our method of *in vivo* photo-activation of immune cells, we delivered a photo-caged, TRIGIR agonist and activated it in a non-invasive manner with light. Using the TRIGIR method of tagging cells, we can overcome the limitation of spatial control of soluble agonists as well as site-specific cell delivery. Compared to conventional adoptive transfer methods that require activation of cells prior to transfer to the animal our method allows for less steps in preparation of the transferred cells and controls when the cells will be activated following adoptive transfer. In addition to temporal control of cell activation, this method offers for the potential of light dosage dependent mitigation of inflammatory signals where longer irradiation times would activate more cells, allowing for sustained activation without the increasing inflammatory response.

This method can also be applied to a variety of cells to induce different responses to TLR2/6 activation. Because TRIGIR is cell specific, but requires labeling, it is compatible with many different primary cell types that can be adoptively transferred. By changing the types of cells and cell populations, one can dissect not only endocrine signaling, but also paracrine signaling following light activation of cell subsets. The technique will not limit researchers to adoptive transfer in the footpad but can create a depot of tagged, subcutaneous cells placed close to an area of interest and gain spatial and temporal control of elicited cellular response. We offer the

clear caveat that current photo-activation methods will limit this method to dermal or subcutaneous activation of innate immune cells. Our data suggest that this technique will give researchers the potential to customize an innate cellular response depending on the target disease or immunological model. In conclusion, we present a method for light activation of adoptively transferred cells *via* TLR2/6. This technique presents a unique way to answer spatial and temporal questions about the innate immune response.

4. 9. Supplementary Experimental Data

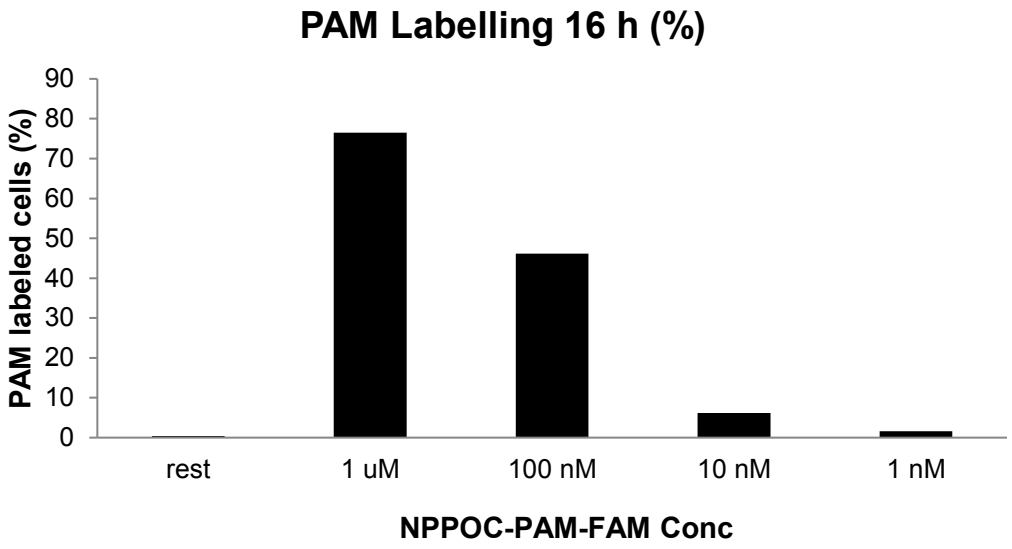

Figure 4. 11. NPPOC-Pam-FAM labeling measured *via* flow cytometry with changing NPPOC-Pam-FAM concentrations. DCs incubated with NPPOC-Pam-Fam overnight.

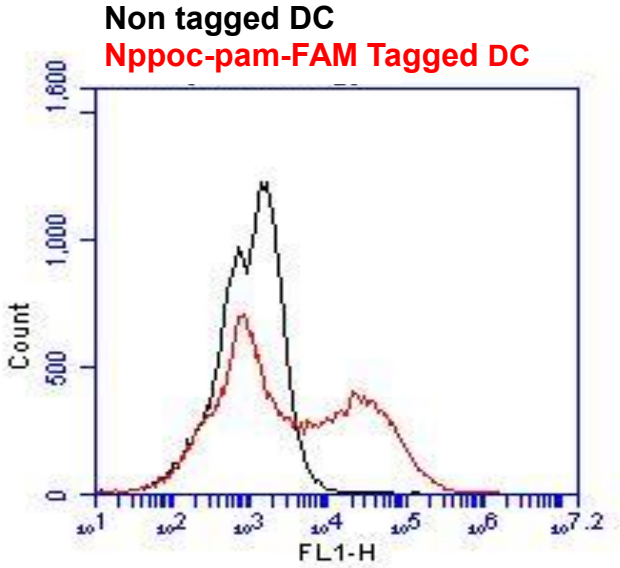

Figure 4. 12. Flow cytometry plot of non-tagged DC (black) and NPPOC-Pam-FAM tagged DC (red).

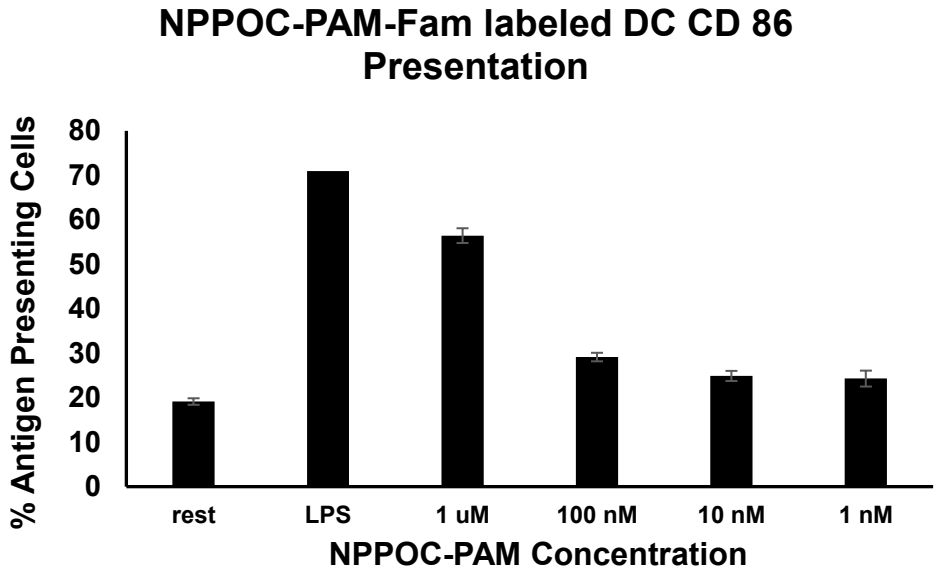

Figure 4. 13. To measure the background activation from the labeling procedure alone (no irradiation), CD86 presentation of DCs tagged with NPPOC-Pam-fam over 16 hrs was measured.

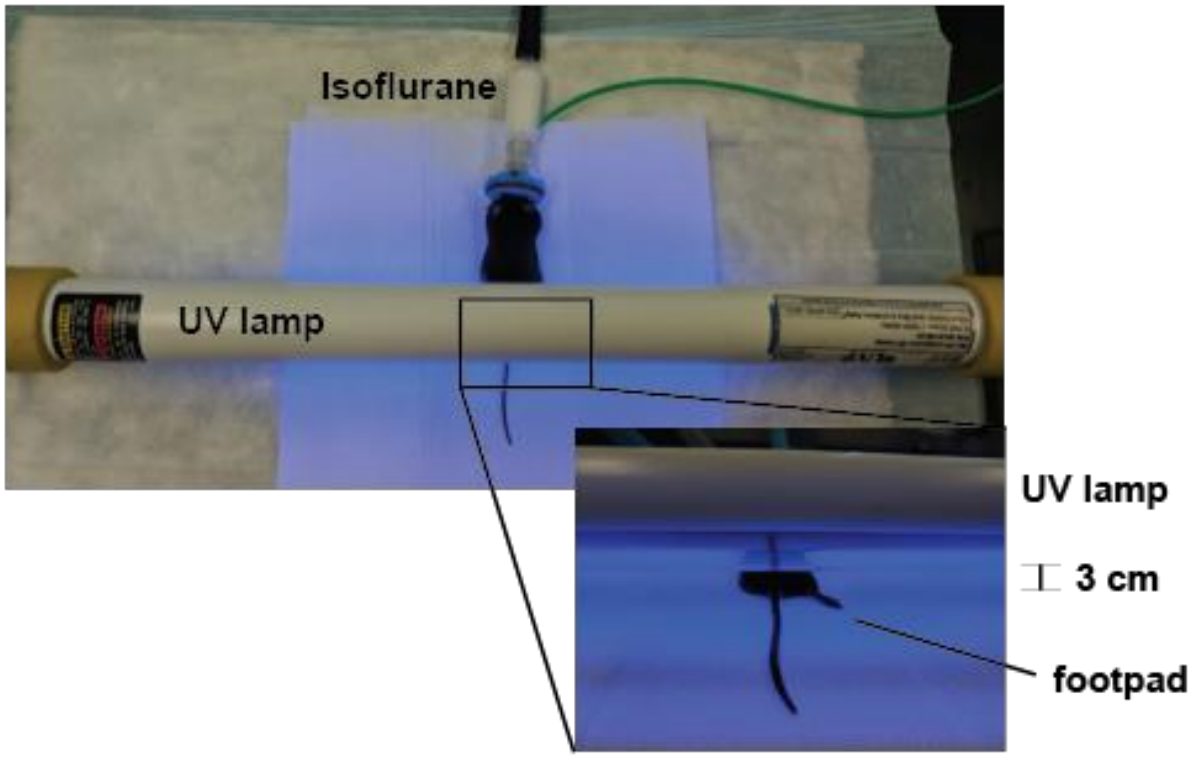

Figure 4. 14. Mouse irradiation set up

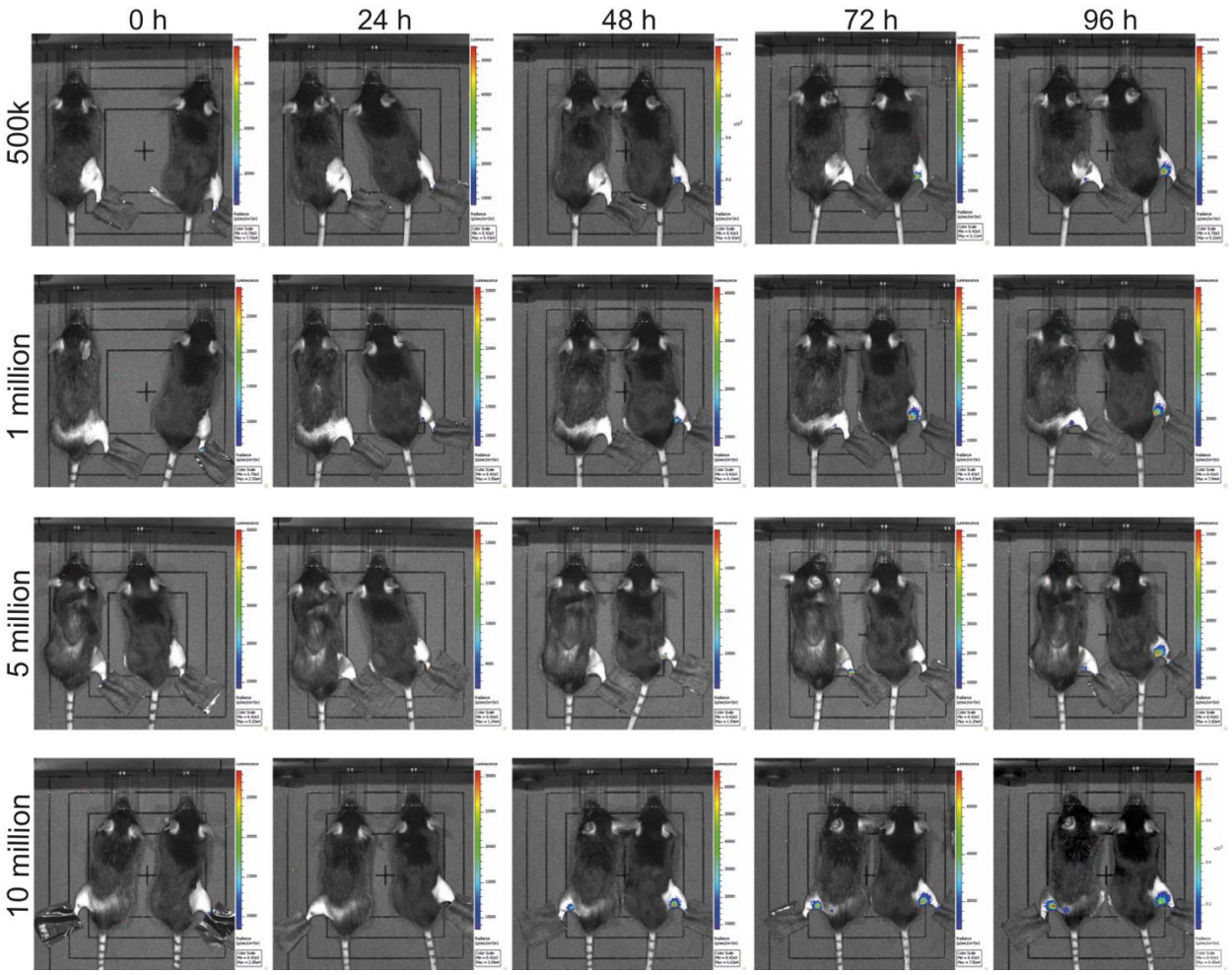

Figure 4. 15. Optimization of cell concentration of adoptive transfer (n=2). Mice injected with $1x10^7$cells showed migration as early as 48 hrs. Migration was similar for concentrations of $5x10^5$, $1x10^6$, and $5x10^6$, however we chose to perform all adoptive transfer assays at $1x10^6$, as previous studies reported loss in efficiency of cell expansion and activity of footpad injected DCs at concentrations higher than $2x10^6$.

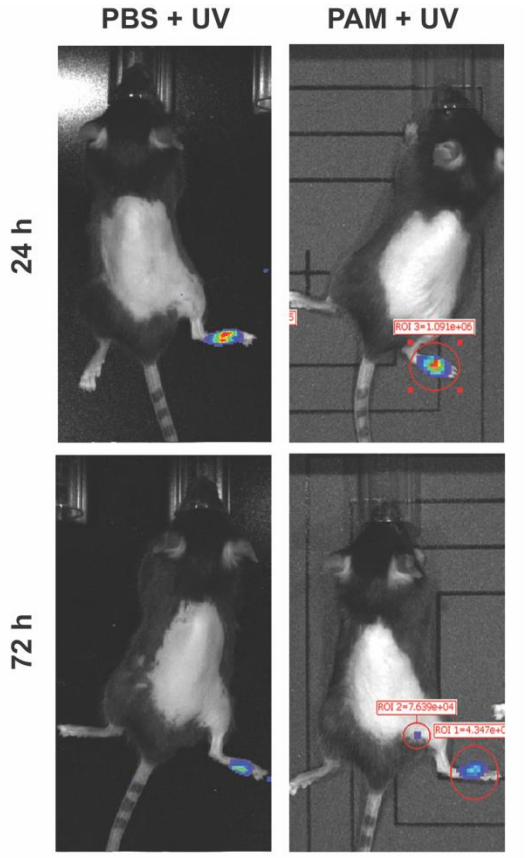

Figure 4. 16. No light dependent migration of control of UV irradiated non-stimulated BMDC (PBS) following footpad injection over 72 hrs was observed.

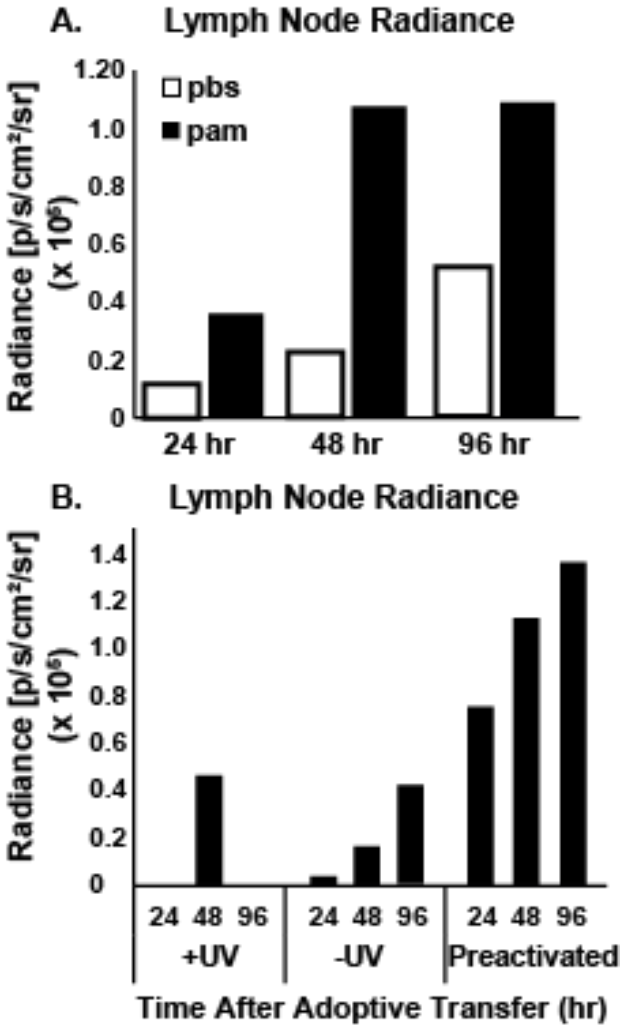

Figure 4. 17. Representative image of radiance of popliteal lymph node following adoptive transfer. (a) Radiance of lymph nodes of non-stimulated DC and Pam_2CSK_4 stimulated DC transferred mice. (b) Radiance of lymph nodes of irradiated, non-irradiated, and pre-activated mice. Data taken from representative group.

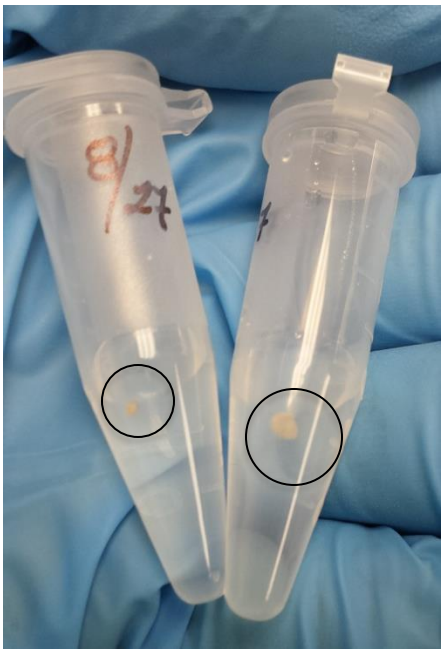

Figure 4. 18. Popliteal lymph node of non-injected footpad (left) and DC injected side popliteal lymph node (right), harvested 96 h after adoptive transfer.

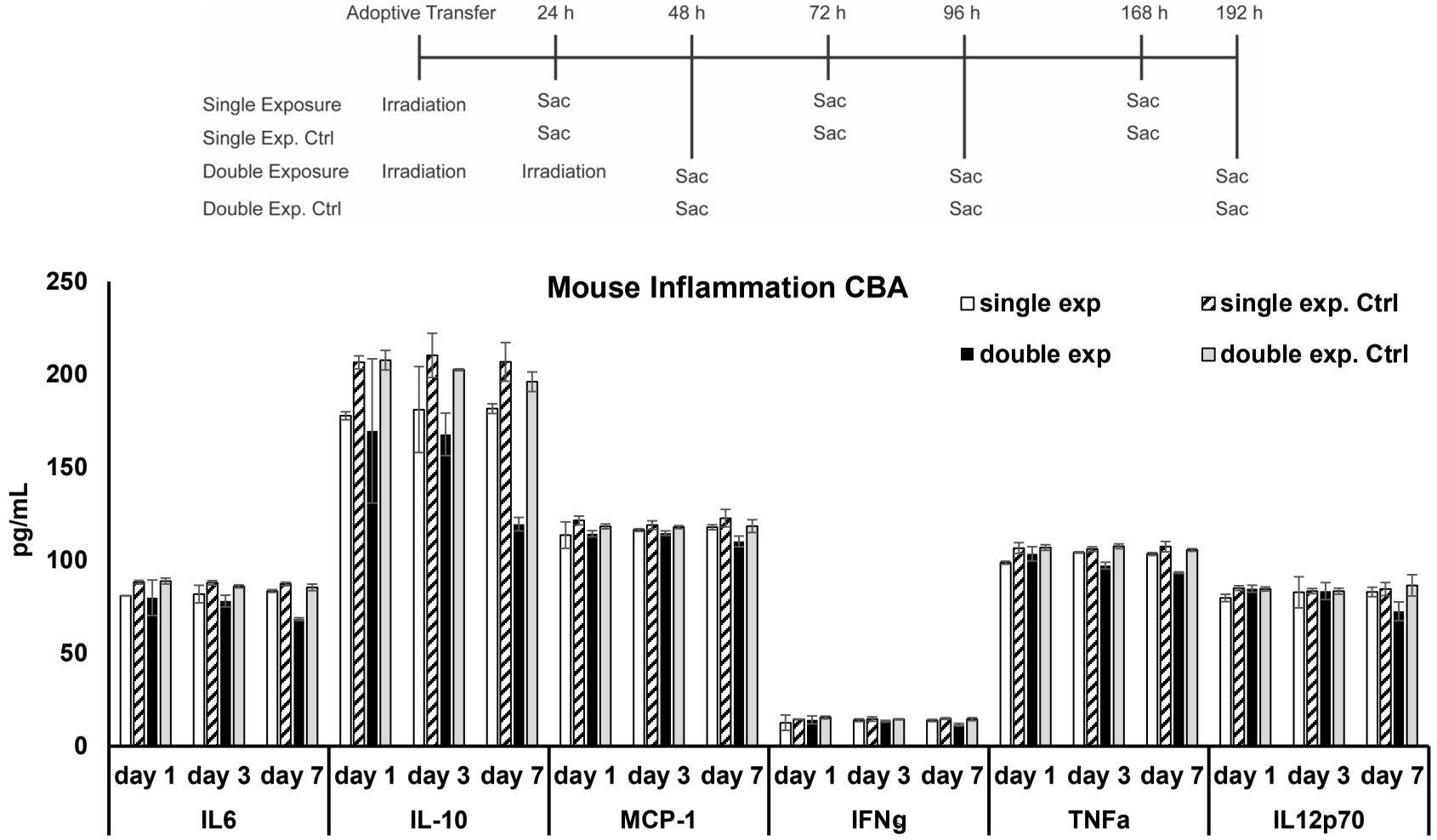

Figure 4. 19. Cytokine analysis of multiple exposure from serum collected from each mouse. Each group consists of 3 mice.

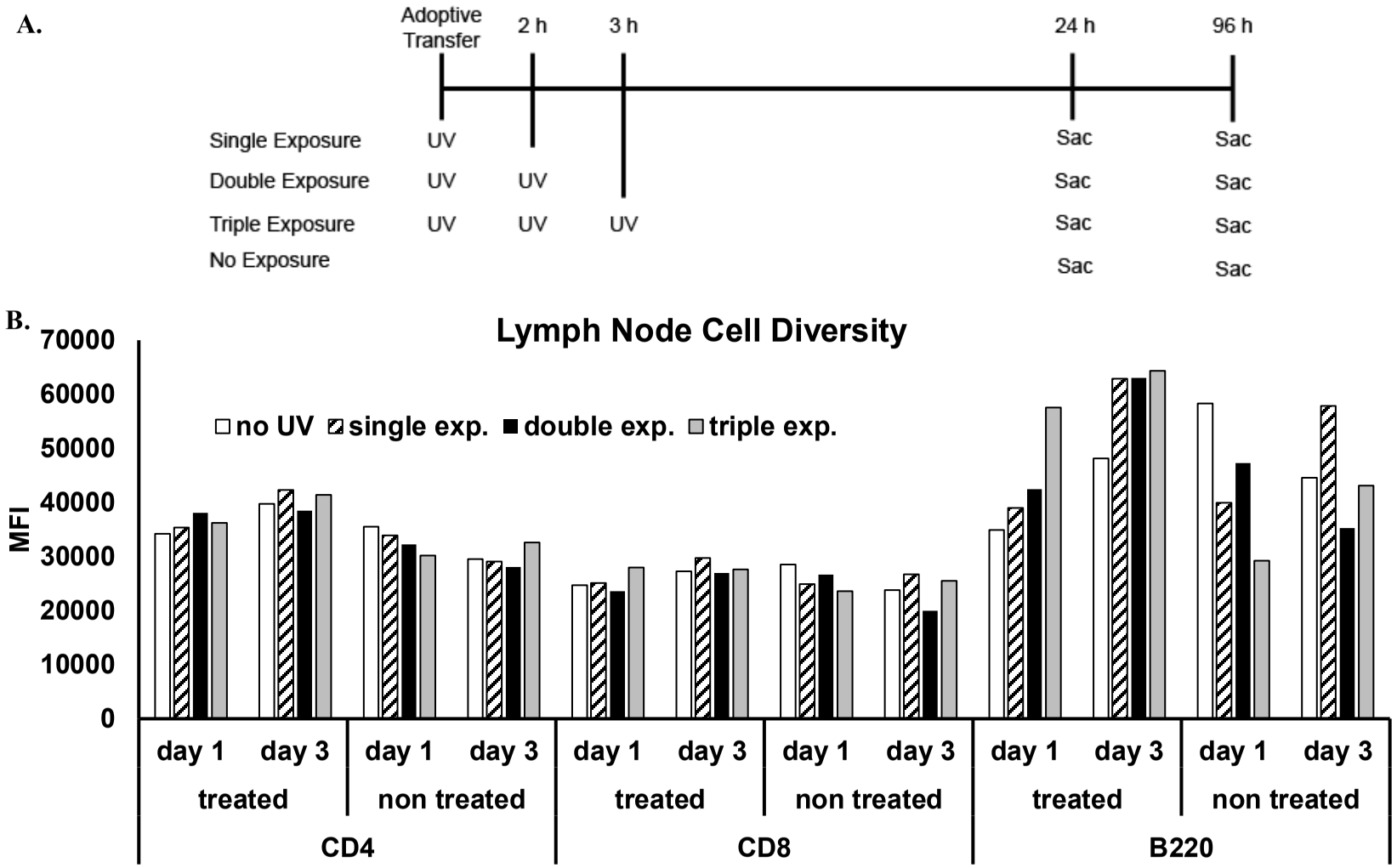

Figure 4. 20. Change in cell diversity following multiple exposures at 1 h intervals. (a) experimental set up, (b) Analysis of change in cell diversity ($CD4^+$, $CD8^+$ T cells and $B220^+$ cells) in the draining lymph node. Each group consists of 2 mice.

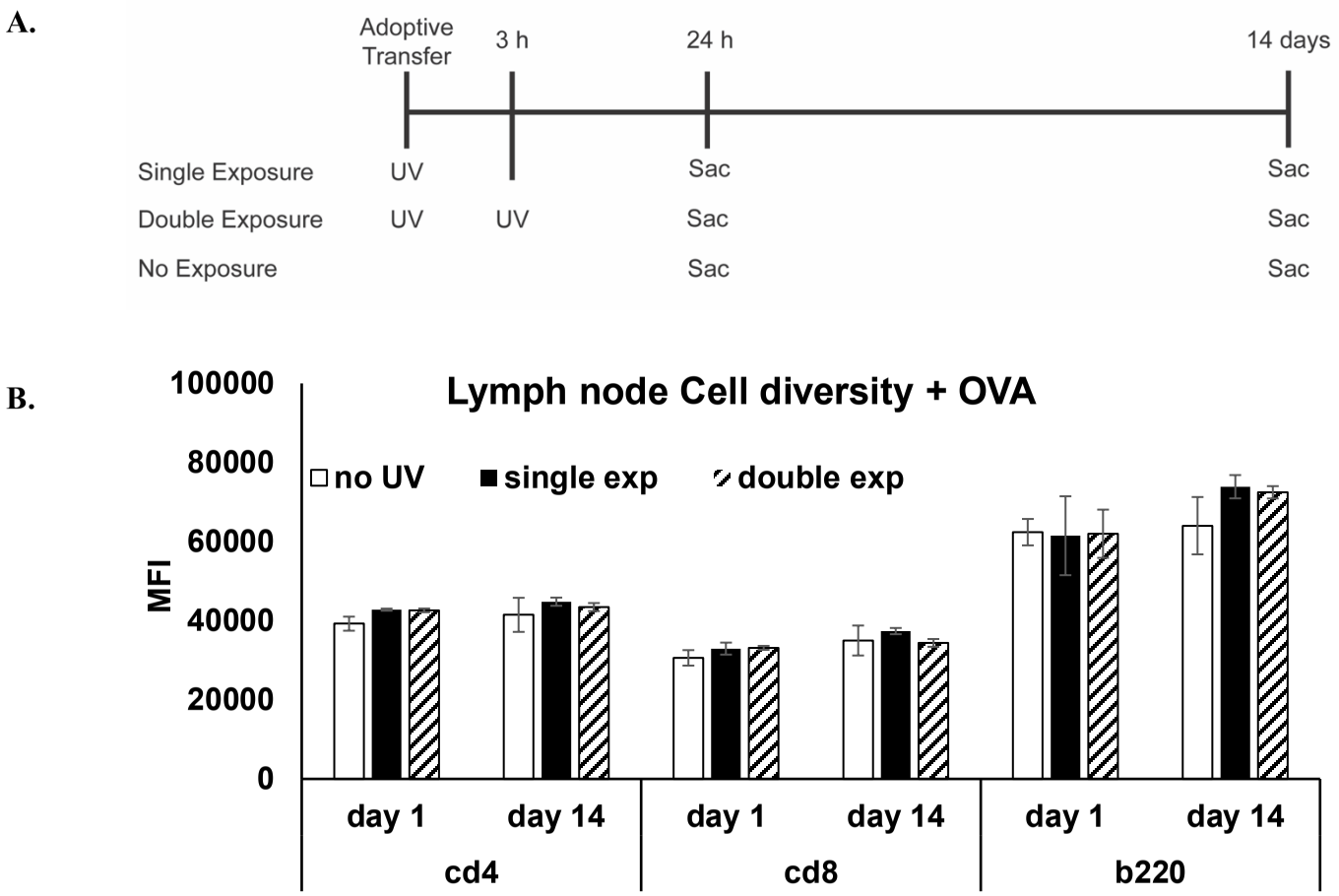

Figure 4. 21. Change in cell diversity following multiple exposures at 3 h intervals and co-administration of OVA. (a) experimental set up, (b) Analysis of change in cell diversity ($CD4^+$, $CD8^+$ T cells and $B220^+$ cells) in the draining lymph node. Each group consists of 3 mice.

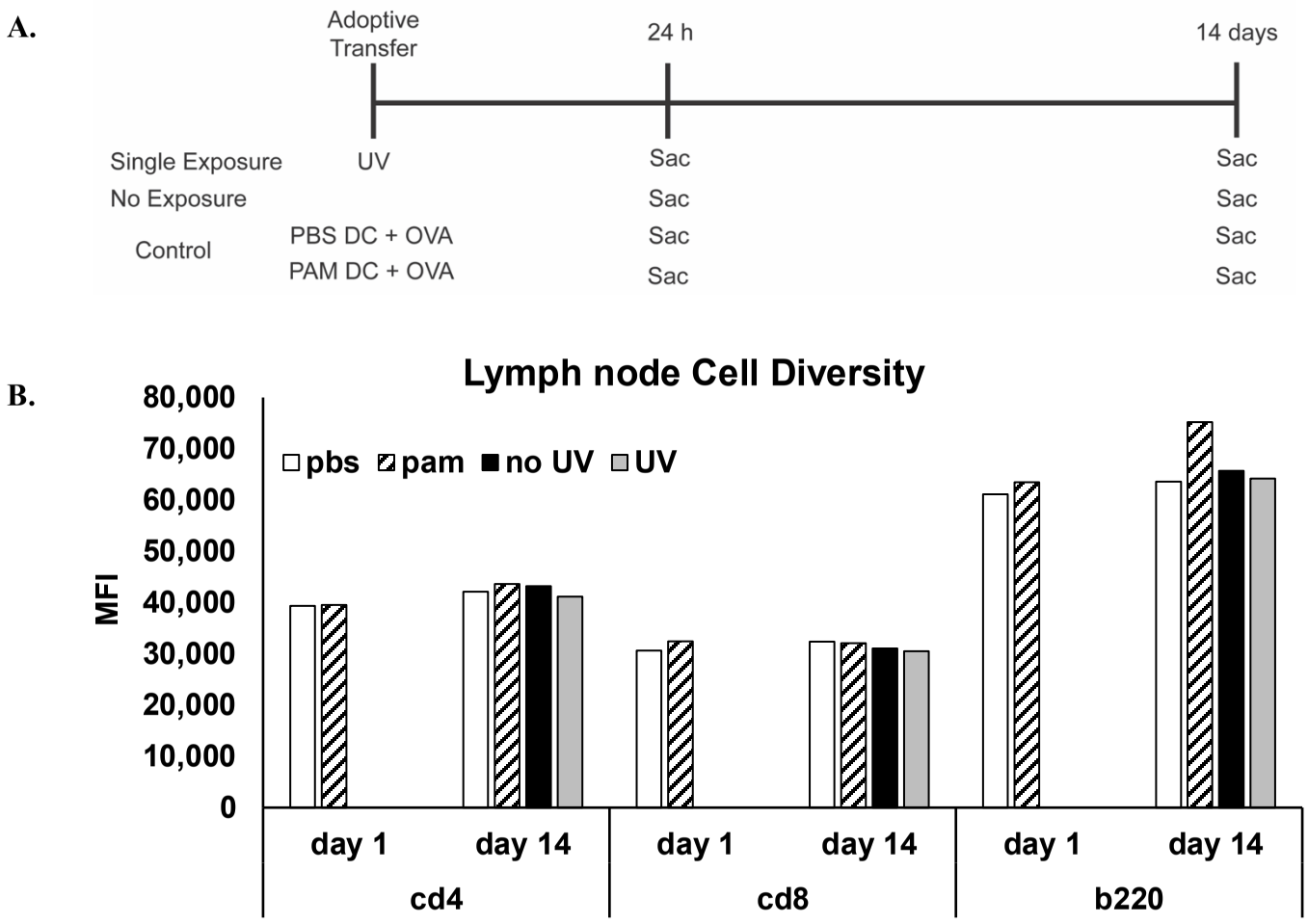

Figure 4. 22. Change in cell diversity following multiple exposures at 3 h intervals and co-administration of OVA. (a) experimental set up, (b) Analysis of change in cell diversity ($CD4^+$, $CD8^+$ T cells and $B220^+$ cells) in the draining lymph node. Each group consists of 2 mice.

4. 10. Experimental Procedures

4. 10. 1. Materials and Methods

Unless otherwise noted, all reagents were purchased from Sigma-Aldrich and used as received. D-Luciferin (potassium salt) was purchased from Gold Biotechnology. Antibodies were purchased from BioLegend. BD Cytofix/Cytoperm Kit for intracellular cytokine flow cytometry and GolgiPlug were purchased from BD Biosciences. Automated solid-phase peptide synthesis was carried out by using a PS3TM Peptide Synthesizer (Protein Technologies, Inc.). Analytical reversed-phase HPLC was performed in an Agilent Zorbax SB-C18 column (50 mm4.6 mm) with a gradient of 5–100% CH_3CN in H_2O with 0.1% TFA and a flow of 1.0 mL/ min over 20 min. UV Vis was measured on Thermo Scientific Nano Drop. Flow cytometry data was acquired using BD Accuri C6 Flow Cytometer and analyzed using the BD Accuri C6 software. RAW-Blue absorbance was measured on a Bio-Tek Quant microplate spectrophotometer MQX200. Microscopy images were obtained on Zeiss 780 confocal microscope in the UCI Optical Biolgy Core. IVIS images were taken on an IVIS Lumina (Xenogen) system. Lymph node tissue work up was done with Genesee Scientific Bead Bug, RNA extraction was done with Qiagen RNeasy mini kit. qPCR was performed on ABI 7300 with Maxima Sybr green (thermo-fisher) and primers ordered from IDT technologies. C57/BL6 (wild type), B6;FVB-*Ptprc*^{a} Tg(CAG-luc,-GFP)L2G85Chco *Thy1*^{a}/J (lucfiferase expressing B6) were purchased from Jackson Laboratories and allowed to equilibrate for a minimum of 48 h. All animal studies and mice maintenance were approved by the Institutional Animal Care and Use Committee (IACUC #2012-3048).

4. 10. 2. Agonist Synthesis Procedures

See preparation in Mancini *et. al*.[16]

4. 10. 3. Bone Marrow-Derived Dendritic Cell Harvest and Culture.

Bone marrow-derived dendritic cells (BMDCs) were harvested from 6-week-old C57Bl/6 mice (Jackson Laboratory). Femur bones were removed from mice and the bone marrow was extracted into PBS buffer and pelleted. ACK Lysing Buffer (3 mL, Lonza) was added to the cell pellet and incubated for 2 min at RT. PBS buffer (13 mL) was then added to the cell suspension, and the cell solution was centrifuged at 300 RCF for 10 min at RT. Thereafter, the cell pellet was resuspended in BMDC complete media composed of RPMI 1640, 10% heat inactivated FBS, 20 ng/mL granulocyte-macrophage colony-stimulating factor (GM-CSF), 2 mM L-glutamine (Life Technologies), 10,000 U/mL penicillin, 10 mg/mL streptomycin, 25 μg/mL amphotericin B, and 50 μM beta-mercaptoethanol. Harvested cells were plated at $1x10^6$ cells/mL in 100 mm petri dishes (10 mL total media) and incubated at 37 °C in a CO_2 incubator (day 0 of cell culture). On day 3, 10 mL of fresh BMDC primary media was added to each petri dish. On day 5, BMDCs were released and plated in 24-well plates at $5x10^5$ cells/mL for cell surface marker activation, cytokine profile flow cytometry experiments.

4. 10. 4. General Procedure for Flow Cytometry for Cell Surface Marker Upregulation.

BMDCs were incubated in individual wells with each agonist (9:1 BMDC:agonist) in 0.5 mL culture media) for 18 h at 37 °C with 5% CO_2. The cells were released from the plate and centrifuged at 2500 RPM at 4 °C for 10 min. The cell pellet was resuspended in cold FACS (composed of PBS (1x), 10% FBS, and 0.1% sodium azide) buffer (100 μL) and incubated with

CD16/32 FcR blocking antibodies (1.0 μg/1x10^6 cells) on ice for 10 min. The cell suspension was pelleted and the supernatant was removed. The cell pellet was resuspended in cold FACS buffer (100 μL) and incubated with PE-CD86 (1.0 μg/1x10^6 cells) on ice and removed from light for 30 min. Each sample was washed twice with 300 μL cold fluorescence-activated cell sorting (FACS) buffer. The dendritic cells were resuspended in cold FACS buffer (150 μL) and kept on ice until being loaded onto the flow cytometer.

4. 10. 5. General Procedure for Cell Labeling.

BMDCs were incubated at 3 million cells in 2 mL of media in a 6 well cell culture plate with the addition of NPPOC-Pam-FAM at 100 nM overnight at 37 °C with 5% CO2. Following incubation, the cells were collected in 15 mL conical tubes and rinsed with PBS 5 times. After the final rinse, the cells were counted and resuspended in PBS at a final cell concentration of 1 million cells/ 30 μL of PBS.

For the ex vivo UV exposed cells, the labeled cells were deprotected with 365 nm light following the last rinse, counted, and resuspended in PBS at a final cell concentration of 1 million cells/ 30 μL of PBS.

4. 10. 6. General Procedure for Adoptive Transfer

Labeled BMDCs were adoptively transferred *via* subcutaneous injection in the footpad of the mouse. The labeled cells were loaded into a syringe (10 cc, insulin syringe) at 1 million cells/ 30 μL of PBS. UV exposed mice were put under isofluorane (2% in 1L/min O2) and exposed to UV light (UVP 95-01300-01 BL-15 long wave UV lamp, 15W) for 15 mins.

4. 10. 7. IVIS imaging procedure

Luciferin was injected into each mouse (15 mg/mL in sterile PBS, 10 μL/g/mouse) *via* intraperitoneal injection. After 10 mins following the luciferin injection, the mice were anesthetized with isoflurane (2% in 1L/min O2). Before taking images the injected foot was taped with black athletic tape and black electrical tape to enhance the bioluminescent signal from the lymph node. Images were analyzed using Living Image Software.

4. 10. 8. Lymph node tissue harvest and RNA extraction

Popliteal lymph nodes were harvested following each desired time point and suspended in RNAlater solution for up to 2 weeks. The harvested RNA was homogenized with prefilled 2mL, 1.5 mm Zirconium bead tubes at 250G for 90 secs. The homogenized tissue solution was extracted for RNA following the procedures for RNeasy Mini Kit (Qiagen). cDNA was reverse transcribed using the extracted RNA (KIT). Murine CCR7, CD34, CD28, nfkb1 expression was quantified using Maxima SYBR Green/ROX qPCR Master Mix (Thermo Fisher) in the ABI 7300 detection system (Applied Biosystems). GAPDH gene expression was measured as endogenous reference. The relative fold change was calculated following the 2^-ΔΔCT method.[34] Fold change was normalized to the average of non-irradiated mice (non treated group) and UV mice (treated group) of triplicate of 6 different mice in each group.

4. 10. 9. Lymph node harvest and cell labeling

The lymph node was suspended in 1 mg/mL solution of collagenase in RPMI. The lymphnodes are incubated at 37 °C with 5% CO2 for 45 min. Using the rugged end of a syringe plunger, the tissue was gently dissociated, using a new syringe plunger for each

lymph. The dissociated tissue was incubated for an additional 10 min at 37 °C with 5% CO2. The tissue was then dissociated further by pipetting and the cell solution was passed through a 0.22 μm cell strainer, including the rinses. The cell solution was then pelleted at 300xg for 10 min. See 3. 10. 4. for general procedure for cell labeling and flow cytometry. Cell suspension was labeled with APC-anti-B220, PE-anti-CD4, and PECy7-anti-CD8.

4. 10. 10. OVA administration

100 μg of Ovalbumin (Invivogen, Ovalbumin Endofit) was administered in 30 μL of PBS including 1 million labeled BMDCs. The OVA-BMDC mixture was adoptively transferred *via* subcutaneous injection in the footpad of the mouse. The labeled cells were loaded into a syringe (10 cc, insulin syringe) at 1 million cells/ 30 μL of PBS. UV exposed mice were put under isofluorane (2% in 1L/min O2) and exposed to UV light (UVP 95-01300-01 BL-15 long wave UV lamp, 15W) for 15 mins.

4. 10. 11. Lymph node harvest and culture

Popliteal lymph nodes were harvested following each desired time point and suspended in 1 mg/mL solution of collagenase in RPMI. The lymph nodes are incubated at 37 °C with 5% CO2 for 45 min. Using the rugged end of a syringe plunger, the tissue was gently dissociated, using a new syringe plunger for each lymph. The dissociated tissue was incubated for an additional 10 min at 37 °C with 5% CO2. The tissue was then dissociated further by pipetting and the cell solution was passed through a 0.22 μm cell strainer, including the rinses. The cell solution was then pelleted at 300xg for 10 min. The supernatant was removed and the cells were resuspended in RPMI + 10% HI FBS and cultured for 72 h.

4. 10. 12. Lymphocyte cytokine production analysis

The supernatant of the cultured of lymphocytes were collected and assayed for IL-4 after 48 h, and for IFN-g and IL-10 72 h after incubation using enzyme linked immunosorbent assay.

4. 11. References

1. Querec, T.; Bennouna, S.; Alkan, S. K.; Laouar, Y.; Gorden, K.; Flavell, R.; Akira, S.; Ahmed, R.; Pulendran, B., *J. Exp. Med.* **2006,** *203* (2), 413-424.

2. Schreibelt, G.; Tel, J.; Sliepen, K.; Benitez-Ribas, D.; Figdor, C.; Adema, G.; de Vries, I., *Cancer Immunol. Immunother.* **2010,** *59*, 1573-1582.

3. Melero, I.; Berman, D.; Aznar, A.; Korman, A.; Gracia, J.; Haanen, J**.,** *Nat. Rev. Cancer* **2015,** *15*, 457–472.

4. Adler; M., E., *Sci. Signal.* **2017,** *10*, eaam5681.

5. Katsikis, P.; Schoenberger, S.; B., P., *Nat. Immunol,.* **2007,** *8*, 899-901.

6. Iwasaki, A.; Medzhitov, R., *Nat. Immunol.,* **2004,** *5* (10), 987-995.

7. Schimmelpfennig, C. H.; Schulz, S.; Arber, C.; Baker, J.; Tarner, I.; McBride, J.; Contag, C. H.; Negrin, R. S., *Am. J. Pathol.* **2005,** *167* (5), 1321-1331.

8. Randolph, G. J.; Angeli, V.; Swartz, M. A., *Nat. Rev. Immunol.* **2005,** *5* (8), 617-628.

9. Wu, W.; Li, R.; Malladi, S. S.; Warshakoon, H. J.; Kimbrell, M. R.; Amolins, M. W.; Ukani, R.; Datta, A.; David, S. A., *J. Med. Chem.* **2010,** *53* (8), 3198-3213.

10. Buwitt-Beckmann, U.; Heine, H.; Wiesmüller, K.-H.; Jung, G.; Brock, R.; Ulmer, A. J., *FEBS J.* **2005,** *272* (24), 6354-6364.

11. Pawlak, J.; Geoffroy, G.; Ruckwardt, T.; Bremmers, J.; Meeuwenoord, N.; Ossendorp, F.; Overkleeft, H.; Filippov, D.; van Kasteren, S., *Angew. Chem. Int. Ed.* **2015,** *54*, 5628–5631.

12. Parasar, B.; Chang, P. V., *Chem. Sci.* **2017,** *8*, 1450-1453.

13. Liu, H.; Kwong, B.; Irvine, D. J., *Angew. Chem. Int. Ed.* **2011,** *50*, 7052-7055.

14. Govan, J. M.; Young, D. D.; Lively, M. O.; Deiters, A., *Tetrahedron Lett.* **2015,** *56*, 3639-3642.

15. Parker, C. G.; Domaoal, R. A.; Anderson, K. S.; Spiegel, D. A., *J. Am. Chem. Soc.* **2009,** *131*, 16392-16394.

16. Mancini, R. J.; Stutts, L.; Moore, T.; Esser-Kahn, A. P., *Angew. Chem. Int. Ed.* **2015,** *54* (20), 5962–5965.

17. Martín-Fontecha, A.; Lanzavecchia, A.; Sallusto, F., Dendritic Cell Migration to Peripheral Lymph Nodes. In *Dendritic Cells*, Lombardi, G.; Riffo-Vasquez, Y., Eds. Springer Berlin Heidelberg: 2009; pp 31-49.

18. Martín-Fontecha, A.; Sebastiani, S.; Höpken, U. E.; Uguccioni, M.; Lipp, M.; Lanzavecchia, A.; Sallusto, F., *J. Exp. Med.* **2003,** *198* (4), 615-621.

19. Spohn, R.; Buwitt-Beckmann, U.; Brock, R.; Jung, G.; Ulmer, A. J.; Wiesmüller, K.-H., *Vaccine* **2004,** *22* (19), 2494-2499.

20. Kang, J. Y.; Nan, X.; Jin, M. S.; Youn, S.-J.; Ryu, Y. H.; Mah, S.; Han, S. H.; Lee, H.; Paik, S.-G.; Lee, J.-O., *Immunity* **2009,** *31* (6), 873-884.

21. Lee, H. W.; Yoon, S. Y.; Singh, T. D.; Choi, Y. J.; Lee, H. J.; Park, J. Y.; Jeong, S. Y.; Lee, S.-W.; Ha, J.-H.; Ahn, B.-C.; Jeon, Y. H.; Lee, J., *Sci. Rep.* **2015,** *5*, 9865.

22. Bertho, N.; Adamski, H.; Toujas, L.; Debove, M.; Davoust, J.; Quillien, V., *Blood* **2005,** *106* (5), 1734-1741.

23. Ritter, U.; Wiede, F.; Mielenz, D.; Kiafard, Z.; Zwirner, J.; Körner, H., *J. Leukoc. Biol.* **2004,** *76* (2), 472-476.

24. Noor, S.; Habashy, A. S.; Nance, J. P.; Clark, R. T.; Nemati, K.; Carson, M. J.; Wilson, E. H., *Infect. Immun.* **2010,** *78* (5), 2257-2263.

25. Clatworthy, M. R.; Aronin, C. E. P.; Mathews, R. J.; Morgan, N. Y.; Smith, K. G. C.; Germain, R. N., *Nat. Med.* **2014,** *20* (12), 1458-1463.

26. Drew, E.; Merzaban, J. S.; Seo, W.; Ziltener, H. J.; McNagny, K. M., *Immunity* **2005,** *22* (1), 43-57.

27. Linterman, M. A.; Denton, A. E.; Divekar, D. P.; Zvetkova, I.; Kane, L.; Ferreira, C.; Veldhoen, M.; Clare, S.; Dougan, G.; Espéli, M.; Smith, K. G. C., *eLife* **2014,** *3*, e03180.

28. Mempel, T. R.; Henrickson, S. E.; von Andrian, U. H., *Nature* **2004,** *427* (6970), 154-159.

29. Baltimore, D., *Cold Spring Harb. Perspect. Biol.* **2009,** *1* (1), a000026.

30. Gerondakis, S.; Siebenlist, U., *d Spring Harb. Perspect. Biol.* **2010,** *2* (5), a000182.

31. Long, E. M.; Millen, B.; Kubes, P.; Robbins, S., *PLoS One* **2009,** *4*, e5601.

32. Inaba, K.; Metlay, J. P.; Crowley, M. T.; Steinman, R. M., *J. Exp. Med.* **1990,** *172*, 631-640.

33. de Heusch, M.; Oldenhove, G.; Urbain, J.; Thielemans, K.; Maliszewski, C.; Leo, O.; Moser, M., *Eur. J. Immunol.* **2004,** *34*, 1861–1869.

34. Livak, K.; Schmittgen, T., *Methods* **2001,** *25* (4), 402-408.

CHAPTER 5. Future Directions: Improving Photoactivation

5. 1. Research Summary

Through photocaged TLR 7/8 agonist, we showed the inhibition of TLR 7/8 activation. Following light exposure, we gain immune cell activation as the photocage undergoes an uncaging event. This control of immune cell activation has been shown in engineered RAW 246.7 cells as well as primary BMDCs. We also verified the activation of a sub-population of cells, by using a photomask to control the area of irradiation.

Further, we could translate this chemical tool to gain photo-control of immune cells *in vivo*. By labeling cells with a photocaged TLR 2/6 agonist, we could keep the photocaged localized on the dendritic cell, which limits the degree of systemic agonist diffusion. Subcutaneous injection of the labeled cells was then activated *via* irradiation of the footpad with a UV lamp. We saw the photo-activated cells migrated to the draining lymph node more quickly compared to the non-activated cells. Gene expression analysis of the harvested draining lymph node showed improved T cell recruitment along a 96 h time line in the activated mice.

5. 2. Limitation of NPPOC and Enhancing Applications *in vivo*

Moving forward, we want to continue developing photocaged agonists to understand the mechanism of TLR synergy at the single cell level. This tool can be used in experiments such as quantifying the number of TLR receptors needed to elicit an immune response of interest. Likewise, the use of orthogonally caged agonists would allow for the study of the mechanism of TLR synergy. To answer these questions, the we are developing 2 photon excitable (2PE) coumarin based photocages (**Figure 5. 10**).[1, 2] These photocages can dramatically enhance the

spatial resolution of deprotection (down to femtoliter resolution)[3], which can enhance resolution in orthogonal deprotection experiments[4] on a microscope to elucidate TLR synergy mechanism *in vitro*.[5]

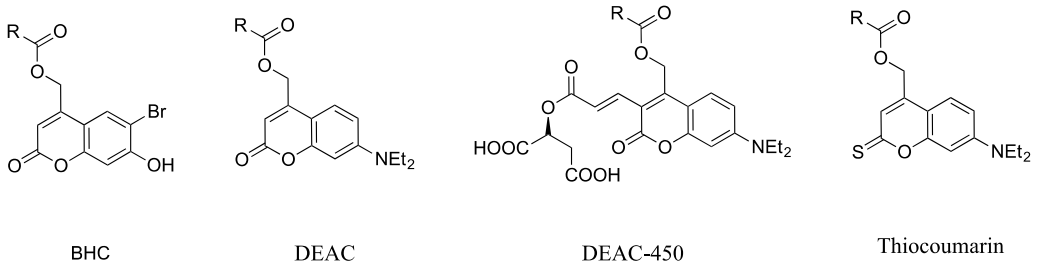

Figure 5. 10. 2PE cleavable coumarin based photocages.

Nonetheless, the NPPOC photocages or the coumarin based photocages are not as efficient *in vivo*. For nitrobenzyl photocages relying on UV irradiation for the uncaging event, UV penetration through the skin is very low. 2PE photouncaging events also require sophisticated pulse lasers which are difficult to translate into *in vivo* experiments. Therefore, there is a need to improve the efficiency of photo-uncaging by improving the tissue penetration of light. With longer wavelength of light, such as near IR (NIR), we gain better spatial resolution with better uncaging efficiencies and we will cause less damage to the irradiated area. However, the challenge remains that there are few photocages that can be uncaged with NIR light.

To overcome this drawback, we investigated the use of upconversion nanoparticles (UCNP) *in vivo*. UCNPs can convert low energy NIR light to high energy ultraviolet (UV) light. The long wavelength of light that is required for excitation enhances the *in vivo* tissue penetration of light required and there is little background activity, as the upconversion process is specific to the excited particles. Recently, UCNP have been used as biomarkers in bioimaging and as nanotranducers for photodynamic therapy.[6-9] Additionally, UCNPs have been used as measures

to uncage biomolecules such as luciferase or DNA/siRNA both *in vitro* and *in vivo*. [10, 11] Following these examples, we wanted to combine UCNPs with our photocaged TLR agonist for better immune cell activation control *in vivo*.

5. 3. UCNP Synthesis

The emission wavelength of lanthanide-based UCNPs can be tuned by changing guest lanthanides within the host matrix. Efforts to enhance the UV emission properties have been rapidly underway. These efforts include changing dopants and synthesis of core-shell UCNPs.[12-14] For application of *in vivo* activation *via* photouncaging, I synthesized $NaYbF_4$ (0.8% Tm) nanocrystals based on the significant enhancement of the 365 nm emission.[15, 16] The synthesis follows a modified co-precipitation method with Yb^{3+} as the host lanthanide and 0.8% Tm^{3+} as the dopant. The synthesized particles were visualized by transmission electron microscopy (TEM)[1] for analysis of the size and morphology (**Figure 5. 11**a). Based on the TEM image, the synthesized particle diameters are in the 10 nm range and shape of the particles are hexagonal plates. However, the nanoparticle mixture is heterogeneous and the size of the particles are about 50 fold smaller than reported. Therefore, the synthetic methods must be optimized for future use.

Though the physical properties of the UCNPs were inconsistent results reported in literature, the emission spectra of the UCNPs following 980 nm excitation showed good emission at 365 nm, comparable to reported values (**Figure 5. 11**b).

[1] Experiment set up and run by Torin Dupper.

A.

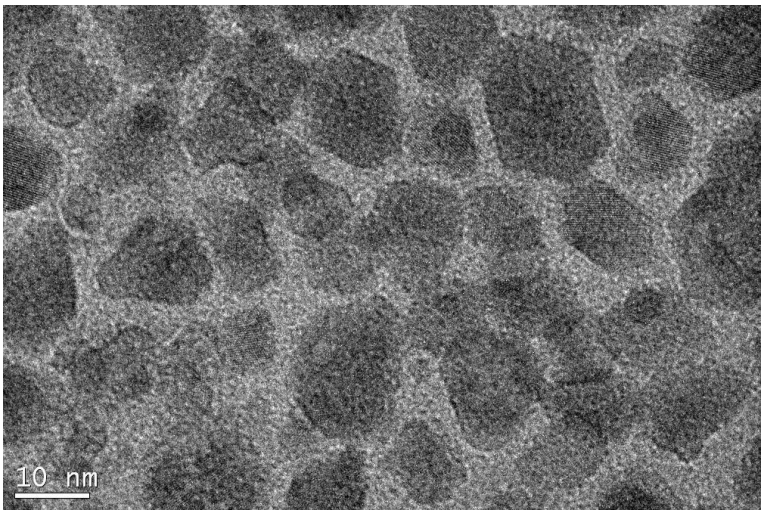

B.

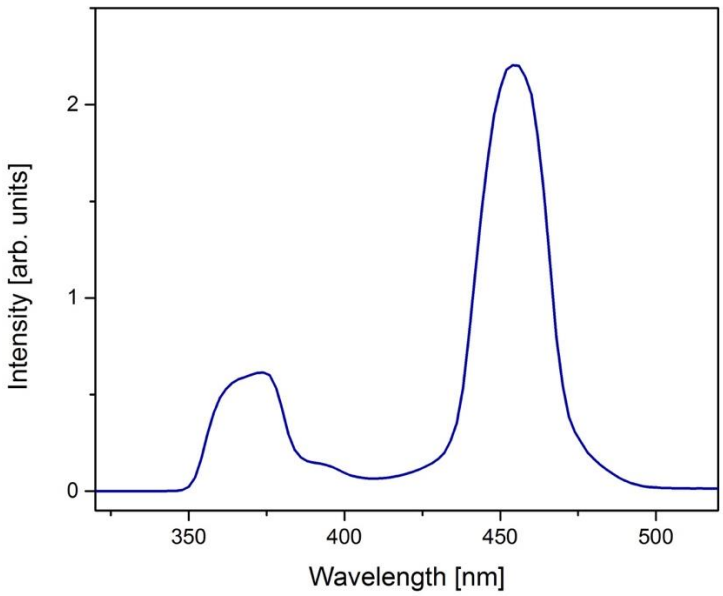

Figure 5. 11. (a) TEM image of synthesized $NaYbF_4$ (0.5% Tm) UCNP, (b) Emission spectra of $NaYbF_4$ (0.5% Tm) UCNP following 980 nm excitation.

5. 4. Photocaged Agonist Adsorption on UCNP and *in vitro* Activation

Following the synthesis of the particles, the particles must be coated with photocaged agonists. We hypothesized we can take advantage of the surface properties of the UCNPs to add a photocaged agonist to the particles. Specifically, we were interested in the hydrophobic property of the synthesized particles due to oleic acids on the surface. These oleic acid residues can interact with the lipid chains on the TLR 2/6 agonist Pam_2CSK_4 *via* hydrophobic interactions. This will allow the adsorption of the agonist NPPOC-Pam_2CKS_4 on the particle which will bring the photocaged agonist in proximity to the UCNP without extra conjugation steps or synthetic changes to the photocaged agonist or the particle itself.

To coat the particles, NPPOC-Pam_2CKS_4 and UCNP is stirred in chloroform overnight. The resulting particles are precipitated and washed multiple times to remove excess NPPOC-Pam_2CKS_4 in solution. The particles (UCNP_NPPOC-Pam) are then suspended in DMSO, filtered through a 0.22 μm filter, and diluted for *in vitro* activation analysis. The UCNP_NPPOC-Pam particles were incubated with RAW-Blue cells at various concentrations and irradiated with a UV lamp (4W) to assess the background immunogenicity of the particles and the amount of activity that can be induced from the adsorbed by full UV irradiation (**Figure 5. 12**).

From the RAW-Blue NF-κB activation assay we concluded that there were large variations in each adsorption reaction, despite following the same adsorption protocol for UCNP_NPPOC-Pam synthesis. Though we see low background activation and NF-κB activity following UV exposure from the UCNP_NPPOC-Pam from Lot 2, very high background activity was observed from Lot 1. This alludes to the inconsistency of the amount of NPPOC-Pam_2CKS_4 that is being adsorbed on to the surface of the particles.

The inconsistency of adsorption is also problematic due to the nature of the NPPOC-Pam agonist. As dicussed previously, because Pam_2CSK_4 is a very potent agonist, small amounts of impurities for background uncaging from NPPOC-Pam can induce a immunological response. Because the adsorption is in consistent, the increased local concentration o the agonist can potentially lead to increased local concentration of uncaged agonist.

To further understand the particle-cell interaction, we imaged RAW-Blue cells incubated with the particles. The cells were also treated with an endosome/lysosome tracker, based on the hypothesis that the particles are endocytosed by the macrophages. Through microscopy of RAW-Blue cells incubated with UCNP_NPPOC-Pam, we observed large aggregates of the fluorescein (FAM) labeled UCNP_NPPOC-Pam (**Figure 5. 13**). This aggregation may be due to the hydrophobic characteristic of the UCNP and the photocaged agonist. The aggregation can occur as the hydrophobic particles are added to aqueous media and can induce inconsistent results.

Though NPPOC-Pam adsorption provides a simple method of coating the particles with the photocaged agonist, there are a variety of parameters that must be optimized for consistent use in the future. These parameters include controlling the amount of adsorption of the agonist on the surface of the UCNP for consistent adsorption for each adsorption reaction. Additionally, because NPPOC-Pam_2CKS_4 induces background immune cell activity at high concentrations, optimizing the concentration of adsorbed agonist to minimize background activation is needed. Following the optimization of these parameters, the UCNP_NPPOC-Pam can be irradiated with 980 nm light to confirm the uncaging of the cage agonist.

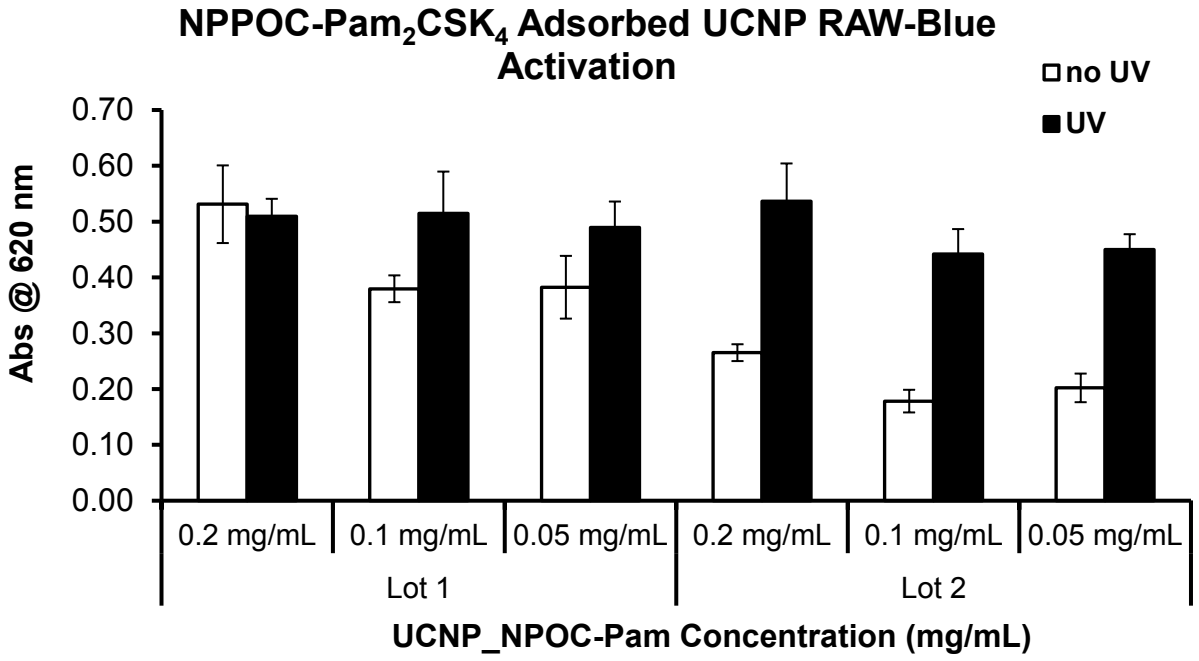

Figure 5. 12. RAW-Blue cell activation with UCNP_NPPOC-Pam particles with (filled) and without (unfilled) UV exposure following 16 h incubation at 37 °C. Each result is from three independent experiments.

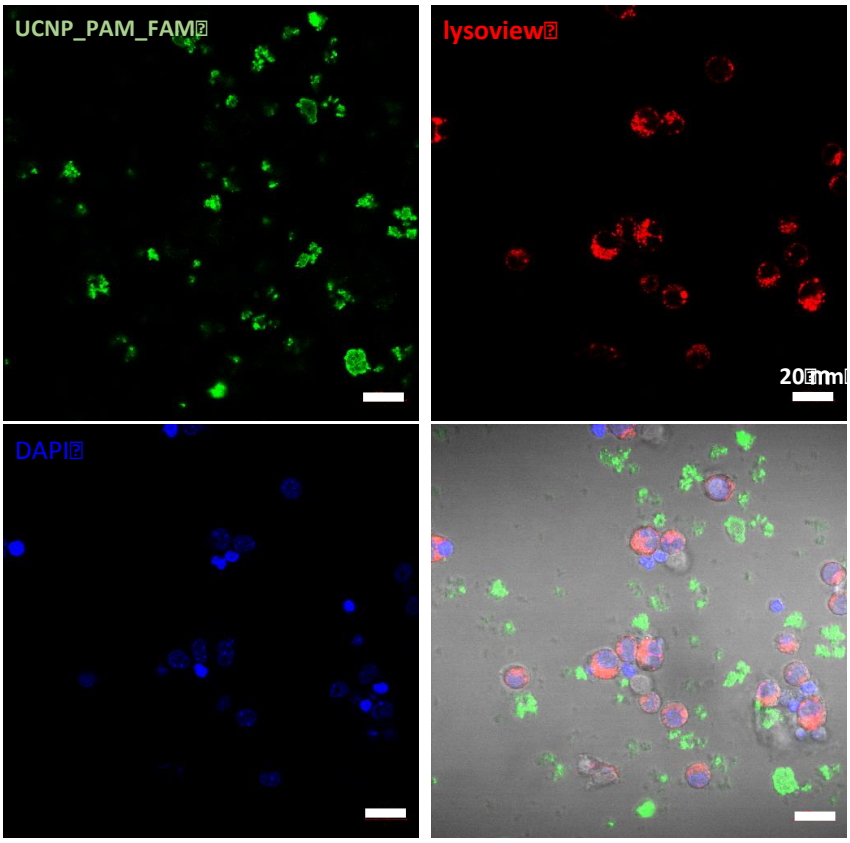

Figure 5. 13. Confocal microscopy of RAW-Blue cells incubated with FAM labeled UCNP_NPPOC-Pam (0.1 mg/mL, green channel). To track the endocytosis mechanism of macrophages, the cells were also stained with rhodamine labeled lysoview (red channel). Scale bar equal to 20 μm for all images.

5. 5. Amphiphilic Polymer Encapsulation of UCNP and *in vitro* Activation

To address the poor water compatibility of the hydrophobic UCNPs, the surface of the particles can be directly modified. The UCNPs can be directly oxidized to form carboxylic acids on the surface of the particle for direct conjugation of the photocaged moiety.[17] For greater stability in biologically relevant conditions, UCNPs can be coated in silica[10] or amphiphilic polymers.[18] One way is to synthesize amphiphilic polymers (C18PMH-PEG) with Poly(maleic anhydride-alt-1-octadecene) (C18PMH) and amine modified PEG (**Scheme 5. 5**). The C18 chain on the maleic anhydride (C18PMH) will interact with the oleic acid chains on the nanoparticle while the PEG component will bring the nanoparticle into water. This will be useful in applying these particles *in vivo* as the particles will be soluble in aqueous media.

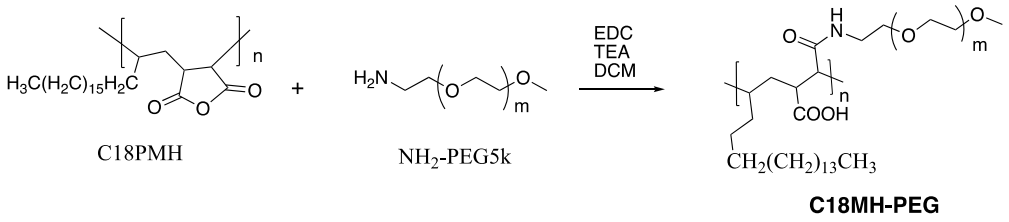

Scheme 5. 5. Synthesis of amphiphilic polymer C18PMH-PEG.

In our efforts, we incorporated the photocaged Resiquimod (ONB-Resiq) in the synthesis of amphiphilic polymer (C18PMH-ONB-Resiq, **Scheme 5. 6**). Though amine functionalized ONB-Resiq can be used to directly modify the surface of an oxidized UCNP, incorporating the moiety into an amphiphile allows for us to use the water stability gained from encapsulating the particle in an amphiphile. Additionally, because no direct modifications are made to the UCNP, we can retain the integrity of the particle.

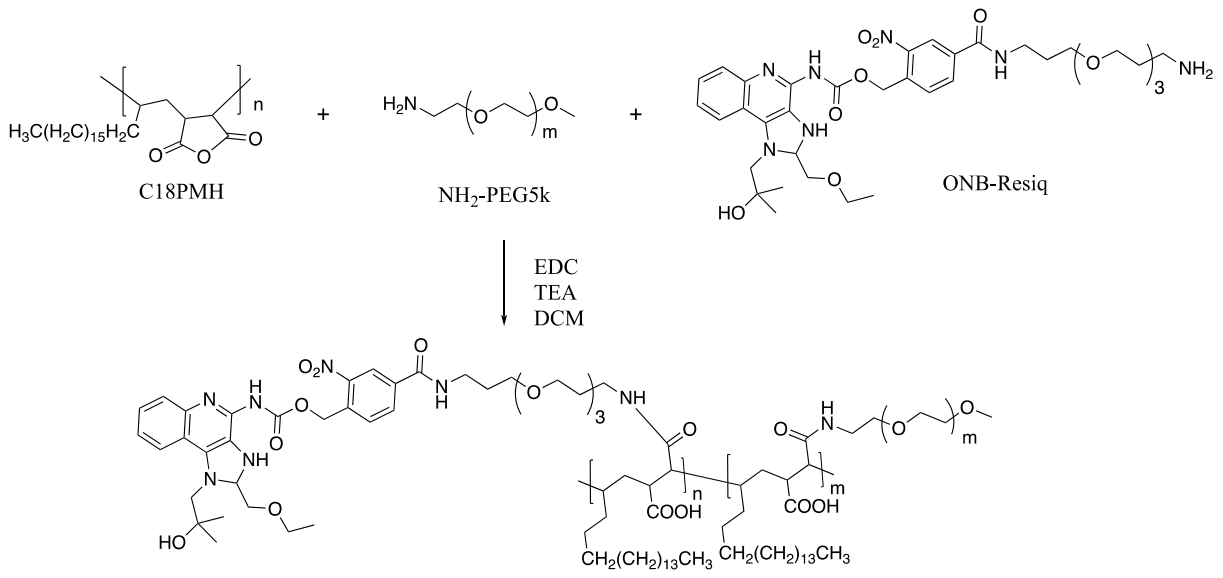

Scheme 5. 6. Synthesis of C18PMH-ONB-Resiq.

Following the synthesis of UCNP and amphiphilic polymers (C18PMh-PEG, and C18PMH-ONB-Resiq) were stirred in chloroform for 2 h. Subsequently, the chloroform was removed and the resulting nanoparticles were resuspended in water at 10 mg/mL. To test the immunogenicity of the polymer encapsulated UCNPs, the UCNPs were incubated with RAW-Blue cells at various concentrations of the modified UCNP (**Figure 5. 14**).

C18PMH-PEG coated particles showed low levels of NF-κB activity across high to low concentrations of the particle (2 mg/mL to 0.2 mg/mL) and no difference in NF-κB activity with or without UV exposure. For C18PMG-ONB-Resiq encapsulated particles, higher concentration (2 mg/mL) of encapsulated UCNP induced high levels of NF-κB activity. However, lower concentrations induced minimal NF-κB activity, comparable to the unmodified C18PMH-PEG encapsulated particles. We also see an increase in NF-κB induction following UV exposure for the C18PMH-ONB-Resiq coated particles.

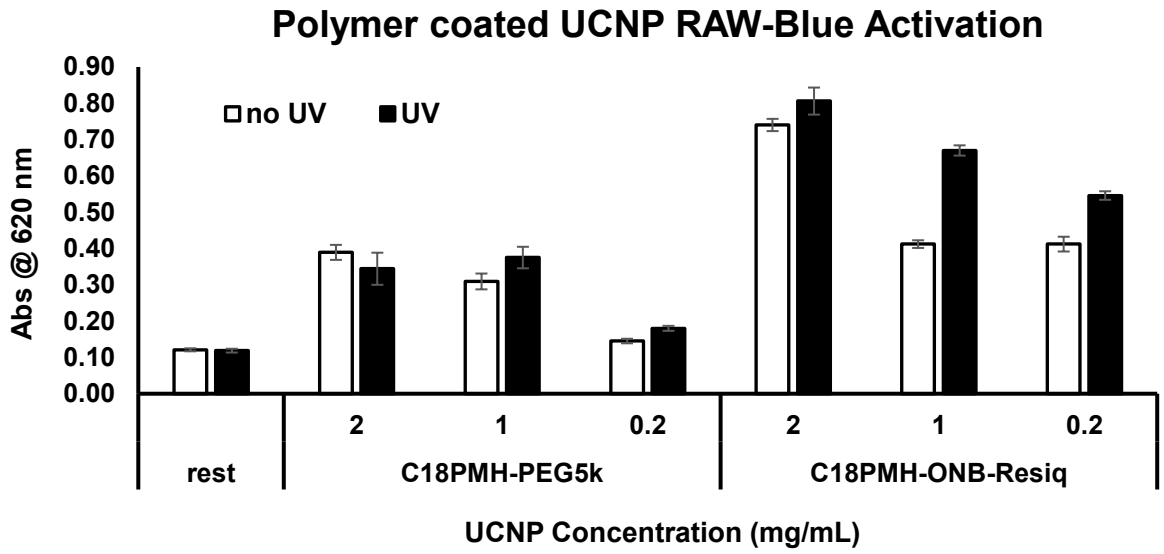

Figure 5. 14. RAW-Blue activation with polymer encapsulated UCNP with (filled) and without (unfilled) UV (4 W) exposure following 16 h incubation at 37 °C. Each result is from three independent experiments.

After confirming the UV dependent Resiquimod uncaging and NF-κB activity induction from the synthesized C18PMH-ONB-Resiq, we can test the upconversion uncaging properties of the particles following 980 nm excitation.[2] First, we confirmed the effect of the 980 nm light irradiation on RAW-Blue macrophages. To test the effect of irradiation, RAW-Blue cells were irradiated with 980 nm (1 W) for times ranging from 30 min to 120 min. For irradiation periods up to 60 min, the cells showed no background NF-κB activity that may be induced from cell stress or death (**Figure 5. 15**a). However, for longer irradiation times (90 min, 120 min), the rapid evaporation of the aqueous solution due to the heat generated from the irradiation procedure made it difficult to keep the cells viable during the irradiation (data not shown). Therefore, the uncaging efficiency of the photocaged agonist coated UCNPs must be sufficient within a 60 min irradiation period.

Before testing the uncaging efficiency of the UCNP in culture with cells. I first tested the uncaging efficiency of the encapsulated nanoparticles in solution and cultured the RAW-Blue cells with the supernantant of the UCNP solution. This was a way of optimizing the irradiation and the UCNP stability before adding a biological parameter into testing the efficacy of the UCNPs. The C18PMG-ONB-Resiq UCNPs were irradiated for 30 min to 120 min. As observed in the previous experiment, the solvent containing the nanoparticles evaporated before the completion of the irradiation experiment (data not shown). 30 min of irradiation did not induce substantial NF-κB activity. However, 60 min of irradiation uncaged enough agonist and the uncaged agonist in solution induced NF-κB activity (**Figure 5. 15**b). This shows that 60 min

[2] Experiment set up and run by Dr. Dima Fishman and Alex Fast at the UCI Laser Spectroscopy Facility.

irradiation is a practical amount of irradiation due to low cell toxicity and efficient agonist uncaging from C18PMG-ONB-Resiq UCNPs that can induce NF-κB activity.

Moving forward, with the general irradiation parameters and irradiation experiment set up optimized, the C18PMH-ONB-Resiq encapsulated UCNPs can be tested with RAW-Blue cells. Once the stable uncaging of the photocaged Resiquimod is shown, the irradiation experiment can be applied to more sensitive primary cells. Further, functionalized UCNPs can be introduced *in vivo* and can be irradiated directly in the living system. By injecting UCNPs in depots at different depths in the body, the irradiation efficiency from 980 nm light can be tested. If the UCNPs are injected in a systemic manner, site specific irradiation can show the spatial control of immune system activation *in vivo*. One can obtain better spatial information of uncaging with using UCNP because the fluorescent properties of the UCNPs can be imaged within the animal. This property can further be used in conjunction with orthogonal animal imaging techniques to visualize the systemic downstream effect of uncaging agonists *in vivo*. Therefore, these tools and methods can be widely applied to elucidate unknown mechanisms and pathways of TLR stimulated immune activation by researchers not only in chemical biology but also immunology, medicinal chemistry, and materials and drug delivery sciences.

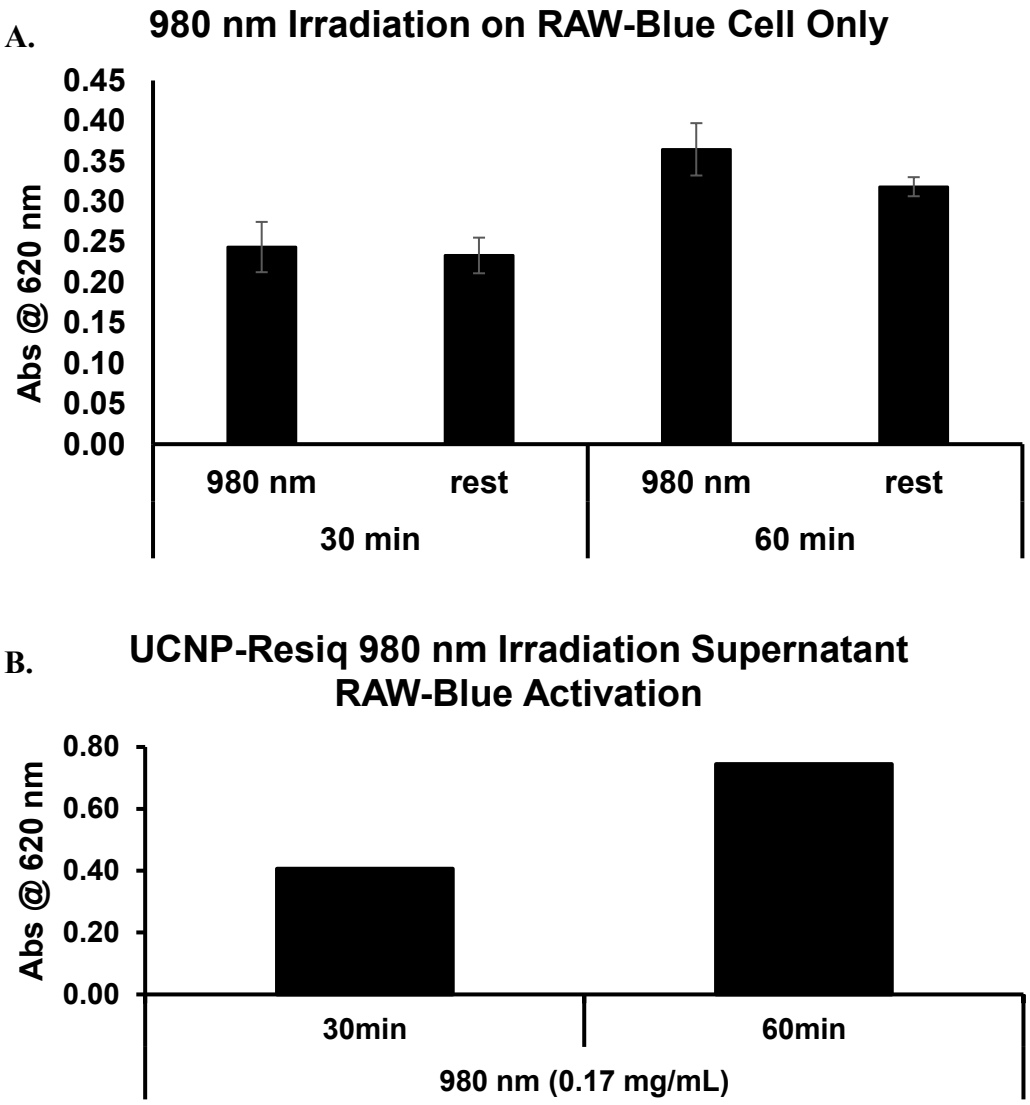

Figure 5. 15. (a) RAW-Blue NF-κB activation following 980 nm (1 W) irradiation for 30 min and 60 min. Each result is from three independent experiments. (b) Measuring uncaging efficiency of 980 nm irradiated C18PMG-ONB-Resiq UCNPs. UCNPs were irradiated for varying durations. The supernatant of the irradiated solution was collected and incubated with RAW-Blue cells to measure the NF-κB activity induced from the uncaged agonist in solution. Each result is from two independent experiments.

5. 6. Supplementary Information

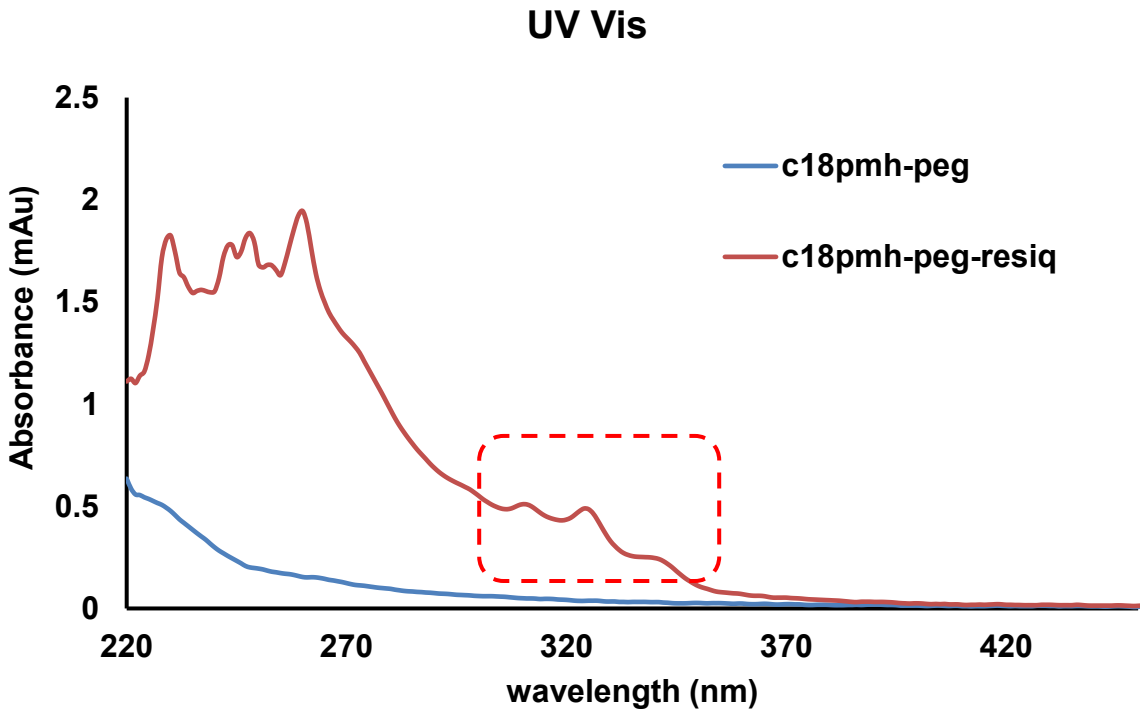

Figure 5. 16. UV absorbance spectra of polymers C18PMH-PEG and C18PMH-ONB-Resiq. The C18PMH-ONB-Resiq shows the addition of ONB-Resiq characterized by the absorbances at 312 nm, 325 nm, and 340 nm.

5. 7. Experimental Procedures

5. 7. 1. General Materials and Methods

Unless otherwise noted, all reagents were purchased from Sigma-Aldrich and used as received. Lysotracker Deep Red was purchased from Thermo Fisher Scientific. ^{13}C and ^{1}H NMR spectra were taken on an AVANCE500 (500 MHz) spectrometer and analyzed using MestreNova software. Mass spectrum was obtained using ESI LC-TOF Micromass LCT 1. UV Vis spectra were obtained using Nanodrop 2000. Confocal microscopy images were taken on Zeiss 780 confocal microscope using a 63x oil immersion. RAW-Blue absorbances were measured on a Bio-Tek Quant microplate spectrophotometer MQX200.

5. 7. 2. Synthesis of particles NP Synthesis[15]

6 mL of $YbCl_3$ (99.6%) and $TmCl_3$ (0.4%) in methanol were added to a 100 mL flask containing 9 mL oleic acid and 21 mL 1-octadecene and the solution was degassed for 30 min at room temperature. The solution was then heated to 160°C for 30 min under argon and then cooled down to room temperature. While the solution was cooling NH_4F (1.6 mmol) and NaOH (1 mmol) were added to 15 mL of methanol and sonicated until the salts were dissolved. The methanol solution was added to the reaction solution and degassed for 30 min, and continued to degas while increasing the temperature slowly to 30°C. After the solution was fully degassed, the reaction was heated to 310°C under argon for 1.5 h and cooled down to room temperature (ramp rate 10°C /min). The resulting nanoparticles were precipitated by the addition of ethanol and centrifugation and resuspended in cyclohexane after decanting the ethanol.

5. 7. 3. NPPOC-PAM$_2$CSK$_4$ UCNP adsorption

0.5 mg of NPPOC-PAM$_2$CSK$_4$ and 3 mg of UCNP was stirred overnight in chloroform. The nanoparticles were when precipitated in EtOH and washed 5 times. The resulting nanoparticles were collected and resuspended in DMSO at 10 mg/mL.

5. 7. 4. C18PMH-PEG5k synthesis[19]

10 mg (1 eq) Poly(maleic anhydride-alt-1-octadecene) (C18PMH) and 143 mg (1 eq) PEG$_{5k}$-NH$_2$ were dissolved in 5 mL DCM with 6 µL triethylamine (TEA) and 11 mg 1-Ethyl-3-(3-dimethylaminopropyl) carbodiimide (EDC). After stirring for 24 h, the solvent was rotovapped and the remaining solid was dissolved in water, forming a transparent clear solution, which was dialyzed against distilled water for 2 days in a dialysis bag with molecular weight cut-off (MWCO) of 14 KDa to remove unreacted mPEG-NH$_2$. After lyophilization, the final product in a white solid was stored at 20°C for future use. ^{1}H NMR (500 MHz, CDCl3) δ 3.85 (t, J = 4.8 Hz, 2H), 3.62 (d, J = 4.8 Hz, 2H), 3.57 (d, J = 5.1 Hz, 2H), 1.32 (s, 16H), 0.94 (d, J = 6.2 Hz, 3H). End group analysis shows 75% pegylation.

5. 7. 5. ONB-Resiq Synthesis[20]

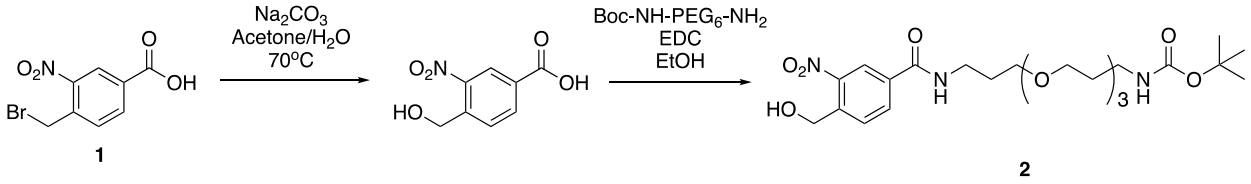

Scheme 5. 7. Synthesis of amine terminated o-nitrobenzyl photocage.

4-bromomethyl-3-nitrobenzoic acid (**1**, 3.88 mmol, 1.0 eq.) and sodium carbonate (13.6 mmol, 4 eq.) was refluxed at 80°C for 5 h in a 1:1 mixture of water and acetone. The solution turned from yellow to dark green. Following reflux, the reaction was cooled to rt and the acetone was evaporated. The resulting aqueous solution was extracted with diethyl ether (x 2) and the organic layers were combined. Concentrated HCl was then added to the aqueous layer, resulting in the formation of yellow precipitate. The aqueous layer was then extracted with ethyl acetate and concentrated under vacuum.

The resulting solid was stirred with N-Boc-PEG_6-NH_2 (1.5 mmol, 1 eq), HATU (1.75 mmol, 1.5 eq), in 10% collidine in anhydrous DMF for 4 h. After 4 h, the reaction was concentrated under vacuum. The residue was dissolved in ethyl acetate and washed with 5% acetic acid followed by sat. sodium bicarbonate solution. The organic layer was dried with anhydrous MgSO4, filtered, and concentrated under vacuum. The product was further purified *via* column chromatography (10% MeOH/DCM) to produce the product, **2**, as a white solid in 90% yield. ^{1}H NMR (500 MHz, DMSO) δ 8.79 (s, 1H), 8.52 (s, 1H), 8.23 (d, J = 8.1 Hz, 1H), 7.95 (d, *J* = 8.4 Hz, 1H), 6.77 (s, 2H), 5.71 (s, 2H), 4.89 (s, 2H), 3.50 (dd, *J*=28.0, 5.6 Hz, 13H), 3.17 – 2.91 (m, 7H), 1.61 (d, *J*=4.6Hz, 3H), 1.38 (d, *J*=1.1Hz, 9H). ^{13}C NMR (500 MHz, DMSO) δ 162.87, 141.70, 134.46, 132.54, 128.94, 123.46, 77.89, 70.23, 70.03, 70.00, 68.64, 68.55, 60.36, 46.23, 37.65, 37.32, 36.29, 31.26, 30.17, 29.65, 28.72, 9.19. Mass m/z $[M+H]^+$ calcd for $C_{23}H_{37}N_3O_9$ 499.25; found $[M+Na]^+$ 522.12.

5. 7. 6. ONB-Resiq

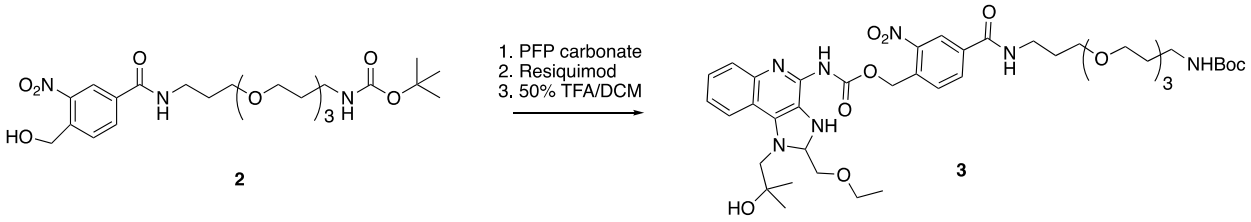

Scheme 5. 8. Synthesis of conjugatable photocaged Resiquimod

Bis-pentafluorocarbonate (1 mmol) was added to a solution of **2** (1 mmol) and DIEA (0.5 mmol) in DMF. The solution was stirred for 3 hr. Resiquimod (0.9 mmol) was added to the reaction and was left to stir overnight. The reaction was concentrated under vacuum and stirred in 1:1 TFA: DCM mixture for 2 h. After concentrating the solution the resulting mixture was further purified by column chromatography (0→ 15 % MeOH/DCM) to produce **3** as a white solid in 10% yield. ^{1}H NMR (500 MHz, DMSO) δ 8.59 (s, 1H), 8.23 (d, *J* = 8.3 Hz, 1H), 8.16 (d, *J* = 7.5 Hz, 1H), 8.05 (d, *J* = 6.9 Hz, 2H), 7.71 (s, 1H), 7.62 (t, *J* = 7.3 Hz, 1H), 7.51 (t, *J* = 7.5 Hz, 1H), 5.77 (s, 2H), 5.34 (s, 1H), 4.83 (s, 2H), 3.76 – 3.56 (m, 14 H), 3.53 – 3.47 (m, 3H), 3.44 (t, *J* = 6.0 Hz, 2H), 1.95 (dd, *J* = 10.9, 5.3 Hz, 2H), 1.69 (p, *J* = 6.2 Hz, 2H), 1.43 (s, 9 H), 1.38 (s, 5H), 1.28 (t, *J*=7.0 Hz, 3H). ^{13}C NMR (500 MHz, DMSO) δ 164.46, 162.80, 156.06, 152.41, 151.40, 147.03, 145.48, 141.73, 136.40, 136.14, 135.28, 134.68, 134.47, 132.55, 128.91, 127.07, 126.51, 123.54, 121.91, 121.12, 115.77, 77.87, 71.15, 70.27, 70.05, 68.66, 68.57, 65.99, 65.78, 65.38, 60.39, 55.33, 37.70, 37.33, 36.24, 31.22, 30.19, 29.67, 28.69, 15.45. Mass m/z $[M+H]^+$ calcd for $C_{41}H_{57}N_7O_{12}$ 839.41; found $[M+H]^+$ 840.31.

5. 7. 7. C18PMH-ONB-Resiq[19]

10 mg (1 eq) Poly(maleic anhydride-alt-1-octadecene) (C18PMH) and 70 mg (1 eq) PEG_{5k}-NH_2,

and 100 mg of **3** were dissolved in 5 mL DCM with 6 μL triethylamine (TEA) and 11 mg 1-Ethyl-3-(3-dimethylaminopropyl) carbodiimide (EDC). After stirring for 24 h, the solvent was rotovapped and the leftover solid was dissolved in water, forming a transparent clear solution, which was dialyzed against distilled water for 2 days in a dialysis bag with molecular weight cut-off (MWCO) of 14 KDa to remove unreacted mPEG-NH_2. ^{1}H NMR (500 MHz, $CDCl_3$) δ 3.85 (t, *J* = 4.8 Hz, 2H), 3.62 (d, *J* = 4.8 Hz, 2H), 3.57 (t, *J* = 5.1 Hz, 2H), 1.32 (s, 17 H), 0.94 (t, *J* = 6.2 Hz, 3H).

5. 7. 8. UCNP C18PMH-ONB-Resiq encapsulation

500 μL of UCNP stock was precipitated in EtOH and pelleted. The resulting nanoparticles were dissolved in a solution of 5 mg C18PMH polymer in chloroform and the reaction was stirred for 2 h. The chloroform was evaporated and the resulting nanoparticles were resuspended in water at 10 mg/mL. After sonicating the solution for 30 min, the solution was filtered through a 0.2 μm syringe filter.

5. 7. 9. UCNP RAW264.7 Macrophage (RAW-Blue) NF-κB Assay

RAW-Blue cells were plated at 5 x 10^5 cells/mL density (180 μL) in 96-well plates using testing media: D-MEM High Glucose medium (Life Technologies), 10% heat inactivated FBS, 2 mM L-glutamine, and antibiotic-antimycotic (1x). RAW-Blue cells were incubated with 20 μL of the aqueous UCNP solution at various UCNP concentrations. The cells were then irradiated with a hand lamp and further incubated for 18 h at 37 °C in a CO_2 incubator. Cell medium (50 μL) from the stimulated RAW-Blue cells was removed, placed into a 96-well plate, and incubated with QUANTI-Blue solution (InvivoGen) (150 μL) for 1.5 h at 37 °C in a CO_2 incubator. The absorbance (620 nm) was measured using a Fisher Scientific MultiSkan FC.

For laser irradiation experiments, UCNP or UCNP-Resiq solutions were irradiated for 30 min and 60 min. The supernatant was collected and added to RAW Blue cells and the NK-κB activity was measured.

5. 7. 10. UCNP RAW-Blue Confocal Microscopy

RAW-Blue cells were plated at 5 x 10^5 cells/mL density (180 μL) in 8-well chamber microscopy plates using testing media: D-MEM High Glucose medium (phenol red free, Life Technologies), 10% heat inactivated FBS, 2 mM L-glutamine, and antibiotic-antimycotic (1x). RAW-Blue cells were incubated with 20 μL of the aqueous UCNP solution at a final concentration of 1 mg/mL overnight. DAPI and lysotracker® was added to the each well 5 min prior to imaging.

5. 7. 11. Laser irradiation of UCNP

Ti:Sapphire femtosecond oscillator (MaiTai, SpectraPhysics, 80 fs, 3W, 76MHz repetition rate) has been utilized as the irradiation source. The laser has been tuned to 980 nm with 1 W power output. The beam was going through the neutral density filter and half-wavelength plate for power and polarization control, then expanded by lens telescope to 5 cm cross-section and then passed through 30 cm lens. The sample has been placed at the distance of about 15 cm from the lens, where the beam size results in about 2.5 mm diameter to fulfill the plate well with the sample. The sample has been irradiated for 0-120 minutes.

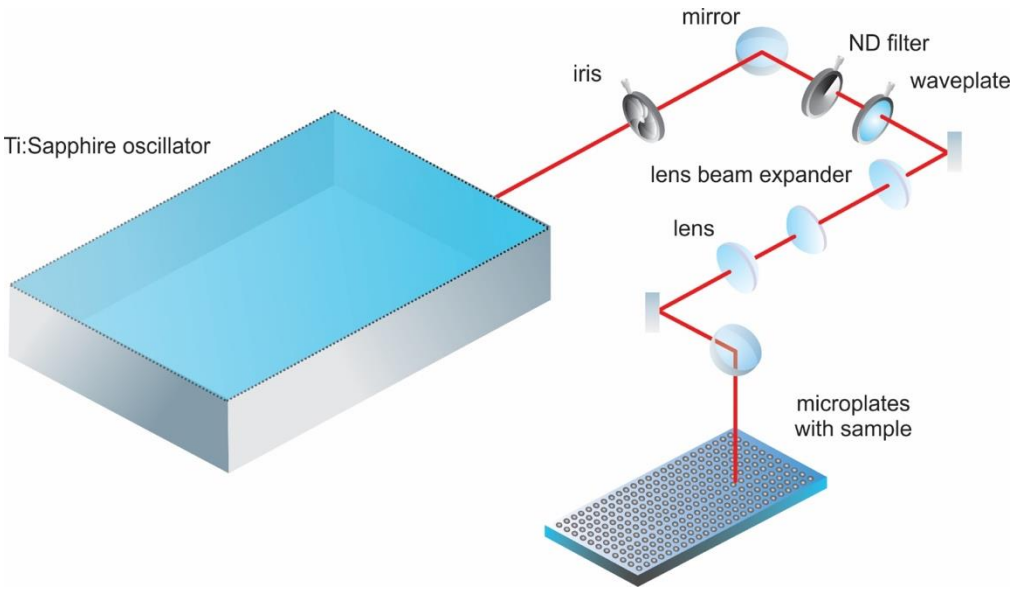

Figure 5. 17. Laser Irradiation set up.

5. 7. 12. Up-conversion fluorescence

The upconversion fluorescence has been measured using modified setup for time-resolved fluorescence studies in time-correlated single photon counting mode (TRFLS, Newport). Ti:Sapphire femtosecond oscillator, tuned to 980 nm (80 fs, 1W, 76 MHz) has been used as an excitation source. The excitation beam has been put through neutral density filter and half-wavelength plate for power and polarization control and expanded to 5 mm diameter by lens based beam telescope. The excitation has been focused then by 5cm lens onto the 1 mm length cuvette. The fluorescence has been collected in the direction collinear to excitation propagation. The excitation radiation has been filtered by appropriate Schott glass filter set. The emission has been coupled in to the double pass grating by focusing on the input slit of the monochromator (Oriel Cornerstone 130) equipped with fast photomultiplier tube (Hamamatsu). The detection bandwidth was set for 2 nm.

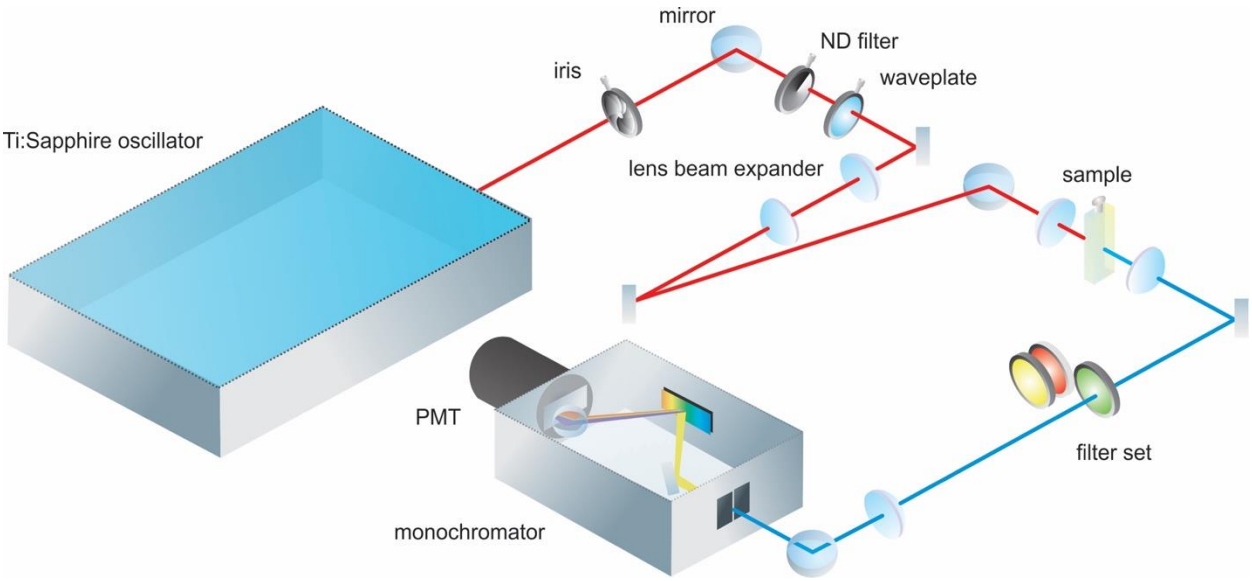

Figure 5. 18. UCNP excitation/emission set up diagram.

5. 8. References and Notes

1. Furuta, T.; Wang, S.; Dantzker, J.; Dore, T.; Bybee, W.; Callaway, E.; Denk, W.; Tsien, R., *Proc. Natl. Acad. Sci. USA* **1999,** *96*, 1193-1200.

2. Olson, J. P.; Kwon, H.-B.; Takasaki, K. T.; Chiu, C. Q.; Higley, M. J.; Sabatini, B. L.; Ellis-Davies, G. C. R., *J. Am. Chem. Soc.,* **2013,** *135* (16), 5954-5957.

3. Brown, E. B.; Shear, J. B.; Adams, S. R.; Tsien, R. Y.; Webb, W. W., *Biophys. J.,* **1999,** *76*, 489-499.

4. Kantevari , S. M., M Kanemoto , Y. Kasai , H. Ellis-Davies , G. C. R., *Nat. Methods,* **2009,** *7*, 123-125.

5. Helmchen, F.; Denk, W., *Nat. Methods,* **2005,** *2*, 932-940.

6. González-Béjar, M.; Liras, M.; Francés-Soriano, L.; Voliani, V.; Herranz-Pérez, V.; Duran-Moreno, M.; Garcia-Verdugo, J. M.; Alarcon, E. I.; Scaiano, J. C.; Pérez-Prieto, J., *J. Mat. Chem. B* **2014,** *2*, 4554-4563.

7. Idris, N. M.; Gnanasammandhan, M. K.; Zhang, J.; Ho, P. C.; Mahendran, R.; Zhang, Y., *Nat. Med.* **2012,** *18*, 1580-1585.

8. Li, Z.; Zhang, Y.; La, H.; Zhu, R.; El-Banna, G.; Wei, Y.; Han, G., *Nanomaterials* **2015,** *5*, 2148-2168.

9. Zhou, J.; Sun, Y.; Du, X.; Xiong, L.; Hu, H.; Li, F., *Biomaterials* **2010,** *31*, 3287-3295.

10. Gnanasammandhan, M. K.; Idris, N. M.; Bansal, A.; Huang, K.; Zhang, Y., *Nat. Prot.* **2016,** *11*, 688-713.

11. Yang, Y.; Shao, Q.; Deng, R.; Wang, C.; Teng, X.; Cheng, K.; Cheng, Z.; Huang, L.; Liu, Z.; Liu, X.; Xing, B., *Angew. Chem. Int. Ed.* **2012,** *51*, 3125-3129.

12. Wang, F.; Deng, R.; Wang, J.; Wang, Q.; Han, Y.; Zhu, H.; Chen, X.; Liu, X., *Nat. Mater.* **2011,** *10* (12), 968-973.

13. Zhang, Y. Y.; Yang, L. W.; Xu, C. F.; Zhong, J. X.; Sun, C. Q., *Appl. Phys. B: Lasers Opt.* **2010,** *98*, 243-247.

14. Shen, J.; Chen, G.; Ohulchanskyy, T. Y.; Kesseli, S. J.; Buchholz, S.; Li, Z.; Prasad, P. N.; Han, G., *Small* **2013,** *19*.

15. Kale, V.; Lastusaari, M.; Holsa, J.; Soukkaa, T., *RSC Adv.* **2015,** *5*, 35858-35865.

16. Wang, F.; Han, Y.; Lim, C. S.; Lu, Y.; Wang, J.; Xu, J.; Chen, H.; Zhang, C.; Hong, M.; Liu, X., *Nature* **2010,** *463*, 1061-1065.

17. Chen, Z.; Chen, H.; Hu, H.; Yu, M.; Li, F.; Zhang, Q.; Zhou, Z.; Yi, T.; Huang, C., *J. Am. Chem. Soc.,* **2008,** *130*, 3023-3029.

18. Xiong, L.-Q.; Chen, Z.-G.; Yu, M.-X.; Li, F.-Y.; Liu, C.; Huang, C.-H., *Biomaterials* **2009,** *30*, 5592-5600.

19. Wang, C.; Cheng, L.; Liu, Z., *Biomaterials* **2011,** *32*, 1110-1120.

20. Eisenfuhr, A.; Arora, P.; Sengle, G.; Takaoka, L.; Nowick, J.; Famulok, M., *Bioorg. Med. Chem* . **2003,** *11*, 235-249.